Title
Acoustic Confinement and Characterization of a Microwave Plasma

Permalink
https://escholarship.org/uc/item/3163g59k

Author
Pree, Seth

Publication Date
2020

Peer reviewed|Thesis/dissertation

UNIVERSITY OF CALIFORNIA

Los Angeles

Acoustic Confinement and Characterization of a Microwave Plasma

A dissertation submitted in partial satisfaction

of the requirements for the degree

Doctor of Philosophy in Physics

by

Seth Lee Pree

2020

ABSTRACT OF THE DISSERTATION

Acoustic Confinement and Characterization of a Microwave Plasma

by

Seth Lee Pree

Doctor of Philosophy in Physics

University of California, Los Angeles, 2020

Professor Seth J Putterman, Chair

High amplitude acoustic fields are used to confine, characterize, and manipulate collisional plasmas with temperatures of a few thousand Kelvin. This dissertation describes the theory, experimental techniques, and apparatus necessary both to generate high amplitude sound in a few thousand Kelvin plasma and to use that sound field to manipulate the plasma within a resonant acoustic cavity. The acoustic field in a spherically symmetric oscillating plasma has been measured to have a Mach number of .03, which is sufficient to cause acoustic radiation pressure effects to confine the plasma to the center of its container. This field also generates convection in the conducting gas, which we study by measuring its effect on the acoustic spectrum, watching the convection occur on high speed video, and by measuring the microwave signal reflected off of the convecting plasma. I also discuss how the varying electrical conductivity due to a high amplitude acoustic field in a plasma may enable a new type of 3D thermoacoustic oscillation.

The dissertation of Seth Lee Pree is approved.

Jonathan M Aurnou

Troy A Carter

Gary A Williams

Seth J Putterman, Committee Chair

University of California, Los Angeles

2020

To my parents, Catherine and Wayne Pree

"Science is a bit like the joke about the drunk who is looking under a lamppost for a key that he has lost on the other side of the street, because that's where the light is. It has no other choice."

- Noam Chomsky

TABLE OF CONTENTS

List of Figures

List of Tables

<div align="center">CURRICULUM VITAE</div>

1991	Born, Iroquois County, Illinois, USA
2009	Diploma, Illinois Mathematics and Science Academy, Aurora, Illinois, USA.
2013	B.S. in Applied and Engineering Physics, Cornell University, Ithaca, New York, USA.
2013 – Present	Ph.D. student in Physics, University of California, Los Angeles (UCLA), Los Angeles, California, USA.

<div align="center">PUBLICATIONS</div>

[1] S. Pree, S. Putterman, and J. P. Koulakis, Physical Review E **100**, 033204 (2019).

[2] J. P. Koulakis, S. Pree, A. L. Thornton, and S. Putterman, Physical Review E **98**, 043103 (2018).

[3] J. P. Koulakis, S. Pree, and S. Putterman, The Journal of the Acoustical Society of America **144**, 2847 (2018).

[4] N. Majernik, S. Pree, Y. Sakai, B. Naranjo, S. Putterman, and J. Rosenzweig, Instruments **2**, 6 (2018).

[5] A. Bataller, S. Putterman, S. Pree, and J. Koulakis, Physical review letters **117**, 085001 (2016).

[6] A. Bataller, J. Koulakis, S. Pree, and S. Putterman, Applied Physics Letters **105**, 223501 (2014).
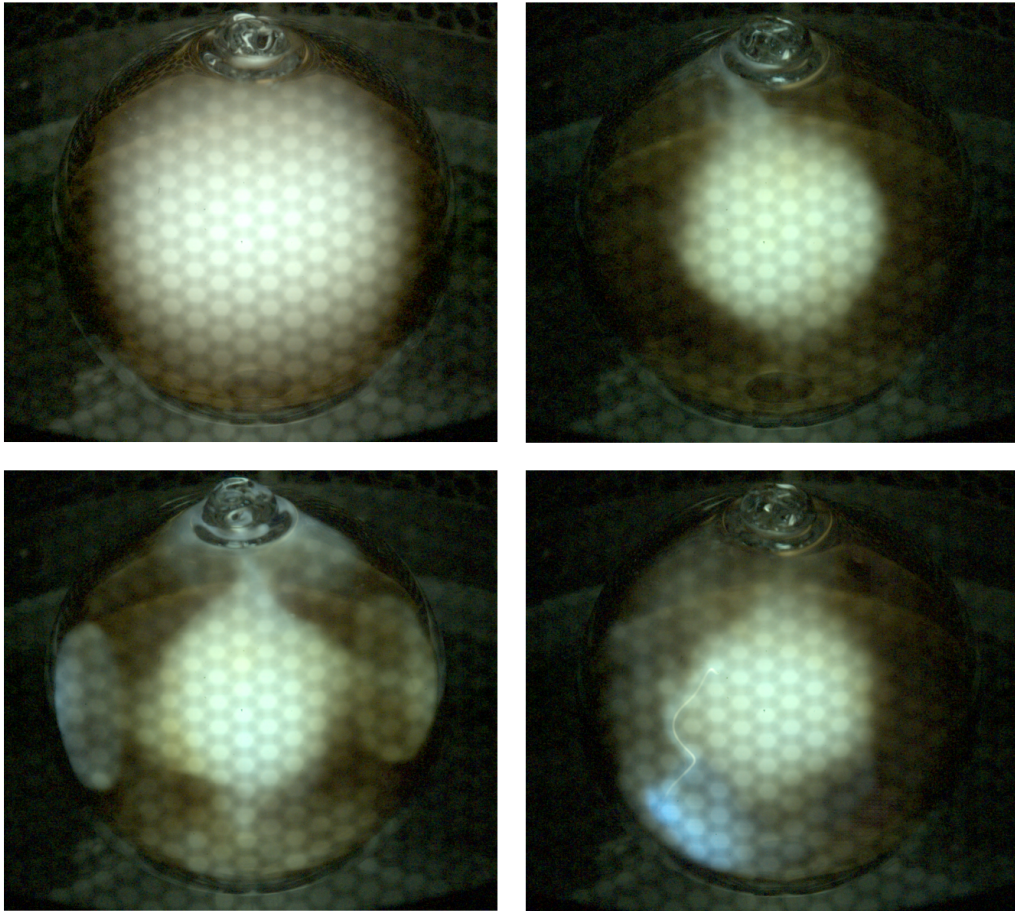
Figure 0.1: A series of photos depicting a microwave plasma subjected to an acoustic field. The top left image shows a luminous sulfur plasma inside a $3\,\mathrm{cm}$ diameter spherical bulb contained in a microwave cavity in its quiescent state in the absence of acoustic oscillations. The top right image depicts the plasma when the microwaves are pulsed near an acoustic resonance frequency of the spherical cavity. In that case, the microwaves generate sound in the plasma which has such a high amplitude that acoustic radiation pressure forces the plasma to be confined to the center of the cavity. The bottom left image shows acoustically driven convection made apparent by the luminous gas. The last image shows a constricted arc which likely has a much higher plasma temperature. The primary purpose of this thesis is to explain the acoustics, fluid dynamics, and plasma dynamics necessary to develop techniques to enable the acoustic manipulation of plasma.

1

CHAPTER 1

Introduction

An ionized gas such as that produced by the sulfur plasma lamp shown in Figure 0.1 mediates between electric fields and sound. Electric fields accelerate the gas's constituent free electrons until they collide with their neutral counterparts inciting acoustic motion, and the luminous edge of the gas exposes motion the sound induces in the gas. The earnest study of plasma physics may have arisen as a consequence of a similar observation in 1900 when the flame of Welsbach mantle, a contemporary lamp, responded to the sound produced by a radiofrequency (RF) wave generator. Although that particular flame responded to the sound and not to the RF generated by the RF generator, this series of events inspired the Barnum and the Bailey of early electrical engineering - Lee de Forest - to forge onward to study a prescient research question

> Here in the flame around this incandescent mantel was matter in a most mobile, tenuous state, extremely sensitive to sound and heat vibrations, infinitely more delicate than any arrangement of solid or liquid particles. Why should it not then in some phase or fashion respond to the hertzian vibrations also? [17].

Pursuing this question, de Forest plugged his headphones into a bunsen burner, alkali salt doped flames, and electric arcs until he arrived at the Audion shown in Figure 1.1, along with a theatrical demonstration. The Audion amplifier was not only the first triode amplifier, which enabled much of the first half-century of power electronics it was also the object of Irving Langmuir's attention at General Electric when he undertook his foundational study of what he would come to name plasma [64, 65, 3].

Plasma is an ultimate and ubiquitous state of matter. As any substance's temperature
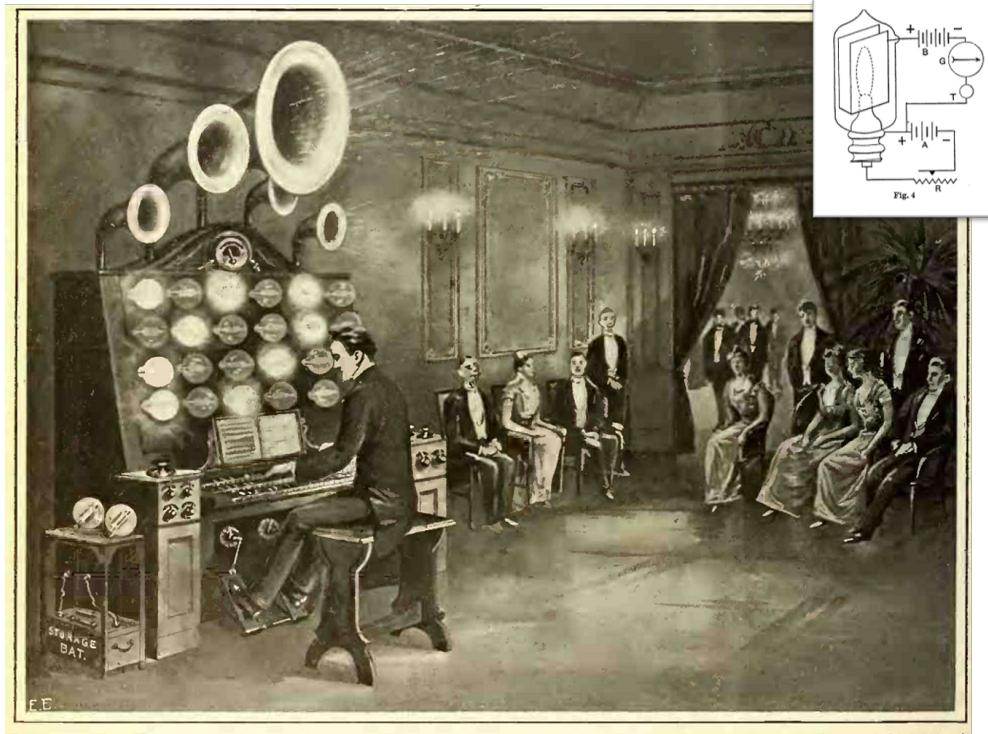
Figure 1.1: The audion amplifier, shown in the inset [17], was the first practical electrical amplifier. Its inventor pursued the idea after observing that a flame responded to a sound wave and mistakenly attributed the effect to an RF signal. The illustration was an early prediction of how the audion and electrical amplifiers may enable electrically generated music [18]. In this thesis we use microwaves to generate sound in a plasma which then induces motion within the plasma.

is increased beyond a few thousand Kelvin, it transforms into a luminous mixture of free electrons, ions, and remaining neutral atoms. Beyond its extreme temperature, a plasma is characterized by its electrical conductivity and interaction with electromagnetic (EM) radiation, which enable its study via electromagnetic measurements such as spectroscopy, RF measurements, videography, and Langmuir probes. Although plasma's major role in electronics fell by the wayside in the first half of the twentieth century due to the rapid development of solid state electronics, it has remained a subject of intensive research as it is central both to the means of and the obstacles to the realization of controlled fusion, which is thought to be a panacea for the purpose of electrical energy generation. It also enables

many manufacturing technologies from joining materials as in arc-welding and the treatment and activation of materials for specialized electronics.

As suggested by a laundry list of its applications and shown in Figure 1.2, the breadth of parameter space in which plasmas exist requires logarithmic axes. In order to introduce the type of plasma explored throughout this thesis, we consider the region labeled sulfur bulb. In particular and to keep in mind, the sulfur plasma such as shown in the title figure peaks around $4000\,\mathrm{K}$, and exists in a gas with a neutral density of more than $1 \times 10^{19}\,\mathrm{cm}^{-3}$, which is comparable to the density of air at STP. This temperature and density in sulfur lead to an electron density around $1 \times 10^{14}\,\mathrm{cm}^{-3}$. The electron neutral collision time of the plasma shown in Figure 0.1 is on the order of $1\,\mathrm{ps}$. This collisionality is so high that some would hesitate to use the word plasma [12]. With these properties, the plasma is sufficiently collisional and cool that an initial treatment will consider it a normal gas which happens to be conducting.

Inspired anew by the observation that an acoustic field enabled the apparent spherical confinement of the weakly ionized plasma found in a man-made light source [15, 58], the purpose of this thesis is to consider again the interaction of the sound with a 'tenuous state of matter' and to widen the set of tools with which plasma and its dynamics can be manipulated and studied to include nonlinear acoustic techniques. In the present study, the RF generator after more than a century of improvements indeed elicits a response from the plasma because of its sensitivity to heat vibrations and by proper modulation generates a sound wave directly within the plasma which has sufficient amplitude that the plasma takes different shapes, is kept from rising due to buoyancy, and is trapped to the center of a spherical cavity as shown in Figure 0.1.

For the most part, the familiar equations of fluid dynamics dictate the motion of the sulfur plasma, and for this reason, this thesis will begin by introducing the fluid dynamics and acoustics necessary to explain how variable heating within a gas could generate sound sufficient to move the plasma around. To explain that motion, after an introduction to nonlinear acoustics and acoustic radiation pressure I will introduce the first theoretical insight
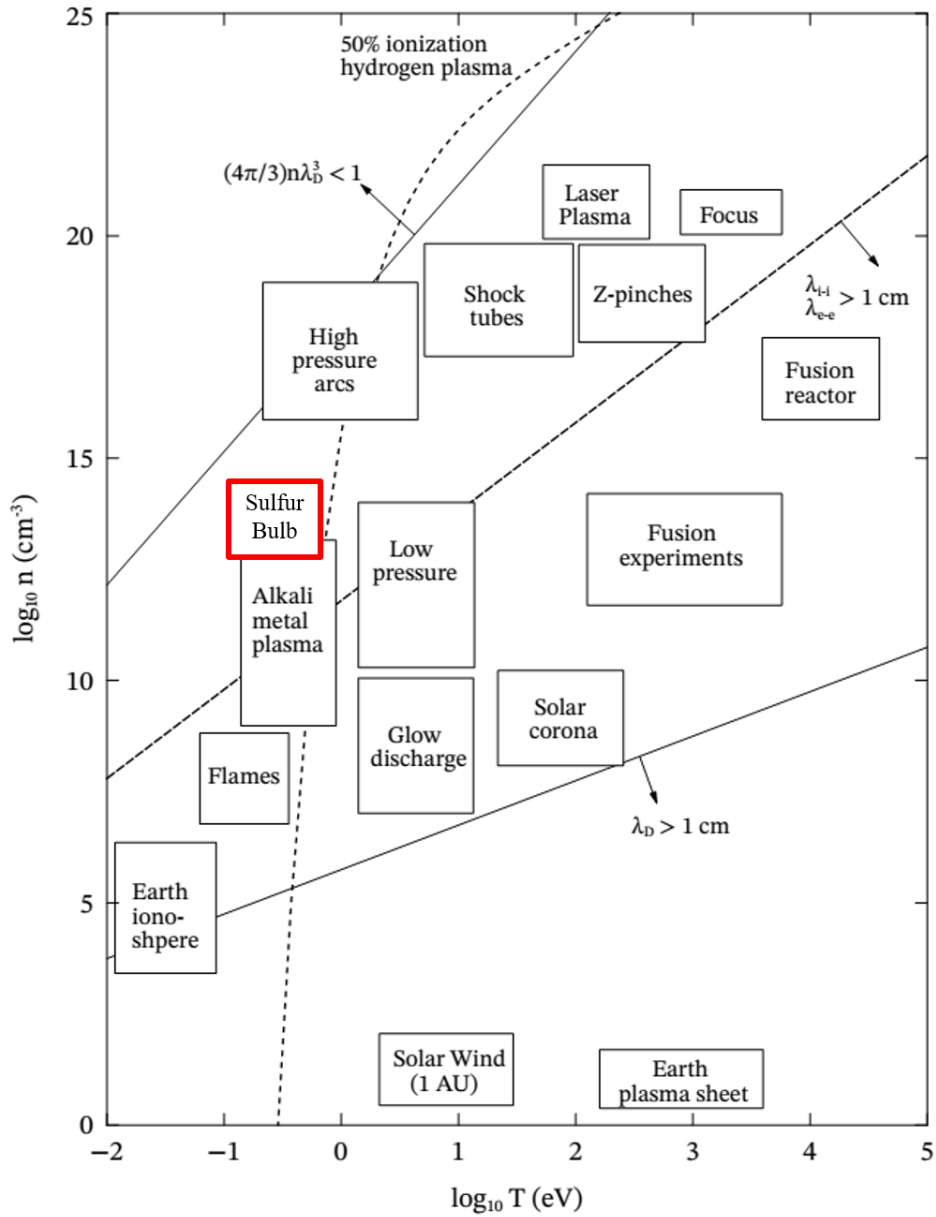
Figure 1.2: A comparison of many types of plasmas. The sulfur plasma, which is highlighted in red and the main focus of this thesis, is unique in that it has such a high neutral density and short electron, neutral collision time that the electrons and molecules are very near thermal equilibrium. Adapted from [88]

.

spun off from this work - that the pycnoclinic acoustic force (PAF) can be used to manipulate plasma. This work was described in [57]. The PAF is a generalization of the acoustic radiation pressure which acts on density gradients in the fluid through which sound propagates. In the plasma lamp a large density gradient is established by the temperature variation which necessarily exists between the center of the plasma and the quartz wall which melts at temperatures below 2000 K. As evidenced by an independent observation of a radiation force described by identical equations in inhomogeneous microfluidic solutions a few years prior [50], the luminous nature of the plasma enables discovery of new consequences of the underlying fluid dynamics.

The third chapter will introduce the aspects of plasma physics essential to explain how microwaves can generate heat within a gas and outline the general apparatus used to generate a plasma with high intensity microwaves. It will also introduce the basic thermodynamic properties of the substance of which the present plasma is made. The fourth chapter will review several experiments which studied the transduction of EM fields into sound.

The fifth and sixth chapters explain the measurements made using two implementations of plasma acoustic drives at UCLA. The fifth chapter will show how a pulsed source revealed the PAF and acoustic plasma trapping, and also how the plasma trapping is accompanied by significant acoustically driven convection. I will show how high speed videography enabled direct measurement of acoustic amplitudes and also a direct observation of pycnoclinic acoustic convection where individual plumes of plasma are slammed into the bulb. Much of the discussion in chapter five was published in [82, 58].

The sixth chapter will demonstrate how a solid state microwave source enabled more precise acoustic measurements of the plasma such as its acoustic spectrum and how that spectrum can be used to determine the temperature as a function of radius throughout the bulb. This technique was published in [56]. The onset of convection due to the spherically central pycnoclinic acoustic force can also be studied with tone bursts which can characterize the onset of pycnoclinic acoustic convection as it begins to cool the gas. Such measurements as how the acoustic spectrum of a rotating plasma filled sphere is affected by its rotation

rate may have implications for modal acoustic velocimetry - a popular tool of astronomers.

Maintaining and enhancing pycnoclinic acoustic convection suggests a route to generating a type of steady-state convective turbulence in a plasma, the onset of which we characterize using microwave perturbation techniques in the seventh chapter. These techniques also measure the extent to which PAF driven fluctuations in the gas change its plasma parameters.

The eighth chapter discusses the second theoretical highlight of this work which is the prediction of a new type of 3D thermoacoustic oscillator based on the acoustically oscillating temperature's effect on a plasma's electrical conductivity. Such an oscillator would enable the generation of high amplitude sound using only a continuous wave (CW) microwave source. This theoretical topic was published in [83].

CHAPTER 2

Introductory Fluid Dynamics

The equations of fluid dynamics are an emergent theory of continuous media that explain the motion of liquids and gases. When applied to a single fluid, they are a complete set of five equations and five unknowns [63]. The five unknowns are generally taken to be: the velocity in three dimensions $v = (v_x, v_y, v_z)$, and two thermodynamic variables which may be the temperature, T, the density, ρ, the entropy per unit mass, s, or the pressure, p.

Though very compact, these equations along with an equation of state describe many, varied behaviors at nearly any scale. To usefully apply them, however, it is necessary to make assumptions and simplifications. The next few sections will use different approximations of these equations in order to introduce several acoustic phenomena which manifest in the plasma acoustic system that is the subject of this thesis.

For example, a first order or linear approximation suffices to show how sound propagates through a fluid, which enables calculations of the speed of sound and acoustic resonances. By approximating to an additional level of perturbation, it becomes apparent that high amplitude sound can cause time averaged forces capable of moving objects. Keeping track of the heating of a fluid demonstrates how a time varying heat source such as a flame or driven plasma can excite sound and also how a continuous heat source can establish the conditions for self-oscillation or thermoacoustics. The lion's share of progress in fluid dynamics comes from the repeated poking and prodding of a small number of equations, and in following tradition those equations are included here for the purpose of further poking and prodding.

2.1 Equations of Fluid Dynamics

The first equation, the continuity equation, is the fluid dynamics statement of the conservation of mass and relates the density and the velocity of the fluid as

$$\frac{\partial \rho}{\partial t} + \nabla \cdot (\rho v) = 0. \tag{2.1}$$

If the fluid under consideration is an ideal fluid, or one without dissipation due to viscosity or irreversible thermal processes, its dynamics are well-explained by the Euler equation,

$$\frac{\partial v}{\partial t} + (v \cdot \nabla)v = -\frac{\nabla p}{\rho}. \tag{2.2}$$

This equation describes how forces effect motion throughout a fluid. The first term is the acceleration of a fluid, the second term ensures Galilean invariance, and p is the pressure, which is a thermodynamic function of ρ and s via the equation of state of the fluid. When viscous or thermal losses are to be considered, the Euler equation is replaced with the Navier-Stokes equation [63].

In an ideal fluid, the last necessary equation is the conservation of entropy,

$$\frac{\partial}{\partial t}(\rho s) + \nabla \cdot (\rho s v) = 0, \tag{2.3}$$

which holds if the whole fluid under consideration is adiabatic. If irreversible processes (e.g. heating) occur within the fluid, entropy increases as required by the second law of thermodynamics.

2.1.1 Conservation of energy in a fluid

As mentioned, in order to completely determine the motion of a fluid, two thermodynamic variables are necessary. The choice of convenient variables is often determined by the particular circumstances of a physical system, such as the source of energy or boundary conditions. The flexibility this affords is realized by writing the fluid dynamic statement of the conservation of energy. Consider the energy of a unit volume of fluid,

$$E = \frac{1}{2}\rho v^2 + \rho \epsilon \tag{2.4}$$

9

where ϵ is the internal energy of a fluid element. By taking a time derivative of this quantity, using the fluid equations, and the first law of thermodynamics,

$$d\epsilon = Tds + \frac{p}{\rho^2}d\rho, \tag{2.5}$$

the fluid dynamic statement of the conservation of energy can be reached

$$\frac{\partial}{\partial t}\left(\frac{1}{2}\rho v^2 + \rho\epsilon\right) = -\nabla \cdot \left(\rho v \left(\frac{1}{2}v^2 + w\right)\right) \tag{2.6}$$

where, w is another thermodynamic potential, the enthalpy, which is a function of entropy and pressure. In order to describe the system with known physical parameters it is often necessary to invoke the thermodynamic relations in order to exploit the fact that five equations is a complete set. Instances of this procedure will be presented in later sections.

2.1.2 Conservation of momentum in a fluid

The momentum of a unit volume of fluid is the product of the density and velocity, ρv. We look for a conservation law of this quantity by taking a partial derivative with respect to time

$$\frac{\partial}{\partial t}\left(\rho v\right) = \rho\frac{\partial v}{\partial t} + \frac{\partial \rho}{\partial t}v, \tag{2.7}$$

and use the the conservation of mass (eq. 2.1) and the Euler equation (eq. 2.2) in order to group all of the components on the right hand side so that they take the form of a divergence [85]. The result is often written in index notation as,

$$\frac{\partial}{\partial t}\left(\rho v_i\right) = -\frac{\partial}{\partial x_k}\left(p\delta_{ik} + \rho v_i v_k\right) = -\frac{\partial}{\partial x_k}\Pi_{ik} \tag{2.8}$$

because the right hand side is the divergence of a tensor [63].

2.2 Sound (linear)

Oscillating pressure, density, velocity, and often temperature fluctuations propagate through a fluid as a sound. The fluctuation is said to be linear when the oscillating quantity, is small

compared to a reference quantity. For example, the oscillating pressure, p_1, is small compared to the ambient, static pressure p_0, the oscillating density fluctuation ρ_1 is small compared to the ambient density, ρ_0, or the oscillating velocity v_1 is small compared to the speed of sound c_s. The ratio of the oscillating quantity to the ambient (e.g. $\frac{v_1}{c_s}$) is the unitless parameter of linearity sometimes known as a Mach number. If the oscillating quantities are small, we can perturb around the ambient values. We will first consider a stationary, $(v_0 = 0)$ fluid that is in mechanical equilibrium, in the absence of an external force field, so p_0 is constant, but we allow for a gradual variation in the density,

$$
\begin{aligned}
p(r,t) &= p_0 &+ p_1(r,t) \\
\rho(r,t) &= \rho_0(r) &+ \rho_1(r,t) \\
v(r,t) &= &v_1(r,t)
\end{aligned}
\tag{2.9}
$$

If these perturbations are substituted into the continuity equation (eq. 2.1) and the conservation of mass (eq. 2.2) and terms to leading order are kept, the resulting equations will be

$$
\frac{\partial \rho_1}{\partial t} + \nabla \cdot (\rho_0 v_1) = 0,
\tag{2.10}
$$

and

$$
\frac{\partial v_1}{\partial t} = -\frac{\nabla p_1}{\rho_0}.
\tag{2.11}
$$

If the fluid is in thermodynamic equilibrium, its thermodynamic properties can be described using two variables, so the pressure, for example, can be written as a function of the density and the entropy, $p(\rho, s)$. The differential form of the pressure is then,

$$
\delta p = \left(\frac{\partial p}{\partial \rho}\right)_s \delta\rho + \left(\frac{\partial p}{\partial s}\right)_\rho \delta s,
\tag{2.12}
$$

and can be used along with the conservation of entropy (eq. 2.3) to reduce the perturbative Euler equation and continuity equation to a system of two equations and two unknowns. In particular, if there is no heat source and the sound field propagates adiabatically, $\delta s = 0$, taking the total or convective derivative ($\frac{d}{dt}$) of equation 2.12,

$$
\frac{\partial \rho_1}{\partial t} + (v_1 \cdot \nabla)\rho_0 = \left(\frac{\partial \rho}{\partial p}\right)_s \left(\frac{\partial p_1}{\partial t} + (v_1 \cdot \nabla)p_1\right)
\tag{2.13}
$$

11

In mechanical equilibrium, the second term on the right hand side will be higher order and can be neglected. Combining the time derivative of equation 2.10 and the divergence of equation 2.11, while substituting equation 2.13, we arrive at an equation

$$\frac{\partial^2 p_1}{\partial t^2} = \rho_0 \left(\frac{\partial p}{\partial \rho}\right)_s \nabla \cdot \left(\frac{\nabla p_1}{\rho_0}\right). \tag{2.14}$$

This equation describes the propagation of sound in a fluid which has a spatially varying density.

If the density ρ_0 is instead constant, equation 2.14 reduces to the form of a wave equation,

$$\frac{\partial^2 p_1}{\partial t^2} = \left(\frac{\partial p}{\partial \rho}\right)_s \nabla^2 p_1. \tag{2.15}$$

Recognizing this equation as a wave equation, the quantity in parenthesis must be the square of the speed of sound, c_s,

$$\left(\frac{\partial p}{\partial \rho}\right)_s = c_s^2. \tag{2.16}$$

As such the speed of sound in a fluid can be calculated if the equation of state is known. In a uniform fluid, the relationship between the acoustic pressure and density fluctuations can be conveniently simplified to

$$p_1 = c_s^2 \rho_1. \tag{2.17}$$

In the case of an adiabatic compression in a gas, the equation of state

$$\frac{p}{p_0} = \left(\frac{\rho}{\rho_0}\right)^\gamma, \tag{2.18}$$

and the ideal gas law,

$$p = \frac{\rho k_B T}{m_g}, \tag{2.19}$$

can be used with the partial derivative in equation 2.15 to calculate the speed of sound in terms of the temperature, T, of the gas

$$c_s = \sqrt{\frac{\gamma k_B T}{m_g}}, \tag{2.20}$$

where γ is the ratio of specific heats and m_g is the atomic weight of the constituent molecules.

The adiabatic equation of state and the ideal gas law can be combined to calculate the temperature of a gas subjected to the compression and rarefaction of a passing sound wave. As long as $p_1/p_0 << 1$, acoustic variation on the temperature, T_1 of a sound field with pressure p_1 is

$$\frac{T_1}{T_0} = \frac{(\gamma - 1)}{\gamma} \frac{p_1}{p_0} \tag{2.21}$$

When a flow field is irrotational, the velocity can be described by the gradient of a scalar potential. An entire sound field can also be described using the velocity potential, ϕ.

$$v_1 = \nabla \phi \tag{2.22}$$

$$p_1 = -\rho \frac{\partial \phi}{\partial t} \tag{2.23}$$

Because it is a scalar, ϕ is often a convenient quantity to use when describing how sound scatters and is particularly useful in some formulations for describing acoustic radiation pressure as will be discussed in section 2.3.5.

Another useful tool for considering sound waves it to treat a sound wave as a plane wave. A propagating acoustic plane wave with pressure amplitude $\overline{p_1}$, will have an oscillating pressure described as a function of position and space of the form,

$$p_1(r, t) = \overline{p_1} e^{i(\vec{k} \cdot r - \omega t)}, \tag{2.24}$$

where k is the wave number, and ω is the angular frequency. Such a wave will appear as an oscillating pressure moving in the $\vec{k}$ direction. The other quantities in equation 2.9 are related to this plane wave via equations 2.11, 2.10, and 2.12. The acoustic velocity if assumed to also be a plane wave can be found by substituting the pressure plane wave into equation 2.11

$$v_1(r, t) = \frac{k}{\omega \rho_0} \overline{p_1} e^{i(\vec{k} \cdot r - \omega t)}, \tag{2.25}$$

Note that the speed of sound is also the phase velocity of the sound wave, $\frac{\omega}{k} = c_s$, so the amplitude of the velocity is the pressure scaled by the product of the density and speed of sound.

$$v_1(r, t) = \frac{1}{c_s \rho_0} \overline{p_1} e^{i(\vec{k} \cdot r - \omega t)}. \tag{2.26}$$

13

One property of these two traveling plane waves is that the acoustic pressure and velocity are in phase with one another. In section 2.2.2 we will introduce resonances which generate acoustic standing waves, where this property no longer holds.

2.2.1 Thermally driven sound

The wave equations, 2.14 and 2.15 describe the propagation of sound through a fluid, but not its generation. Typically when we think of the generation of sound, the source is the oscillatory motion of a solid object such as a speaker cone, a guitar string, or vocal chords. The expansion of a gas caused by the introduction of heat may also generate sound. This is the type of source which generates sound in a plasma.

If a fluid contains a localized source of heat which has a heating per unit volume H, the entropy will increase according to the first law of thermodynamics. In such a case, to first order, the conservation of entropy (eq. 2.3) will be

$$\rho_0 T_0 \frac{\partial s}{\partial t} = H, \tag{2.27}$$

If the term proportional to a change in entropy from equation 2.12 is kept in order to consider how heating changes the pressure within the gas, the resulting formula can be rearranged to

$$\delta \rho = \frac{1}{c^2} \delta p - \frac{1}{c^2} \left(\frac{\partial p}{\partial s} \right)_\rho \delta s \tag{2.28}$$

taking a second derivative of that with respect to time, substituting equation 2.27, and assuming the density and pressure fluctuations are acoustic oscillations,

$$\frac{\partial^2 \rho_1}{\partial t^2} = \frac{1}{c^2} \frac{\partial^2 p_1}{\partial t^2} - \frac{1}{\rho_0 T_0 c^2} \left(\frac{\partial p}{\partial s} \right)_\rho \frac{\partial H}{\partial t}. \tag{2.29}$$

By using the Maxwell relation,

$$\left(\frac{\partial p}{\partial T} \right)_\rho = \left(\frac{\partial s}{\partial V} \right)_T, \tag{2.30}$$

the thermodynamic relation,

$$\left(\frac{\partial p}{\partial s} \right)_\rho = \left(\frac{\partial p}{\partial T} \right)_\rho \left(\frac{\partial T}{\partial s} \right)_\rho = \left(\frac{\partial p}{\partial T} \right)_\rho \frac{T}{c_V}, \tag{2.31}$$

14

and

$$c_P = c_V + T \left(\frac{\partial s}{\partial V} \right)_T \left(\frac{\partial V}{\partial T} \right)_P, \tag{2.32}$$

equation 2.29 can be rewritten as

$$\frac{\partial^2 \rho_1}{\partial t^2} = \frac{1}{c^2} \frac{\partial^2 p_1}{\partial t^2} + \frac{\gamma - 1}{T_0 c^2} \rho_0 \left(\frac{\partial T}{\partial \rho} \right)_P \frac{\partial H}{\partial t}, \tag{2.33}$$

or in terms of the coefficient of thermal expansion, $\beta = -1/\rho \left(\frac{\partial \rho}{\partial T} \right)_P$

$$\frac{\partial^2 \rho_1}{\partial t^2} = \frac{1}{c^2} \frac{\partial^2 p_1}{\partial t^2} - \frac{\gamma - 1}{T_0 c^2 \beta} \frac{\partial H}{\partial t}. \tag{2.34}$$

By taking the time derivative of the conservation of mass (eq. 2.1) and a divergence of the Euler equation (eq. 2.2), and using equation 2.34, a wave equation with a forcing function can be derived,

$$\nabla^2 p_1 - \frac{1}{c_s^2} \frac{\partial^2 p_1}{\partial t^2} = \frac{\gamma - 1}{T_0 c_s^2 \beta} \frac{\partial H}{\partial t}. \tag{2.35}$$

In an ideal gas, the coefficient of thermal expansion leads to the acoustic wave equation with a driving term which is due to a time variable heating,

$$\nabla^2 p_1 - \frac{1}{c_s^2} \frac{\partial^2 p_1}{\partial t^2} = -\frac{\gamma - 1}{c_s^2} \frac{\partial H}{\partial t}. \tag{2.36}$$

This key equation derived in [6, 75] describes how sound is generated in microwave plasma acoustics and will be referred to throughout this thesis. In the ideal gas, this relation can be understood more intuitively by considering that the internal energy of the gas, ϵ is proportional both to the temperature and the pressure of the gas. So, if some external heating acts to locally increase the temperature it will also locally increase the pressure. If that heat source oscillates, it will cause a sound.

The use of heat to drive a sound has been explored in many contexts for example by throttling and choking the fuel source for a flame [5], a device known as the "Dragon Loud Speaker" was developed in order to improve a modulated-airstream loudspeaker.

A device known as a thermophone was also proposed which would use alternating current in a thin wire or metallic strip in order to generate sound via time varying Ohmic heating [4]. The sound generated in the sulfur plasma here is similarly generated via Ohmic heating. More detail on how plasma or conducting gas is uniquely able to generate sound using this mechanism will be the subject of chapter 4.

2.2.2 Acoustic resonance

When sound propagates in a bounded volume such as the spherical bulb which holds the plasma in this experiment (shown in Figure 0.1) at certain, quantized or resonant frequencies, reflections off of the walls constructively interfere and generate a standing wave pattern. This constructive interference enables the generation of a high amplitude acoustic wave for the same acoustic drive. Such high amplitudes as can be achieved with a standing wave resonance enabled acoustic levitation [87, 90]. Secondly, the comparison between predicted and measured acoustic resonances is a tried and true method of determining thermodynamic properties of a gas [28] and under the right experimental conditions has proven to be very precise [71].

To calculate at what frequencies such a resonance occurs, both the wave equation, (eq. 2.15) and a set of boundary conditions must be satisfied. When the fluid is much less dense and much more compressible than its container, as is the case with a gas contained in a quartz sphere, the boundary conditions are the rigid wall boundary condition which assumes that the normal component of the acoustic velocity at a wall is zero.

In order to reference later, I present results for a 1D tube and a sphere assuming that a homogeneous fluid fills either volume.

The simplest case is a 1D closed tube of length L as shown in the first frame of Figure 2.2, where all acoustic losses have been ignored. If the end caps of such a tube are rigid, the acoustic velocity must be 0 at each end of the tube. By using equation 2.11 these boundary conditions can be stated in terms of the acoustic pressure as

$$\left(\frac{\partial p_1}{\partial x}\right)_{x=0,L} = 0, \tag{2.37}$$

which result in solutions of the form

$$p_1(x,t) = \overline{p_1}\cos\left(k_n x\right)e^{ic_s k_n t}, \tag{2.38}$$

where the allowed, discrete wavenumbers are $k_n = \frac{n\pi}{L}$. The oscillation frequency of the resonant tones is $f_n = c_s\frac{n}{2L}$. Again using equation 2.11, the acoustic velocity in this case

16

will be

$$v_1(x,t) = -i\frac{\overline{p_1}}{c_s\rho_0}\sin(k_n x)\, e^{ic_s k_n t}, \tag{2.39}$$

which has a $\pi/2$ phase offset both in space and time as compared to the pressure.

Standing waves in a spherical geometry still satisfy the wave equation but the gradients result in the spherical Helmholtz equation (see [53]). In a homogeneous sphere, the standing wave solutions are separable and take the form

$$p_{lmn}(r,\theta,\phi,t) = A_{lmn} j_l(k_{ln}r) P_l^m(\cos(\theta))\cos(m\phi + \gamma_l mn)e^{ick_{ln}t}, \tag{2.40}$$

where j_l are the spherical Bessel functions, P_l^m are the associated Legendre polynomials of the first kind. In a sphere with rigid walls and radius R, the condition that the velocity normal to the walls be zero at the walls,

$$\left(\frac{\partial p_1}{\partial r}\right)_{r=R} = 0, \tag{2.41}$$

determines the allowed wave numbers, k_{ln}, which must satisfy

$$k_{ln}R = \xi'_{ln}, \tag{2.42}$$

where ξ'_{ln} are the extrema of the spherical Bessel function which can be found in the appendix [53]. The nodal surfaces of the pressure field of the first few modes are shown in Figure 2.1.

The oscillating pressure and velocity field of the lowest frequency spherically symmetric resonance, sometimes referred to as the breather mode, take the forms

$$p_1(r,t) = \overline{p_1}\frac{\sin(kr)}{kr}\exp(i\omega_{02}t) \tag{2.43}$$

and

$$\vec{v}_1(r,t) = \frac{\overline{p_1}}{\rho_0 c_s}\frac{kr\cos(kr) - \sin(kr)}{k^2 r^2} i\exp(i\omega_{02})\hat{r}, \tag{2.44}$$

where $k = 4.49/R$, and $\omega_{02} = 4.49 c_s/R$. Note that the velocity is radially inward and outward and out of phase with the pressure.

The spherically symmetric acoustic resonances have several useful properties when trying to generate high amplitude fields and also to characterize the contents of the bulb. Greenspan

17
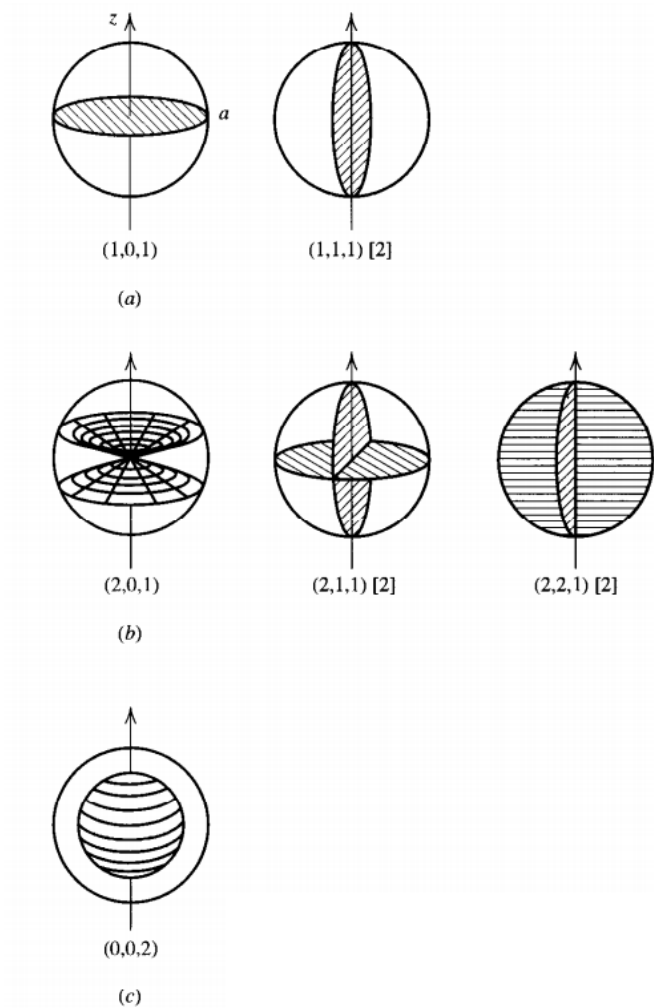
Figure 2.1:

The nodal surfaces of the first few acoustic standing waves in a sphere. The spherically symmetric mode, labeled here as (0,0,2) is excited in these experiments in order to confine the plasma. At least 20 acoustic modes have been observed within the plasma. Figure taken from [53].

et al. who used a spherical acoustic resonator to make an accurate thermometer that was used to set a NIST standard for the universal gas constant in [72] highlighted several reasons why a spherical cavity was well suited for that purpose: 1) in the breather modes the velocity is everywhere perpendicular to the surface, so there is no viscous damping, 2) spheres maximize the volume to surface ratio, so surface losses are minimized, 3) the acoustic energy density is maximized at the center and away from the walls, and 4) the higher order resonances are not linear multiples of the breather and so not inadvertently excited [71, 73].

2.2.3 Thermally driven sound in a cavity

If the gas within a spherical cavity is heated with a time varying heat source such as in equation 2.36, the resulting acoustic field will take the form of equation 2.40. The amplitude of sound generated by a harmonically oscillating heat source $H(r)e^{i\omega t}$ generates sound can be calculated by writing that heating function as a Fourier sum of the eigenmodes

$$H(r,t) = H_0 e^{i\omega t} \sum_{l,m,n} h_{lmn} j_l(k_{ln}r) P_l^m(\cos(\theta)) \cos(m\phi + \gamma_l mn) \tag{2.45}$$

where h_{lmn} are the Fourier weights. If the heating of the fluid in a cavity were completely uniform, the Fourier weights would all be zero. So some variation in how heat is absorbed within the cavity is necessary. Similarly, if a spherical cavity is heated in a spherically symmetric way, only the spherically symmetric modes can be excited. For the heat absorption we expect in the plasma, h_{002} is generally around .5.

With this form of the driving function, and the orthogonality of the spherical Bessel functions, it is possible to write the driven wave equation in a form like a driven simple harmonic oscillator. For example, if we consider the lowest spherically symmetric mode,

$$p_1(r,t) = \overline{p_1}(t) j_0 (k_{02}r), \tag{2.46}$$

the wave equation reduces to a driven harmonic oscillator

$$\frac{\partial^2 \overline{p_1}}{\partial t^2} + c_s^2 k_{02}^2 \overline{p_1} = (\gamma - 1)h_{002} \frac{\partial H_0}{\partial t}. \tag{2.47}$$

In terms of the resonance frequency of that mode, ω_{02} and taking the derivative of the heating, and adding a damping term

$$\frac{\partial^2 \overline{p_1}}{\partial t^2} + 2\alpha \frac{\partial \overline{p_1}}{\partial t} + \omega_{02}^2 \overline{p_1} = (\gamma - 1)H_0 h_{002}\omega e^{i\omega t}. \tag{2.48}$$

When the drive frequency ω approaches the resonance frequency of the cavity, the amplitude will grow.

2.2.4   Acoustic damping in a spherical resonator

The damping added into equation 2.48 is due to acoustic losses. The total quality factor of the mode, Q is $\omega_0/2\alpha$. In the volume of the cavity, the principal losses are viscous damping in the gas and thermal conduction. At the walls of the cavity losses are due to viscous damping due to the no slip condition, thermal losses due to the isothermal boundary condition, and the sound radiated out of the cavity [73, 71]. As long as these losses are fairly small their contribution to the cavity's quality factor can be calculated in the reciprocal sum

$$\frac{1}{Q} = \frac{1}{Q_1} + \frac{1}{Q_2} + \dots \tag{2.49}$$

In the spherically symmetric modes, the oscillating velocity is everywhere perpendicular to the walls of the cavity and so viscous losses at the wall can be ignored. In that case, the largest loss is the thermal loss at the wall and the corresponding quality factor is

$$Q_{wall} = \sqrt{\frac{R^2 \omega_{02}}{2(\gamma - 1)^2 D_t}}, \tag{2.50}$$

where D_t is the thermal diffusivity of the fluid in the cavity [71]. In a gas, the thermal diffusivity is of the same order as the mean thermal velocity times the mean free path λ_{mfp}, or because the mean thermal velocity is approximately the speed of sound,

$$D_t \sim \lambda_{mfp} c_s, \tag{2.51}$$

as is discussed in [63].

2.3 Nonlinear Acoustics

2.3.1 Energy density of a sound wave

When a sound passes through a fluid, the fluid's energy density will change due to both the compression of the sound field doing work on the fluid and the motion the sound causes. To determine the increase in the internal energy in equation 2.4 due to the sound wave we expand $\rho\epsilon$ to second order as

$$\rho\epsilon \approx \rho_0\epsilon_0 + \left(\frac{\partial\rho\epsilon}{\partial\rho}\right)_s \delta\rho + \frac{1}{2}\left(\frac{\partial^2\rho\epsilon}{\partial\rho^2}\right)_s (\delta\rho)^2 \tag{2.52}$$

The compression due to the sound field will do work on the fluid according to the first law of thermodynamics in equation 2.5. If the sound is adiabatic, the change in internal energy is due entirely to the compression of the gas, and will be

$$\left(\frac{\partial\epsilon}{\partial\rho}\right)_s = \frac{p}{\rho^2} \tag{2.53}$$

By substituting this relationship and the first order perturbations of equation 2.9 into equation 2.52, the internal energy in the fluid as the sound passes is calculated to be

$$\rho\epsilon = \rho_0\epsilon_0 + (\epsilon_0 + \frac{p_0}{\rho_0})\rho_1 + \frac{1}{2}\frac{c_s^2}{\rho}\rho_1^2. \tag{2.54}$$

Because the sound passing conserves mass, the term proportional to ρ_1 is zero if a volume the size of a wavelength is considered. This term can also be neglected if the energy is to be measured over several oscillation periods. This different time scale averaging will be explained and applied in deriving aspects of the radiation pressure force in a latter section. Using equation 2.17, the change in energy due to the work done by the sound field and the kinetic energy added by the sound field is

$$E_{ac} = \frac{1}{2}\frac{p_1^2}{\rho_0 c_s^2} + \frac{1}{2}\rho_0 v_1^2 \text{ [63].} \tag{2.55}$$

This energy includes terms to second order. A traveling sound wave will cause an energy flux density. A sound wave may also induce a mass flux density or carry momentum. Consequences of these quantities will be considered in section 2.3.2.

2.3.2 Acoustic radiation pressure

An acoustic wave is an oscillating disturbance in a fluid, and can generally be well described by an approximation of the fluid equations that includes terms linear in the Mach number. Because an acoustic wave is a rapidly oscillating pressure and velocity disturbance, to first order it does not cause a time averaged mechanical effect - i.e. everything occurring in the first half of an acoustic cycle is reversed in the next half. As the amplitude becomes large, however, the approximation should include more terms in the Mach number expansion. If the fluid equations are held to be correct up to second order in that expansion, terms which do not time-average to zero are present. These terms cause pressure and velocity fields that are called acoustic radiation pressure and acoustic streaming, respectively. Such averaging is similar to the process used in calculating the energy density of a sound field as was done to arrive at equation 2.55.

A sound wave both carries momentum and an energy density. As such when sound scatters off an inhomogeneity it imparts a force or a pressure. In this section I will introduce the theoretical techniques that have been developed to quantify the strength of the acoustic radiation force and describe how those techniques have been developed to address acoustic levitation or to answer what is the radiation force on the boundaries of a cavity. In the following chapter, we will extend those techniques to address how acoustic radiation forces will impact variation in the fluid through which sound travels. This subject has proven theoretically tricky and by way of disclaimer I begin with a quote from a famous lecture on radiation pressure from Beyer in [8]:

"It might be said that radiation pressure is a phenomenon that the observer thinks he understands – for short intervals, and only every now and then."

2.3.3 Brillouin stress tensor

A sound passing through an otherwise homogeneous fluid will carry momentum. By substituting the acoustic perturbations (eq. 2.9) into the conservation of momentum (eq. 2.8),
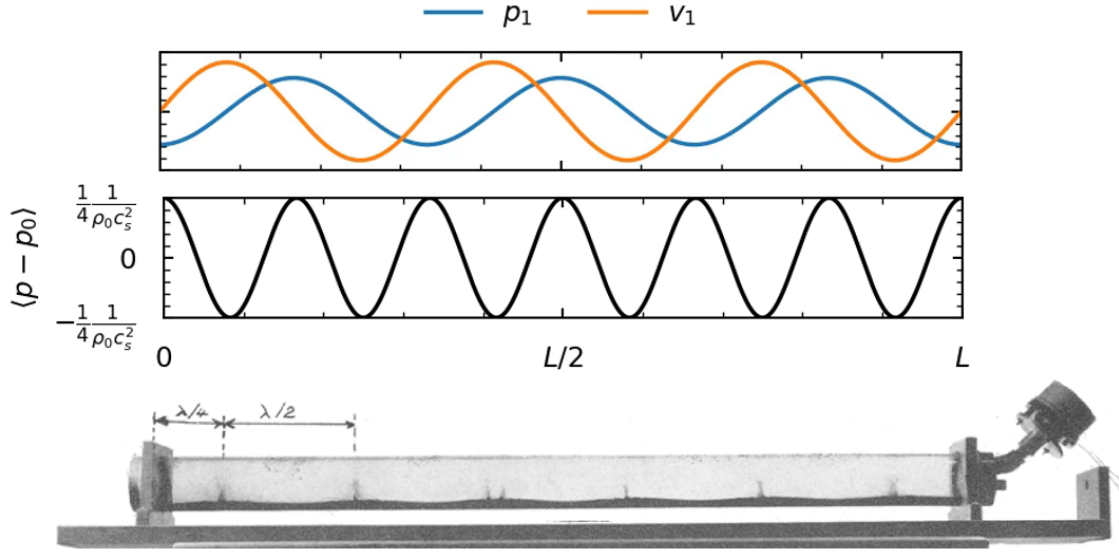
Figure 2.2:   The top frame shows a snapshot in time of the velocity v_1, and pressure p_1 of the $n = 6$ standing wave in a 1D tube where all acoustic losses have been ignored. After one half of an oscillation period the curves would invert. Note that in a rectangular cavity, the pressure antinodes or extrema coincide with velocity nodes. The central frame graphically depicts the excess pressure from equation 2.64 calculated from the standing wave from the top frame. The bottom frame depicts an experimental result from [41], where the excess pressure due to the $n = 6$ acoustic standing wave in a long rectangular air-filled cavity deformed the surface of water pooled at the bottom. The standing wave is driven by the speaker on the right hand side. The water is pushed down where the radiation pressure is high such as near the walls and pulled up where it is low. Compare the shape of the water's surface in the lowest frame to the excess pressure calculated in the second frame. The jet at each pressure minimum are due to a surface wave instability as discussed in [39]. The pycnoclinic acoustic force discussed in section 2.4 is a similar effect which acts on the more subtle density gradients present in the plasma-filled bulb.

and keeping terms up to second order, the momentum change throughout the volume is

$$\frac{\partial}{\partial t} \langle \rho_0 v_{1,i} + \rho_1 v_{1,i} + \rho_0 v_{2,i} \rangle_t = -\frac{\partial}{\partial x_i} \langle (p_0 + p_1 + p_2) \rangle_t \, \delta_{i,j} - \frac{\partial}{\partial x_j} \langle \rho_0 v_{1,i} v_{1,j} \rangle_t .$$ (2.56)

As mentioned above, the acoustic radiation pressure is a time-averaged effect (i.e. observed over many acoustic periods) - denoted as $\langle f \rangle_t$, so it should still be observed if equation 2.56 is averaged over many acoustic periods. If such an average is carried out for harmonically oscillating sound fields, the first term on the left hand side will average to zero because of the oscillation of v_1. The second term on the left hand side does not generally time average to zero and may give rise to certain acoustic streaming effects such as Gedeon streaming [101, 27], but in an acoustic standing wave when the density and velocity oscillations are out of phase it will average to zero. The third term in the time derivative is a transient that approaches zero as mechanical equilibrium is established, but may play a significant role until that point. The p_1 term will average to zero as it also oscillates at the acoustic frequency.

The terms that remain on the right hand side after time averaging define a momentum flux density often referred to as the Brillouin stress tensor, $S_{i,j}$

$$\frac{\partial}{\partial x_j} S_{i,j} = -\frac{\partial}{\partial x_j} \langle p \delta_{i,j} + \rho_0 v_{1,i} v_{1,j} \rangle_t = 0 \ [66]$$ (2.57)

The excess pressure due to the sound field can be calculated by subtracting the mean or ambient pressure from p, this does not effect the satisfaction of equation 2.57 if p_0 is a constant. Thus, the stress tensor due to the sound field is

$$S_{i,j} = -\langle p - p_0 \rangle \, \delta_{ij} - \rho_0 \langle u_i u_j \rangle \ [66].$$ (2.58)

The pressure p may be composed of first and second order terms. In the simplest case, the first order term, p_1 is the sound field and will time-average to zero. Then, the goal is to look for a second order pressure, p_2 which remains after taking the average. Such a remnant pressure will exert time averaged forces on the surroundings or objects in the cavity. This pressure is sometimes referred to as an 'excess pressure'.

2.3.4 Excess pressure

In order to calculate the excess pressure, which is a scalar quantity, we follow [66, 25] and consider the simplest case - a standing sound field in a stationary homogeneous fluid. We assume the sound field, though high amplitude, is still irrotational, and the Euler equation (eq. 2.2) can be written as

$$\frac{\partial v}{\partial t} + \nabla \frac{v^2}{2} = -\frac{\nabla p}{\rho}. \tag{2.59}$$

We will again treat sound as adiabatic and on time average we assume that the gas is in mechanical equilibrium. As such it is convenient to consider the enthalpy, $h(s, p)$, which is the thermodynamic potential with pressure and entropy as the independent variables, and so in differential form is

$$dh = T ds + \frac{dp}{\rho}. \tag{2.60}$$

If the entropy is constant throughout the fluid, $dh = \frac{dp}{\rho}$, so in a uniform fluid the right hand side of equation 2.59 can be written as the gradient of the enthalpy. By using the velocity potential $\nabla \phi = v$, the entire equation can be written as the gradient of scalar quantities

$$\nabla \left(\frac{\partial \phi}{\partial t} + \frac{v^2}{2} \right) = -\nabla h. \tag{2.61}$$

Taking both sides out from under the gradient, the enthalpy can be written entirely in terms of the velocity and the velocity potential as

$$h = h_0 - \frac{\partial \phi}{\partial t} - \frac{v^2}{2}. \tag{2.62}$$

This is sometimes referred to as the strong form of the Bernoulli's equation, because it holds throughout an irrotational fluid as opposed to only along streamlines [25]. The enthalphy $h(s, p)$, can also be Taylor expanded in terms of the pressure,

$$h = h_0 + \left(\frac{\partial h}{\partial p} \right)_s \delta p + \frac{1}{2} \left(\frac{\partial^2 h}{\partial p^2} \right) \delta p^2, \tag{2.63}$$

where according to equation 2.60, the derivatives $\left(\frac{\partial h}{\partial p} \right)_s$ and $\left(\frac{\partial^2 h}{\partial p^2} \right)$ are $1/\rho$ and $-1/\rho^2 c^2$. If the perturbations in the pressure and velocity are considered up to second order, where v_1 and p_1 are an acoustic standing wave, these two representations of the enthalpy, equations

2.62 and 2.63 are equated in order to compute the second order excess pressure. To first order, the relationship between acoustic velocity potential and pressure in equation 2.23 is recovered.

Considering the terms of second order and taking a time average over many acoustic cycles, we ultimately arrive at the often quoted form of the acoustic radiation pressure

$$p_2 = \frac{1}{2} \left\langle \frac{p_1^2}{\rho c^2} \right\rangle_t - \frac{1}{2} \left\langle \rho v_1^2 \right\rangle_t, \tag{2.64}$$

which can also be written entirely in terms of the velocity potential as

$$p_2 = \frac{1}{2\rho_0 c^2} \left\langle \left(\frac{\partial \phi}{\partial t} \right)^2 \right\rangle_t - \frac{\rho_0}{2} \left\langle (\nabla \phi)^2 \right\rangle_t. \tag{2.65}$$

If the acoustic radiation pressure is calculated for the linear standing wave as in equations 2.38 and 2.39, the $n = 6$ mode would have an excess pressure as shown in Figure 2.2. How the radiation pressure might move objects around is rendered visible in the last frame of Figure 2.2. In that experiment described in [41], the acoustic amplitude in a rectangular cavity was sufficient to deform the surface of water of density, ρ_l, and surface tension, σ_l, pooled at the bottom. The extent of the deformation of the water's surface, η_l, is described by

$$-\rho_l g \eta_l + \sigma_l \nabla^2 \eta = p_2, \tag{2.66}$$

which is a force balance between the excess pressure acting on the water's surface, the gravitational force on the water, and the surface tension of the deformation. In addition to the gradual variation across the surface, it was observed that at sufficient amplitude fountains would erupt from the water's surface at pressure nodes or velocity antinodes occasionally resulting in free floating water channels [39]. Similar standing wave fields have been shown to be capable of levitating discrete objects isolated from their surroundings. In the case of levitation, a pressure becomes insufficient to describe the motion of the object and instead a radiation force must be calculated. Furthermore, when the radiation force levitates an object within the bulk of a standing wave, the mode can be appreciably changed due to the sound scattering off of the object which must be taken into account of both in the excess pressure and in the Brillouin stress tensor.

2.3.5   Acoustic levitation

As mentioned above, when a sound wave scatters off of an object it imparts a force. This force can be calculated by integrating the momentum flux from equation 2.8 over a surface surrounding the object,

$$F_i = - \oint \Pi_{ik}. \tag{2.67}$$

Such a force has been shown to levitate and manipulate objects in acoustic standing waves such as the fish suspended in mid air, and the bubble held from rising due to buoyancy shown in Figure 2.3. The ability to levitate and manipulate objects with sound was realized and used long before complete theoretical explanations were developed for example this levitation was used to measure the speed of sound in [61]. The magnitude and the direction of these levitation forces depends on the location of the object within the standing wave, and the relative properties of the fluid and the object. Here we will outline the derivation of the acoustic radiation force using the method laid out by King [52], extended by Yosioka and Kawasima [115], and probably best explained by Gor'kov [32]. This approach has subsequently been refined and expanded by many others [67, 117, 44], because it demonstrates clearly how the radiation force of an acoustic standing wave acts on objects of different composition.

The scattering of the incident sound wave off of the object modifies the standing wave, and so must be taken into account when the force on the object is calculated via equation 2.67. For example, both the pressure component of the stress tensor and the velocity dependent component need to be written in terms of the total standing wave including the incident and scattering wave's contributions.

Such a calculation would appear as

$$F_i = - \oint \left(\frac{1}{2\rho_0 c^2} \left\langle \left(\frac{\partial \phi}{\partial t} \right)^2 \right\rangle_t - \frac{\rho_0}{2} \left\langle (\nabla\phi)^2 \right\rangle_t \right) \delta_{ik} + \rho \left\langle (\nabla\phi)_i (\nabla\phi)_k \right\rangle_t. \tag{2.68}$$

With this formula, the calculation of this radiation force, which enables levitation can be conducted by knowing only the velocity potential of the acoustic field. That velocity potential can often be written as the sum of incident and scattered sound fields as

$$\phi(r,t) = \phi_{in}(r,t) + \phi_{sc}(r,t) \tag{2.69}$$

27

The field, and therefore the calculation of the force, can be simplified by making a few assumptions about the scatterer - for example if the scattering object is much smaller than the acoustic wavelength, the scattered field can be usefully expanded in terms of multipoles. In that case, only leading terms need to be computed, because the integrating surface away from the scatterer can be taken far enough away the the higher order terms are moot.

There are basically two effects relevant to the multipole expansion of the scattered potential, one is due to the difference in compressibility between the scattering object and the surrounding fluid, and the second is due to the oscillating fluid flow which induces motion in the object which either leads or lags the motion in the surrounding fluid. For a sphere in a standing acoustic wave, the scattered potential is

$$\phi_{sc}(r,t) = -\frac{R^2}{3\rho r}\rho_{in}f_1 - \frac{R^3}{2}f_2\nabla \cdot \left(\frac{v_{in}}{r}\right), \tag{2.70}$$

with

$$f_1 = 1 - \frac{c^2\rho}{c_{sc}^2\rho_{sc}} \tag{2.71}$$

and

$$f_2 = 2\frac{(\rho_{sc} - \rho)}{2\rho_{sc} + \rho}. \tag{2.72}$$

The writing of the scattered wave entirely in terms of the incident wave is useful because it enables the determination of the radiation force on the object in terms of the standing wave and the relative properties of the levitated object. Furthermore, this enables writing the levitation force as the gradient of a scalar potential energy. If the particular object under consideration is a sphere with radius R, that potential energy landscape takes the form

$$U = 2\pi R^3\rho\left(\frac{p_{in}^2}{3\rho^2c^2}f_1 - \frac{v_{in}^2}{2}f_2\right). \tag{2.73}$$

By finding the minima of this potential, it is possible to determine where one might expect a sphere of density, ρ_{sc} and speed of sound c_{sc} to be moved due to the radiation pressure of a standing sound wave propagating through a fluid with density ρ and speed of sound c. For example, in the case of the fish levitated in Figure 2.3.5, both the density and the speed of sound in the fish are comparable to that of water, so $\rho_{sc} > \rho$, and $c_{sc} > c$. Under these
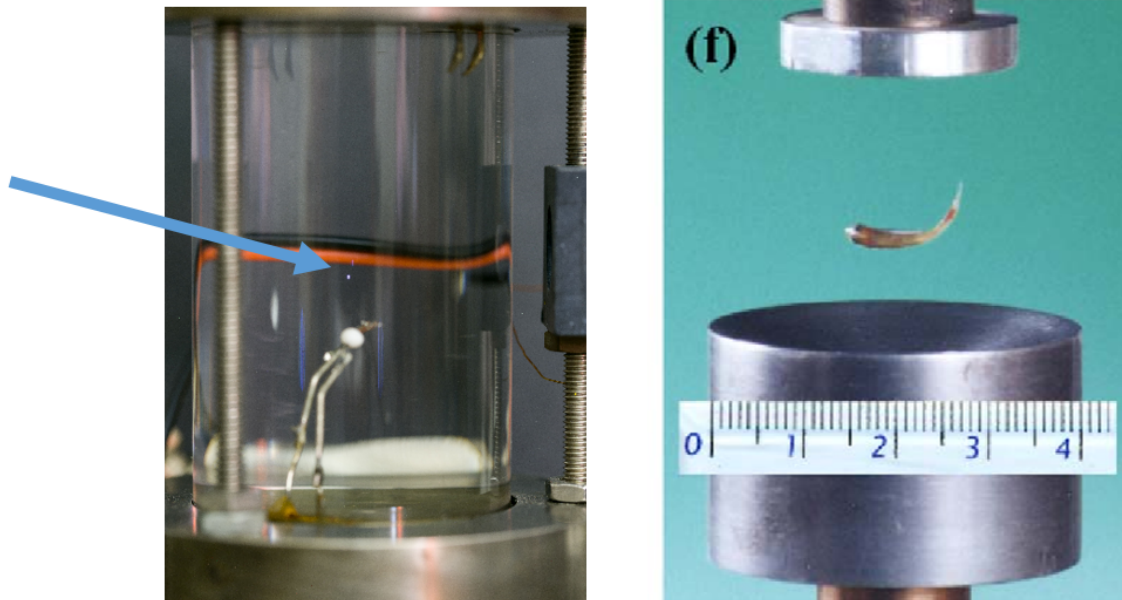
Figure 2.3:   Examples of objects being levitated by an acoustic standing wave. On the left is a sonoluminescing bubble indicated by a blue arrow. Photo by Christian Lee, Hassan Farhat, and Cai Boer during the 180D Acoustics Laboratory at UCLA. To the right is small fish levitated in a standing wave. Photo of levitated fish taken from [114]

conditions, $f_1 > 0$, and $f_2 > 0$, and so the potential energy is minimized if the scatterer is located at a velocity maxima which in a linear standing wave correspond to pressure nodes. For a sense of the acoustic amplitudes necessary to levitate an object in air, to levitate a sphere of material much denser than air a Mach number of around 4×10^{-4} at the point of maximum force will balance the gravitational force.

If the scatterer were instead considered to be a small pocket of warm ideal gas suspended in a standing wave propagating through cooler ideal gas of the same composition, the density of the small pocket would be lower than the surrounding volume. In order to maintain mechanical equilibrium its pressure, however, would be the same and so $\rho_{sc} c_{sc}^2 = \rho c^2$. In this case, $f_1 = 0$, and $f_2 < 1$, and so the object would be forced by the radiation pressure force

toward a velocity node.

This latter case begins to approximate our picture of how an acoustic radiation force could act on the density gradients caused by large density gradients in the plasma bulb. In the experiment, however, the region of changing temperature is not small compared to a wavelength of the sound - in fact, based on the upper right image in the opening figure of this dissertation (Fig. 0.1) and as will be discussed it is approximately the same size.

Some of the literature gives hints about how to handle such a case. For example in order to address how an object levitated in an acoustic wave which propagates through a fluid with a significant temperature gradient, [14] used a procedure similar to Gor'kov, but replaced the velocity potential with a mass flux potential. That this work anticipated the PAF can be observed by considering that it predicts an acoustic radiation force on an object with both f_1 and f_2 equal to zero (i.e. the region becomes acoustically indistinguishable from its surroundings) when the sound field propagates in a temperature gradient. This consequence suggests that the sound field may act on density gradients in a fluid despite the absence of a discrete object. This possibility will be the subject of the next section.

2.4   Pycnoclinic Force

The acoustic radiation pressure demonstration in Figure 2.2 and the levitation of a bubble and fish in Figure 2.3.5 demonstrate how time averaged acoustic radiation forces can manipulate objects with abrupt boundaries. Such theories are insufficient, however, to explain how the plasma is confined to the center of the sphere in Figure 0.1, or how bromine gas, and frozen water vapor are pulled into an acoustic standing wave in Figure 2.4. In these instances, the acoustic radiation pressure acts on gradients in the fluid through which the sound propagates.

In order to determine how second order acoustic radiation forces can manipulate variations in a fluid, we will consider sound passing through a fluid which has variations in its
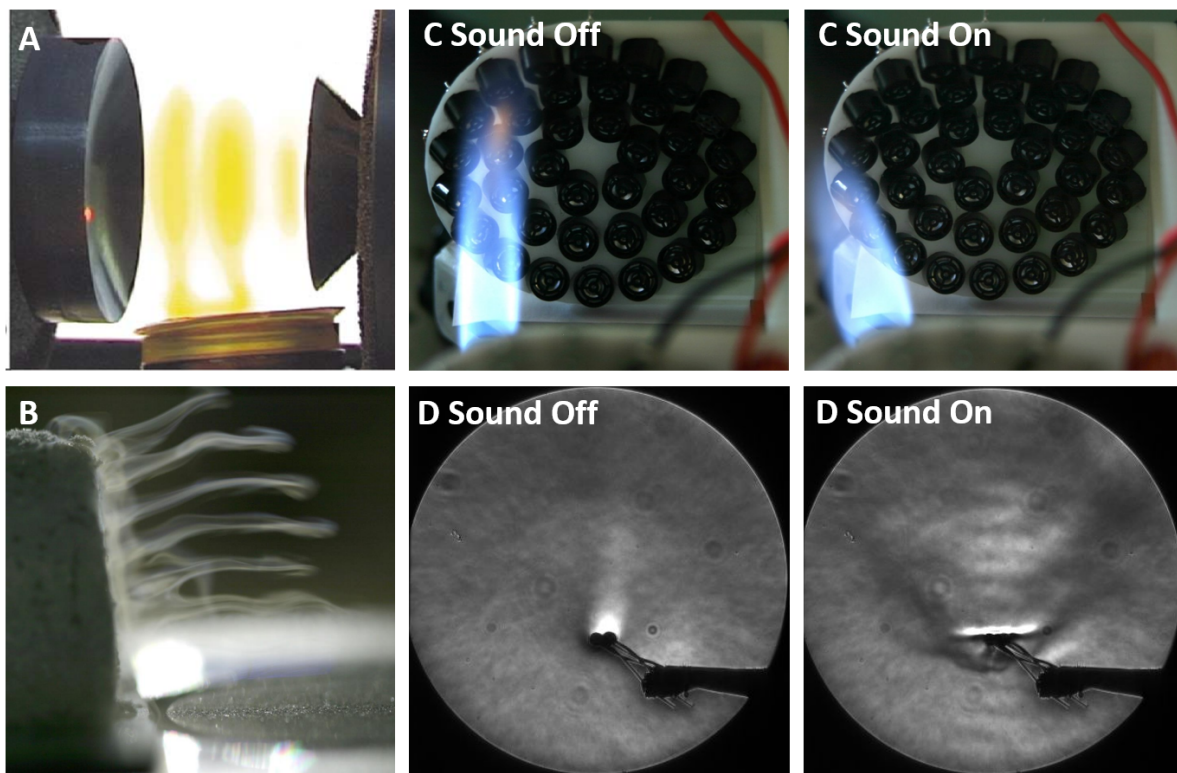
Figure 2.4: Several demonstrations of a high amplitude acoustic standing wave pulling and pushing on density gradients in a gas. A) Yellow bromine vapor, which is denser than air, is pulled upward from a dish into an acoustic standing wave. The yellow color is due to molecular transitions. Photo from [104]. B) Cold, dense vapor fingers emanating from a piece of dry ice are formed by and pulled into an acoustic standing wave via the pycnoclinic acoustic force. Photo used from [57]. C) The low-density flame of a bunsen burner is expelled from the center of the gaussian standing beam of an acoustic levitator. D) The thermal plume of a $\frac{1}{4}$ W resistor is visualized using Schlieren imaging which renders density gradients in a fluid visible. In the first frame, the thermal plume which appears lighter than the surroundings rises due to buoyancy. When the sound field is turned on, the thermal plume is squeezed in the vertical direction by the pycnoclinic acoustic force of an acoustic levitator. The pycnoclinic force due to the levitator, however, does not confine the thermal plume in the horizontal direction, so it escapes from the sides and rises due to buoyancy. The photos in C and D were taken at UCLA using a device described in [68].

temperature and density. The fluid has temperature and density variations, so that

$$\nabla \rho_0 \neq 0, \tag{2.74}$$

but to first order it is in mechanical equilibrium, and for now we neglect gravity, so that p_0 is treated as constant. To address how the variation in the density of the fluid impacts the propagation of a sound wave it is also necessary to consider the wave equation derived for an inhomogeneous fluid as was derived for equation 2.14. For example, when density gradients in a fluid became sizable, the velocity field is no longer necessarily curl free as can be seen by taking the curl of the first order Euler equation (eq. 2.2)

$$\nabla \times \left(\rho_0 \frac{\partial v_1}{\partial t} \right) = -\nabla \times \nabla p_1 = 0. \tag{2.75}$$

Instead,

$$\frac{\partial}{\partial t} \left(\nabla \times \rho_0 v_1 \right) = 0 \tag{2.76}$$

demands that the curl of $\rho_0 v_1$ must be a constant. If the velocity field is still harmonically oscillating, the time average, $\langle \rho_0 v_1 \rangle_t$, must be zero and therefore, $\rho_0 v_1$ is curl free. As such that quantity can be rewritten as a scalar potential

$$\nabla \psi = \rho_0 v_1, \tag{2.77}$$

which has been labeled the mass flux potential [14, 50], this relationship along with Euler's equation gives another useful relationship between the pressure and the momentum flux,

$$\frac{\partial \psi}{\partial t} = -p_1. \tag{2.78}$$

By using Gauss' law on the surface integral which was used to calculate the radiation force necessary to levitate an object (eq. 2.67), it is possible to determine the force density, f_{ac} on a volume element, dV, within the fluid to be

$$F = -\int_V dV \nabla \cdot \Pi_{ik} = \int_V dV f_{ac}. \tag{2.79}$$

By considering the momentum flux tensor as was done by [50], we will determine how the force on a fluid due to a sound wave propagating through the fluid impacts the force density throughout that fluid - this we will call the pycnoclinic force as was labeled in [58].

The force density can be written in terms of the divergence of the momentum flux tensor as

$$f_{ac} = -\nabla \cdot \Pi_{ik} = -\nabla \cdot (p\delta_{ik}) - \nabla \cdot \left(\rho v_1 v_1^T\right). \tag{2.80}$$

We follow [50] and [57] to rewrite this force density in terms of the acoustic field. The first term on the right hand side can be written as the gradient of a pressure, and the second term is the divergence of a tensor which can be broken up into two parts as

$$f_{ac} = -\nabla p - \langle v_1 \cdot \nabla \rho_0 v_1 \rangle_t - \langle \rho_0 v_1 (\nabla \cdot v_1) \rangle_t, \tag{2.81}$$

where the first term in brackets is the dot product of the velocity vector and the gradient of the mass flux vector [i.e. a tensor]. That bracketed term can be rewritten in terms of the mass flux potential, equation 2.77, as

$$f_{ac} = -\nabla p - \left\langle \frac{1}{\rho_0} \nabla \psi \cdot \nabla (\nabla \psi) \right\rangle_t - \langle \rho_0 v_1 (\nabla \cdot v_1) \rangle_t \tag{2.82}$$

The divergence of the velocity field can also be written in terms of the mass flux potential by combining equation 2.13, and the conservation of mass (eq. 2.1), so that the second bracketed term is also entirely in terms of the mass flux potential,

$$f_{ac} = -\nabla p - \left\langle \frac{1}{\rho_0} \nabla \psi \cdot \nabla (\nabla \psi) \right\rangle_t - \left\langle \nabla \psi \left(\frac{1}{\rho_0 c^2} \frac{\partial^2 \psi}{\partial t^2} \right) \right\rangle_t. \tag{2.83}$$

Using vector the vector identity $\nabla(A \cdot B) = (A \cdot \nabla)B + (B \cdot \nabla)A + A \times (\nabla \times B) + B \times (\nabla \times A)$ to pull the gradient out of the second term and that integration by parts on harmonic functions yields $\left\langle f_1 \frac{\partial g_1}{\partial t} \right\rangle_t = -\left\langle \frac{\partial f_1}{\partial t} g_1 \right\rangle_t$ the second term is rewritten as

$$f_{ac} = -\nabla p - \frac{1}{2\rho_0} \nabla \langle (\nabla \psi) \cdot (\nabla \psi) \rangle_t + \frac{1}{\rho_0 c^2} \left\langle \left(\nabla \frac{\partial \psi}{\partial t} \right) \frac{\partial \psi}{\partial t} \right\rangle_t. \tag{2.84}$$

Pulling the gradient out of the last term simplifies the expression to

$$f_{ac} = -\nabla p - \frac{1}{2\rho_0} \nabla \langle (\nabla \psi) \cdot (\nabla \psi) \rangle_t + \frac{1}{2\rho_0 c^2} \nabla \left\langle \left(\frac{\partial \psi}{\partial t} \right)^2 \right\rangle_t, \tag{2.85}$$

where the definition of the mass flux potential equation 2.77 and relation 2.78 can be substituted back in to arrive at a force in terms of the acoustic field quantities,

$$f_{ac} = -\nabla p - \frac{1}{2\rho_0} \nabla \langle (\rho_0 v_1) \cdot (\rho_0 v_1) \rangle_t + \frac{1}{2\rho_0 c^2} \nabla \langle (p_1)^2 \rangle_t. \tag{2.86}$$

and finally each term can be separated in order to isolate the familiar acoustic radiation pressure force from the new terms which are due to inhomogeneities in the fluid

$$f_{ac} = -\nabla p - \langle v_1^2 \rangle_t \nabla \rho_0 - \frac{\rho_0}{2} \langle \nabla v_1^2 \rangle_t + \frac{1}{2\rho c^2} \langle \nabla p_1^2 \rangle_t. \tag{2.87}$$

By grouping the right hand side under a gradient as,

$$f_{ac} = -\nabla \left(p + \frac{\rho_0}{2} \langle v_1^2 \rangle_t - \frac{1}{2\rho c^2} \langle p_1^2 \rangle_t \right) - \frac{\langle v_1^2 \rangle_t}{2} \nabla \rho_0 - \frac{\langle p_1^2 \rangle_t}{2} \nabla \left(\frac{1}{\rho c^2} \right), \tag{2.88}$$

we point out that the first term on the right hand side would recover the standard acoustic radiation pressure (eq. 2.64) for a homogeneous gas in equilibrium. The two terms outside of the gradient are the components of the force which arise due to variation in the fluid. Although $1/\rho_0 c^2$ is in general a quantity that may vary in space, for an ideal gas with a uniform pressure it is constant, so we will neglect it from here on. The remaining term is what we call the pycnoclinic acoustic force (PAF). The PAF indicates that a high amplitude acoustic field will act on density gradients in the fluid through which the sound propagates. Comparing again f_{ac} to the momentum flux in the conservation of momentum (eq. 2.8), we can address how the PAF induces motion in a fluid with both large density gradients and a high amplitude acoustic field. The change in momentum of a fluid at some point will be

$$\frac{\partial}{\partial t}(\rho v) = f_{ac} \tag{2.89}$$

How the PAF may induce motion in a fluid can be observed by considering the vorticity it induces. By taking the curl of equation 2.89, only the terms outside of the gradient in equation 2.88 won't be zero and so the vorticity induced is

$$\frac{\partial}{\partial t}\nabla \times (\rho v) = \frac{1}{2}\nabla \rho \times \nabla \langle v_1^2 \rangle_t. \tag{2.90}$$

If this equation is considered, for example in the case of the bromine gas in Figure 2.4 where the density increases toward the yellow gas in a direction perpendicular to the standing wave sitting above it. This vorticity equation predicts that the dense bromine gas will be accelerated upward into the standing wave near the velocity antinodes. The vorticity generation described in this equation is also central to the formation of the plumes shown in the title Figure 0.1.

34

CHAPTER 3

Necessary Plasma Physics

When a gas contains charged species it is said to be a plasma. Plasmas are generally electrically conducting, luminous, and can absorb or reflect light. Generally, they are at elevated temperature, but can exist under many circumstances. The motion of the charged species due to the Lorentz force dictates how an electric field such as light or a radiofrequency signal will interact with the plasma whether by scattering, reflecting or being absorbed. The parameters which dictate these interactions are the neutral gas density, N, the free electron density N_e, the electron and neutral particle temperature, T_e and T, and the electron neutral collision time τ. Several examples of plasmas are shown in Figure 3.1. In this section, we introduce enough plasma physics to explain how microwave energy is absorbed by a conducting plasma, so that they can then be used to generate sound.

3.1 Saha's Equation

For a gas to be a plasma it must have an appreciable number of free electrons. When the gas is in thermal equilibrium, $T_e = T$, the fraction of gas which is ionized, $x = N_e/N$ is determined by the temperature, T, number density, N, and ionization energy of the gas, χ, via the Saha ionization equation,

$$\frac{x^2}{1-x} = \frac{2g}{N\lambda^3} \exp\left(-\frac{\chi}{k_B T}\right). \tag{3.1}$$

In this equation, $\lambda = h/\sqrt{2\pi m_e k_B T}$ is the thermal de Broglie wavelength, and g is a statistical weight [116]. At temperatures where the thermal energy becomes comparable to the ionization energy of a particular species, (e.g. $k_B T \approx .1\chi$), a gas will begin to ionize
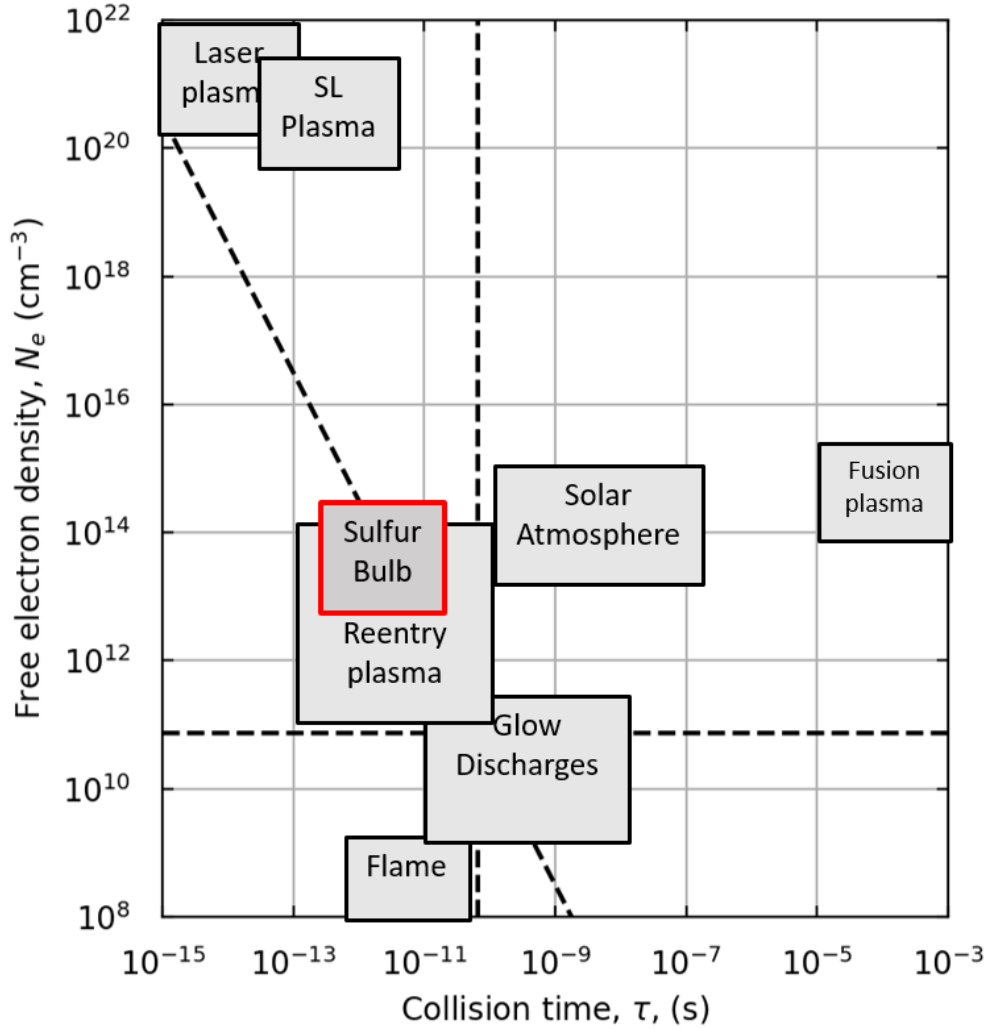
Figure 3.1: A comparison of various plasmas which compares their free electron density and electron-neutral or electron-ion collision rate. The horizontal dashed line indicates when the plasma frequency, ω_p is equal to the microwave frequency, $\omega = 2.45\,\mathrm{GHz}$, the vertical line indicates, $\omega\tau = 1$. The diagonal dashed line depicts when $\omega_p\tau = 1$. Data sourced from [88, 93, 86, 34]

appreciably.

3.2 Plasma Dispersion

A simple model of a plasma can be found in [42]. This model is based on the interaction that an EM plane wave of the form

$$E(r,t) = E_0 e^{i(k \cdot r - \omega t)}, \tag{3.2}$$

will have on the free electrons of a plasma as it passes through.

The dispersion of that EM field through a plasma is generally dictated by the frequency of the EM field, ω and the plasma frequency,

$$\omega_p = \sqrt{\frac{N_e e^2}{\epsilon_0 m_e}}, \tag{3.3}$$

which depends on the concentration of free charges and properties of the electron such as its charge e and mass m_e. In a collisionless plasma, the plasma frequency determines whether an oscillating EM field will be reflected or transmitted through a plasma. As ω_p becomes larger than ω, the plasma begins reflecting the wave.

3.3 Collisional Plasma and Drude's Model

If the neutral density is sufficiently high, the electron-neutral collision time, τ, plays an important role in determining how a plasma will interact with light. The collision time

$$\tau = \frac{\lambda_{mfp}}{v_{th}}, \tag{3.4}$$

is determined by the thermal speed of the electrons,

$$v_{th} = \sqrt{\frac{8k_B T}{m\pi}}, \tag{3.5}$$

and the mean free path of the electrons,

$$\lambda_{mfp} = \frac{1}{Na}, \tag{3.6}$$

which depends on the collision cross section, a, and the density of colliding species, N [95]. In this thesis we assume the most important collision is between electrons and the majority neutral species, which is S_2. For comparison to an atomic gas, the electron, neutral cross section for S_2 is approximately 100 times larger than that for argon at the typical temperatures in the plasma we are studying, and so the collision time is around 100 times shorter. The collision time also influences the time it takes for the charged species to come into thermal equilibrium with the neutral gas. If a temperature disparity between species such as between electrons and the neutral particles the time it takes for the two to reach thermal equilibrium is approximately the product of the ratio of masses and the collision time. The electron-neutral thermalization time, τ_{th} would be

$$\tau_{th} \approx \frac{m_A}{m_e}\tau, \tag{3.7}$$

thus, for an Argon plasma to thermalize a temperature difference between the electrons and neutral species takes approximately 73,000 collision times, and a molecular sulfur plasma would take 120,000. Note however, despite the increased mass, the temperature equilibration time in S_2 is much faster.

The wave number of an RF wave through such a plasma, will satisfy

$$k_p^2 = \frac{\omega^2}{c^2} - \frac{\omega_p^2}{c^2}\left(\frac{\omega^2\tau^2}{1+\omega^2\tau^2}\right) + i\frac{\omega_p^2}{c^2}\left(\frac{\omega\tau}{1+\omega^2\tau^2}\right). \tag{3.8}$$

For an RF wave propagating through a plasma comparable to the sulfur plasma such as seen in Figure 0.1, which has a plasma frequency of $\frac{\omega_p}{2\pi} \approx 100\,\text{GHz}$, and a collision time of $\tau = 1$ ps, the real and imaginary parts of k_p will have the form shown in Figure 3.2. For an EM wave incident on the plasma of the form shown in equation 3.2, the imaginary part of the wave number, k_p, will determine the penetration depth into the plasma.
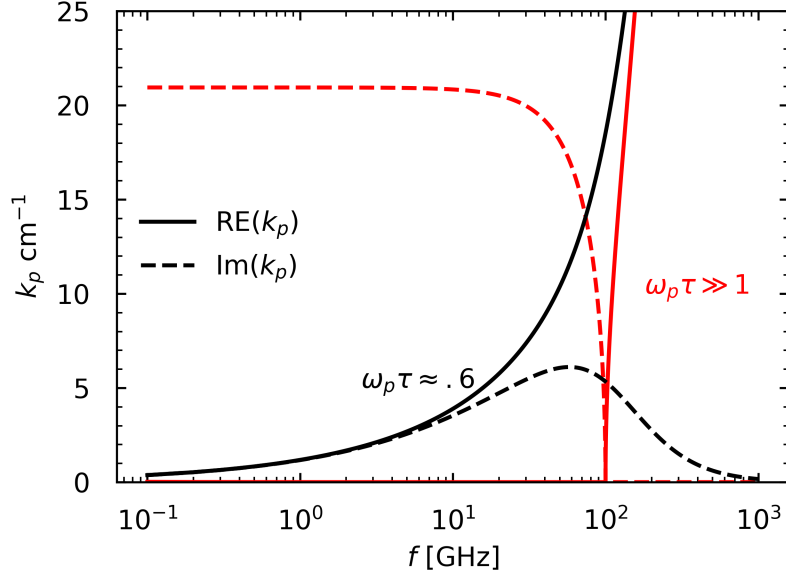
Figure 3.2: Plotted here in black are the real and imaginary parts of the wave number (equation 3.8) of an electromagnetic wave of the form shown in equation 3.2 through a plasma with plasma frequency of $100\,\mathrm{GHz}$. The high electron neutral collision rate for the sulfur bulb plasma and similar systems allows the field to penetrate deeper into the plasma than would be expected if only the plasma frequency were considered. The wave number for a plasma with very large collision time is shown in red for comparison. Both wave numbers converge to that of free space when $\omega > \omega_p$.

The complex dielectric constant of a collisional plasma which has the wave number of equation 3.8 is

$$\epsilon_r\left(\omega\right) = \left(1 - \frac{\omega_p^2\tau^2}{\omega^2\tau^2 + 1}\right) - i\frac{1}{\omega\tau}\frac{\omega_p^2\tau^2}{\omega^2\tau^2 + 1}. \tag{3.9}$$

As with the wave number, the complex dielectric constant depends on the plasma frequency and collision frequency of a plasma. How this can be used to learn about the plasma will be discussed in section 7.1.

When the electron collision frequency, $\nu = 1/\tau$, in a plasma is large compared to the frequency of an RF wave with frequency ω incident on the plasma,

$$\omega < \nu, \tag{3.10}$$

the conductivity, σ, of the plasma is well described by the Drude formula of conductivity

$$\sigma = \frac{N_e e^2}{m_e}\tau = \epsilon_0\tau\omega_p^2, \tag{3.11}$$

and the power absorbed will be determined by the Joule heating equation as described in the next section.

3.4 Microwave Induced Plasmas

With the advent of high power continuous microwave sources it became possible to sustain persistent discharges in high pressure gases. Plasmas generated in this way are known as microwave induced plasmas. A schematic of the basic elements of such a system in a flowing gas configuration is shown in Figure 3.3, an example device where the plasma is contained in a sealed vessel is shown in Figure 3.4. Typical microwave plasma generators will use $1\,\mathrm{kW}$ to $2\,\mathrm{kW}$ of microwave power in order to sustain the plasma, but devices ranging from $100\,\mathrm{W}$ [31] to more than $20\,\mathrm{kW}$ [49] have also been implemented. If the dielectric envelope contains air, nitrogen, or some other molecular gas the typical temperature will range from $4000\,\mathrm{K}$ to $5000\,\mathrm{K}$. If a monatomic gas is used, at these pressures, the electron temperature and ion temperature will be separated due to the monatomic gas's much smaller cross section.

Argon, typically would have an electron temperature of $6500\,\text{K}$ to $7000\,\text{K}$ and a neutral species temperature of approximately $4500\,\text{K}$ [86].

Because microwave radiation is used to sustain the plasma, there are no electrodes in contact with the plasma, so the contents can be well controlled. This control along with the elevated temperatures have led microwave plasmas to be commonly used in chromatography [7, 31]. These plasmas also have found many uses in terms of materials manufacture, surface processing, and abatement of environmentally deleterious gases [106]. The plasma studied throughout the majority of this project was initially used as an efficient source of light, and so that particular application will be studied more closely in the following section.

In this work, the microwave plasma is ignited and sustained by the electric field within a cylindrical microwave cavity. In order for the field to be large enough to ionize the gas, the cavity must have a fairly high quality factor. Quality factors of around 15,000 are routinely achieved [59]. Here I follow the discussion from [83] to describe the coupling of microwave power P_{inc} into a microwave plasma. If the system is well matched, the total incident power will absorbed in the plasma or in the cavity's walls,

$$P_{inc} = P_p + P_w. \tag{3.12}$$

The power absorbed in the plasma will be due to Joule heating with a conductivity given by the drude model (eq. 3.11), which for now we assume is uniform over the plasma's volume V_p. If the plasma is situated near the maximum electric field, it will also absorb microwave power, P_p of

$$P_p = \frac{\sigma}{2} \int_{V_p} \left| \vec{E} \right|^2 dV, \tag{3.13}$$

where $\vec{E}$ is the electric field in the cavity.

Any power not absorbed by the plasma is absorbed due to the finite conductivity of the cavity's walls according to

$$P_w = \frac{1}{2\sigma_w \delta_w} \int_S \left| \hat{n} \times \vec{H} \right|^2 da, \tag{3.14}$$

where $\delta_w = \sqrt{2}\omega\mu\sigma_w$ is the penetration depth of the field into the cavity's walls, σ_w is the conductivity of the walls, and $\vec{H}$ is the magnetic field (not to be confused with volumetric

heating from the driven wave equation), $\hat{n}$ is the unit normal vector relative to the surface of the cavity's wall. The power per unit volume absorbed by the plasma in terms of the total incident power can then be written as

$$H_0 = \frac{P_{inc}}{V_p} \frac{P_p}{P_p + P_w} = \frac{P_{inc}}{V_p} \left[1 + \frac{1}{\sigma_w \sigma \delta_w} \frac{\int_S \left| \hat{n} \times \vec{H} \right|^2 da}{\int_{V_p} \left| \vec{E} \right|^2 dV} \right]^{-1} \tag{3.15}$$

This formula can be written in terms of the unloaded microwave cavity's quality factor Q_c, as

$$H_0 = \frac{P_{inc}}{V_p} \left[1 + A \frac{\epsilon_0 \omega V_c}{\sigma Q_c V_p} \right]^{-1}, \tag{3.16}$$

where A is a unitless constant which is determined by the exact positioning of the plasma within the field. If the plasma's presence doesn't change too much the shape of the fields in the cavity, A is approximately the ratio of the energy in the cavity to that in the plasma, but generally it is

$$A = \frac{V_p \int_{V_c} \left| \vec{E_0} \right|^2 dV \int_S \left| \hat{n} \times \vec{H} \right|^2 da}{V_c \int_{V_p} \left| \vec{E} \right|^2 dV \int_S \left| \hat{n} \times \vec{H_0} \right|^2 da}, \tag{3.17}$$

where $\vec{H_0}$ and $\vec{E_0}$ are the fields in the empty cavity.

If the cavity has a reasonably high quality factor, and the conductivity of the plasma is high enough that the majority of the incident microwave power is absorbed the in the plasma, the volumetric heating reduces to

$$H_0 = P_{inc}/V_p, \tag{3.18}$$

which is the form we will use throughout most of this thesis in order to both heat the plasma and to drive sound within it.

3.5 Sulfur Plasma Lamp

The initial design of this plasma acoustic experiment was based on electrodeless sulfur lamps or sulfur plasma lamps, which are an efficient lighting technology invented in the late 1980's
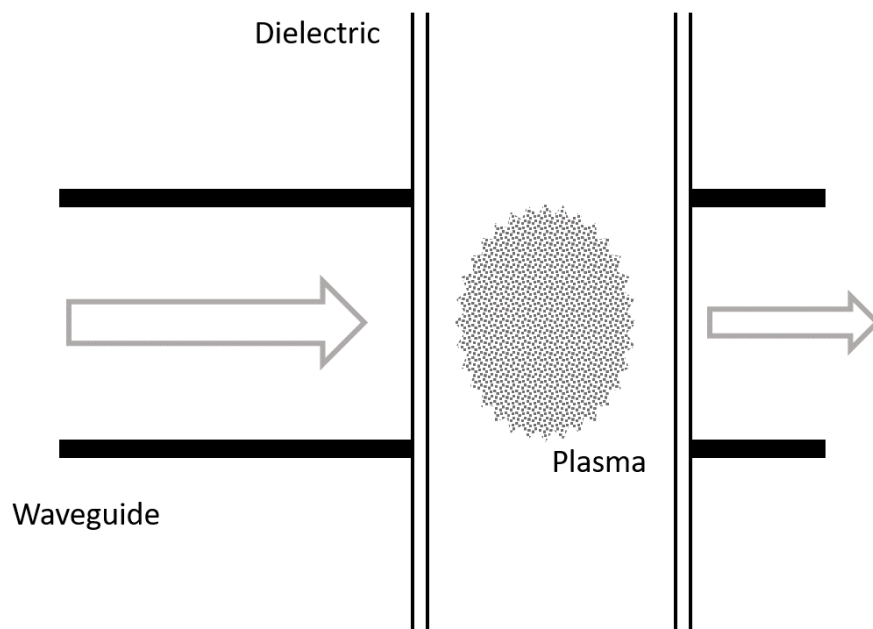
Figure 3.3: A schematic of the basic elements in a typical high pressure microwave plasma system. Microwaves travel through a waveguide and are incident on a plasma filled dielectric container commonly made from a microwave transparent material with a high melting point such as quartz. The dielectric envelope is often situated within a resonant microwave cavity in order to achieve higher electric fields or to increase the efficiency of heating the plasma. The dielectric may either be a tube as shown here which enables gas to be pumped through the plasma region as is the case when the microwave is facilitating a chemical process or chromatography, or sealed and completely within the microwave waveguide or cavity as will be discussed in section 3.5. Schematic is based on a similar image from [86].

that is still used as of 2020 in green houses and on movie sets. An example schematic of a sulfur plasma lamp is shown in Figure 3.4. These lights use a magnetron similar to those found in a microwave oven to generate microwaves with sufficient intensity to turn a material which is solid at room temperature into a luminous plasma by heating it to a few thousand Kelvin. The use of a material which is solid at room temperature enables both the initiation of a plasma with a lower peak electric field and an ultimate plasma in a neutral density greater than 10^{19} particles per cubic centimeter, which leads to the very short collision times mentioned above [110]. At room temperature, the solid material sits beneath approximately 10 torr of argon. Several of the basic thermodynamic properties of the bulb and its contents are listed in Table 10.2.

The sphere is mounted on an axially symmetric stem in order to rotate it. Rotation is necessary to keep the quartz from melting at localized hotspots, but also to ensure the temperature distribution throughout the bulb is at least axially symmetric, and to minimize flickering in the light produced. For a bulb with the dimensions in Table 10.2, the centrifugation balances buoyancy,

$$\frac{\frac{1}{2}\rho\Omega^2 R^2}{\rho g R} > 1, \tag{3.19}$$

when the rotation rate exceeds 5 Hz, but the bulb is typically rotated between 20 Hz to 50 Hz. The mechanical rotation of the bulb is a source of audible noise and is a common point of failure, so other groups had worked to remove that component by instead using a circularly polarized microwave field to mix the plasma [51].

Sulfur is chosen as the working material because it is efficient at converting microwave power into visible light which imitates the visible portion of the solar spectrum without producing much UV or IR [105]. An alternative material used is InBr [51]. These materials work well for lighting because at high temperatures and pressures nearly all of the light generated is due to molecular transitions [45]. The direct generation of visible light obviates the need for phosphors to down convert higher energy photons as is the case in mercury based bulbs.

In terms of practical design, the light emission increases fairly linearly with input power.

44
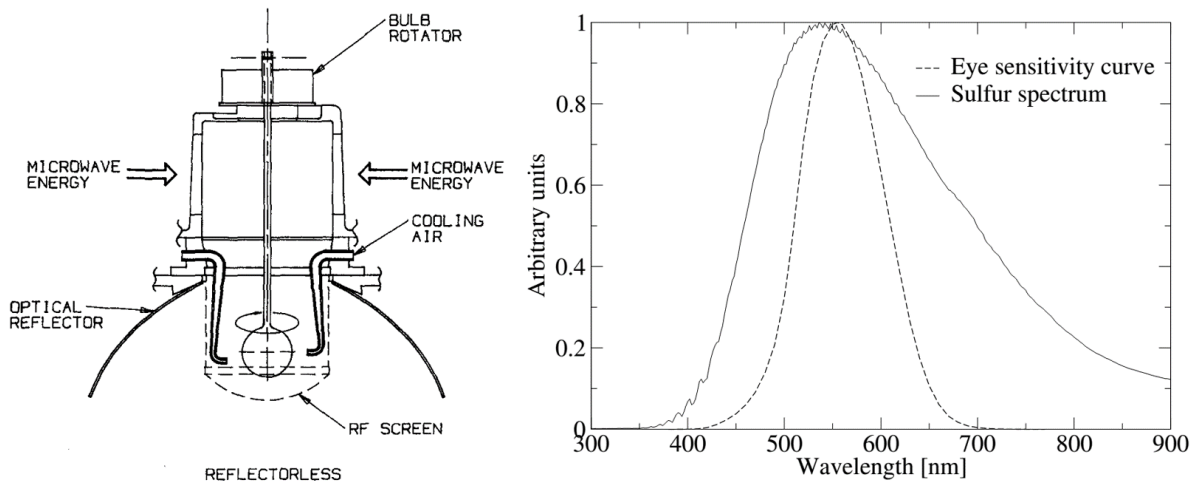
Figure 3.4: Schematic and spectrum of the initial sulfur plasma lamp. One early example was used in the Smithsonian's National Air and Space Museum where the nearly 440000 lumens were distributed through the museum via 100 m of light pipes. Schematic taken from [105], and spectrum of sulfur lamp compared to Eye sensitivity curve is from [47].

In terms of physical modeling, because the emission is due to the molecular transitions, the intensity of the light output is due to each transition is approximately described by a Boltzmann factor with the energy between the excited and ground state in the exponent.

$$I = I_0 \operatorname{Exp}\left(-\frac{E_{exc}}{k_B T}\right), \tag{3.20}$$

where E_{exc} is the energy level of an excited state.

Because of the immense technological promise that sulfur plasma lamps held, they were subject to close study. Attempts at self-consistent models of the light output, electrical conductivity, and microwave absorption were conducted by Johnston et al. in [47]. One particular insight in that body of work which is unique to a molecular plasma is how quickly the electron temperature equilibrates to the rest of the gas. Johnston attributes that to large inelastic losses. These are increased both by the large number of rovibrational states, and the high pressure of the gas assuring that these states are populated. The small temperature

45
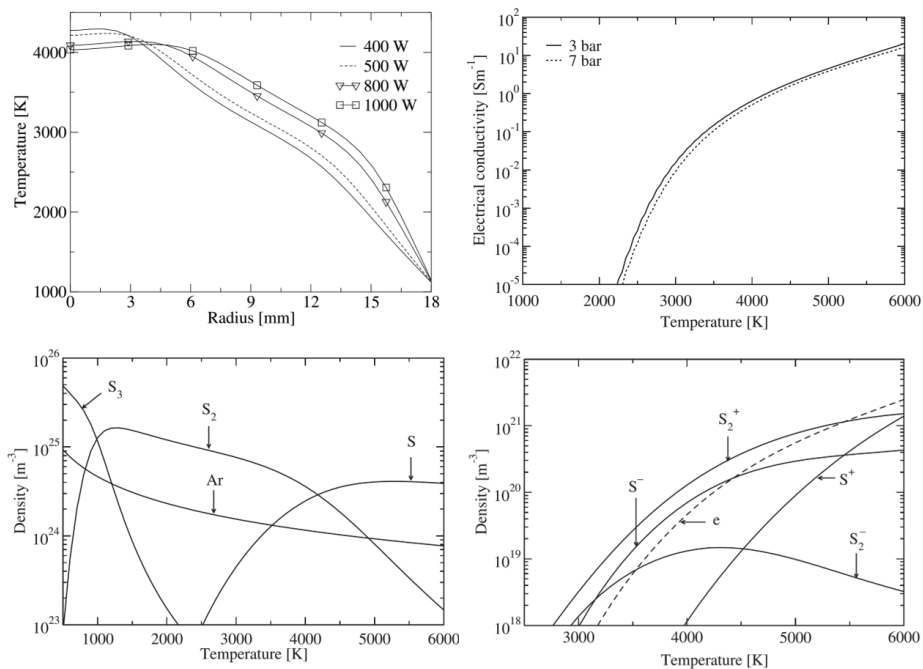
Figure 3.5: Several simulations have been done on the thermodynamics of sulfur plasma lamps. A) A characteristic temperature distribution of the gas in a sulfur lamp. The bulb in this case had a radius of 18 mm. B) The electrical conductivity as a function of temperature. C) The dominant neutral species within an equilibrium sulfur plasma for the parameters of these experiments is diatomic sulfur. D) The free electron density in the equilibrium plasma approaches $1 \times 10^{14}\,\mathrm{cm}^{-3}$. Figures taken from [45, 46].

difference between electrons and heavy particles was established experimentally to be on the order of 3 K by interrupting the power to the lamp [47, 46].

The molecular simulations and experiments conducted by Johnston et al. provide estimates for the steady-state temperature and species concentrations of the plasma contained within a sulfur plasma lamp. In order to reference throughout the thesis, I copy some key figures from his thesis into Figure 3.5.

CHAPTER 4

Plasma Acoustics

Consider walking across a nylon carpet on a dry winter day. As you reach for a doorknob you see, feel, and hear a static shock between your finger and the doorknob. The charge imbalance between your body and the door became so great as you walked across the carpet that as your hand approached the metal an electric field sufficient to cause dielectric breakdown of the air was established (approximately $30\,\mathrm{kV\,cm^{-1}}$). In order for the electric charge to reach equilibrium a current flows through that dielectric breakdown which can routinely heat the air to temperatures exceeding $1000\,\mathrm{K}$ [80]. The cracking sound that you hear is due to that current rapidly heating a thin channel of ionized air.

The sound produced in the previous example may seem modern and quaint, but the same mechanism writ large is at play when lightning strikes generate earth rattling thunder. A lightning strike heats air to around $3 \times 10^4\,\mathrm{K}$ within a microsecond and in so doing generates a strong shock wave which converts approximately 1% of its total energy into a sound wave [23, 108].

Both of these examples involve an impulsive discharge that ends as soon as the initial charge imbalance has been depleted, so the sound they generate at first seems somehow different from what is generated for example by a speaker. If the power source that generated the electrodynamic heating were instead an oscillating current source, however, a persistent tone can be generated. Indeed, many researchers have harnessed a power source to generate sound using a plasma and some have gone so far as to produce commercial speakers. In this chapter, I will review the many ways that sound has been generated via the heating of gas by electric fields whether DC, AC, RF, or via focused laser light.

4.1 Some Previous Experiments in Plasma Acoustics

As discussed in section 2.2.1, a time varying heat source in a gas generates a sound. If the thermal mass of the heat source is small enough and the source of heat intense enough such as that of a flame or plasma, its temperature can be varied rapidly enough to generate sound.

Some of the earliest controlled experiments of using a plasma as a sound source were those of William Duddell who configured a circuit to modulate a direct current through an arc channel between two electrodes open to the atmosphere [20]. A schematic of this early plasma speaker which came to be known as a singing-arc is shown in Figure 4.1. Duddell used a direct current of 10 A to maintain a 5 mm arc and by varying the current by as little as 1 mA up to 100 mA was able to produce audible sound from a few hundred Hertz to the edge of the audible range. By using a keyboard to adjust a capacitance in parallel with the arc, and therefore resonance frequency of the the circuit, Duddell used such a singing-arc device to play songs such as "God Save the Queen" [48].

The generation of sound from such minute perturbations in the current through an arc suggested applications useful for emerging electronic and telephone technology. This led to careful characterization of the frequency established by an arc in a circuit which was determined by its dimensions, the plasma properties, and the connecting circuit [77].The sound produced by a time-varying current through an arc discharge characterized by a persistent current of a few amps and voltages of 10's of Volts is one method of causing pressure oscillations within a gas.

Another series of devices which generated sound by heating an ionized gas were based on a corona discharge which is characterized by a high electric field between two electrodes but insufficient to cause complete dielectric breakdown. The first successful devices sustained a plasma with an RF source with a carrier frequency up to 10 MHz. A prototype device was invented by Siegfried Klein [54] and developed into a commercial product known as an Ionovac speaker [70]. In order to develop a high amplitude, broadband, and high frequency noise source in order to study rodents' response to sound, Ackerman et al. adapted Klein's

design and achieved SPL's of 132 dB re 20 µPa using 3 kW of mains power [1].

A second type of corona-type plasma acoustic drive uses a high voltage, low current corona discharge between appropriately configured electrodes to induce a time-varying corona-wind from one electrode to the other. The earliest such design used a triode configuration where the grid voltage was modulated to control the velocity of the wind [103]. A later design used an array of anodes with 35 kV potential difference and around 1 mA of current which was limited by a series resistor [69].

A glow discharge based loudspeaker was designed in order to test the impact of thermal diffusivity on the low frequency behavior of a plasma speaker. This device used around 1 kV and 300 mA to drive a sound field 80 dB re 20 µPa [70]. Such experiments are useful for determining when the sound generation in a plasma speaker changes from an induced velocity to a thermal effect as derived in equation 2.36.

Another series of devices which generate sound in the open atmosphere generated a high voltage by using a Tesla coil providing a high voltage oscillating at 325 kHz with peak voltage of around 5 kV and a current around 30 mA. When driven with around 20 W that device produced an electron density of around $1 \times 10^{13}\,\text{cm}^{-3}$ [100].

That acoustics may enable the manipulation of a plasma was suggested by [98] who observed kinks forming in a DC glow discharge when the drive was modulated at certain frequencies. These kinks were attributed to nonaxial acoustic modes in the discharge lamp [92]. Researchers studying higher pressure high intensity discharge (HID) lamps also observed kinking of the arc plasma [113, 79]. This kinking was attributed to acoustic streaming [2, 19]. In order to improve such lamps, it has been proposed to use an acoustic field to prevent the separation of gaseous components [97] and to stabilize and straighten the arc channel [78].
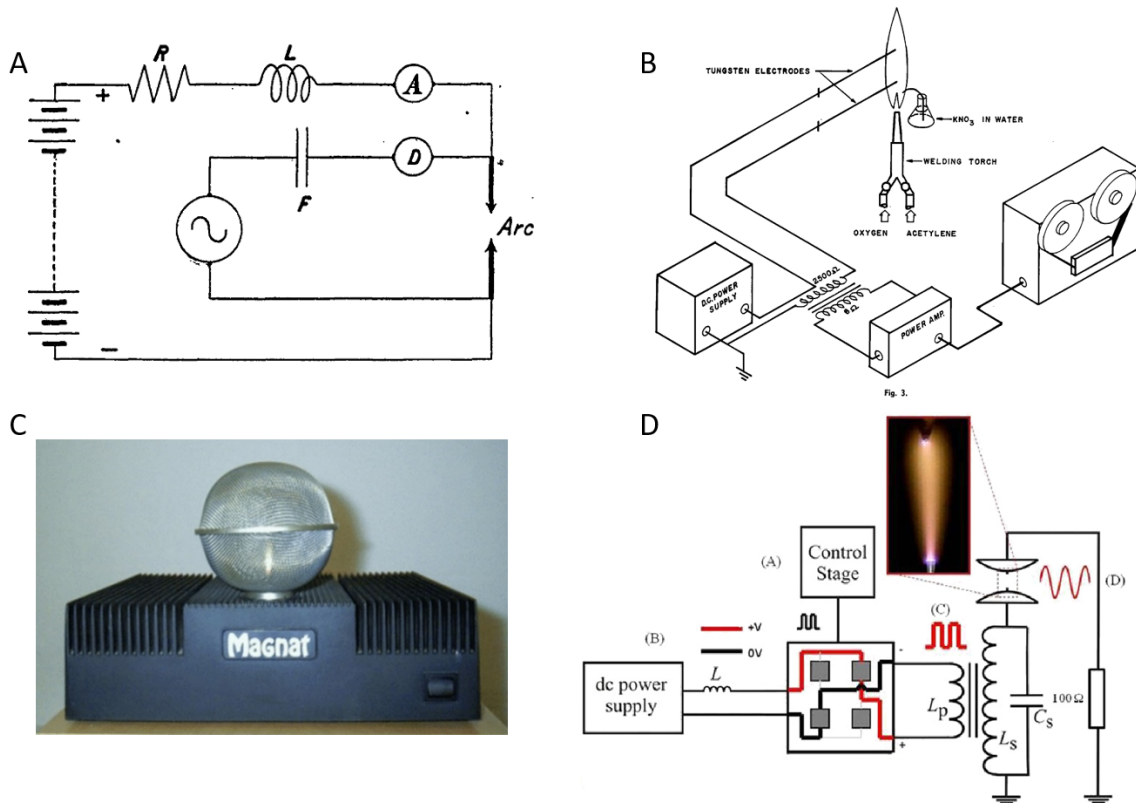
Figure 4.1: Several techniques have been developed to generate sound by varying an electric field in a plasma. A) William Duddell's schematic for a singing arc used $1\,\mathrm{A}$ DC with $100\,\mathrm{mA}$ modulation [20]. B) Several experimenters would run a current through a salt-seeded flame as a means of generating sound [10, 5]. C) The most commercially successful plasma-based speakers used a corona discharge. The example shown is an MP-02 tweeter produced by Magnat [37]. D) More recent devices have used an arc generated by the high voltage of a Tesla coil [100].

CHAPTER 5

Pulsed Magnetron Acoustic Drive

When the acoustic amplitude grows large, the pycnoclinic acoustic force generates a central force with a magnitude of around 1000 times the force due to gravity on earth. In this chapter I will describe how the acoustic amplitude necessary to confine the plasma to the center of the spherical cavity via the pycnoclinic force was first achieved and measured. The second consequence of such high acoustic amplitude was the ejection of convective plumes which are evidence of convection in a central force. In order to explain the convection due to the spherically symmetric pycnoclinic acoustic force I present an attempt to model the temperature fluctuations in the bulb as a whole, and then present evidence that the pycnoclinic force accelerating plumes of hot plasma toward the cavity walls is the mechanism.

5.1 Experimental Apparatus

In order to drive acoustic oscillations within the sulfur plasma, a lamp similar to those discussed in 3.5 was modified by replacing the high voltage power supply which powers the magnetron with a pulsed supply. A schematic and photograph of the microwave circuit for first plasma acoustic drive built at UCLA is shown in Figure 5.1.

A high-voltage circuit designed by Courret et al. and purchased from the Institut d'Energie et Systemese Electriques enables a magnetron to be efficiently pulsed from 5-100 kHz with duty cycles of 5% to 90% [26]. The power supply holds the magnetron at a voltage just beneath the conduction threshold and then pulses an additional few hundred volts to trigger microwave power. An example modulation pattern that they used to excite acoustic resonances in the sulfur plasma is shown in Figure 5.2. The pulse of microwave power is
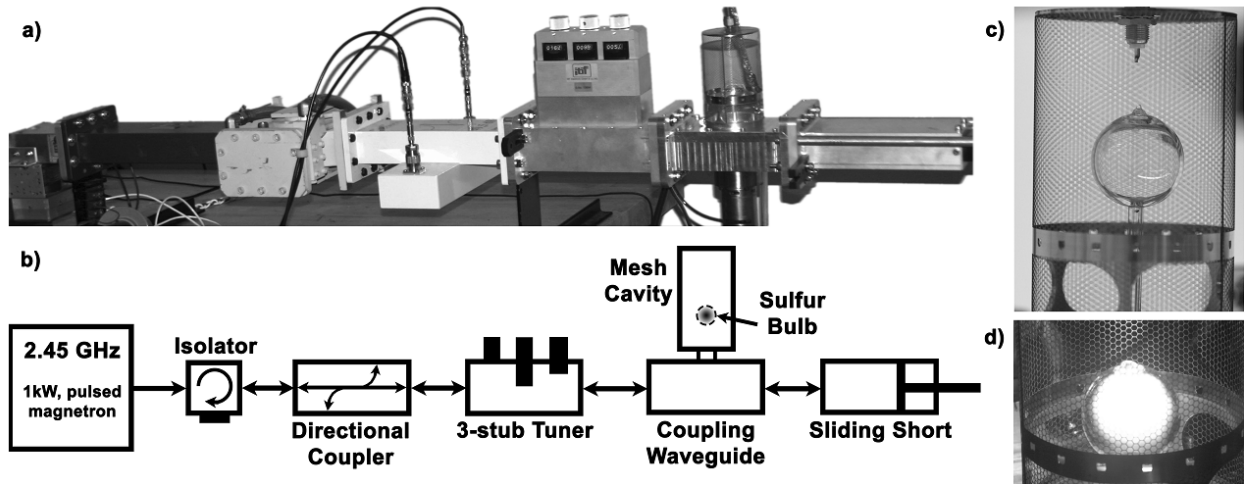
Figure 5.1: A) photograph of the experimental apparatus used to generate sound fields in a microwave plasma. Microwaves are generated by a magnetron like those found in a microwave oven and modified according to [15] B) Schematic of the apparatus. C) Photo of spherical bulb within microwave cavity. D) Photo of plasma filled spherical bulb. Figure adapted from [59]

then absorbed over the volume of the plasma. If the plasma is sufficiently conducting that all of the power is absorbed, but has a skin depth large enough that the field throughout the volume of the plasma is nearly constant, the power shown in Figure 5.2 divided by the volume of the plasma would provide an approximation of the heating per unit volume, H, for equation 2.36.

As shown in Figure 5.1, the magnetron is connected to a series of WR340 waveguides, an isolator, a directional coupler, and a 3-stub tuner in order to deliver power to a cylindrical cavity with a 75 mm diameter and 125 mm height. Beyond the cylindrical cavity is a sliding short which along with the stub tuner enable tuning the microwave resonance frequency and impedance matching. The bulb inside the microwave cavity is a 3 cm diameter quartz sphere, filled with around 30 mg of sulfur sitting beneath around 10 Torr of argon. It is necessary to use an isolator to protect the magnetron from high power reflections because the impedance of the cavity changes dramatically when the contents of the bulb change from nonconducting, solid sulfur and inert argon to a conducting load when the plasma turns on

and the conductivity increases to as much as $1\,\Omega^{-1}\,\mathrm{m}^{-1}$. Furthermore, fluctuations in the plasma cause spurious reflections and can lead to rapid extinction of the plasma such an extinction causes a rapid increase in reflected microwave power.

The impedance tuner and sliding short are necessary to maximize the coupling of the microwave power into the plasma. Although it is necessary to achieve a high field $5\,\mathrm{kV\,cm}^{-1}$ in order to exceed the RF-breakdown threshold of low pressure argon so that the plasma can be ignited, we found that a very high quality factor cylindrical mode was not necessarily the best for igniting and maintaining this plasma. Very high quality factor cavity modes were difficult to use because the magnetron's emission frequency could shift by $10\,\mathrm{MHz}$ due to operating conditions such as changing the pulse frequency or duty cycle [59].

The change in the conductivity of the contents of the microwave cavity as the sulfur goes from an insulating solid to an ionized gas necessitate compromising at which point the coupling should be optimized, and so the cavity is tuned in order to maximize microwave absorption once all of the sulfur is vaporized and the bulb produces the maximum amount of light. This is done by observing the power reflected both at the directional coupler or at a monitoring port on the isolator.

Once the plasma is ignited and the sulfur completely vaporized, if the bulb is not rotating, the plasma floats to the top and often flickers and goes out. It was observed that rotating the bulb at a rate between $10\,\mathrm{Hz}$ and $60\,\mathrm{Hz}$ stabilized it consistent with reports in the literature and the most common design of sulfur plasma lamps [105]. Such rotation also reduces any rotational asymmetry and pulls the plasma toward the axis of rotation. While spinning, the plasma appears stable and apparently fills the bulb. This calm state is observed in Figure 5.3.
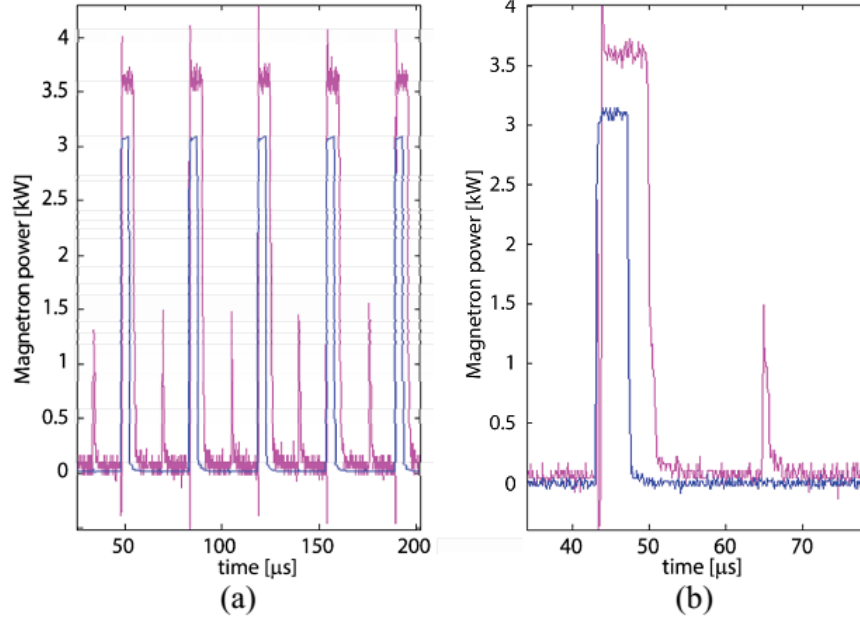
Figure 5.2: Power modulation produced by pulsing a 1 kW average power rated magnetron. Note that the peak power is essentially the average power divided by the duty cycle. Figure adapted from [26]

.

5.2   Initial Observation of High Amplitude Sound and Pycnoclinic Plasma confinement

Using the pulsed magnetron plasma acoustic drive shown in Figure 5.1, several measurements of nonlinear acoustics in a molecular sulfur plasma were made. Due to the design of the high voltage circuit, the magnetron source was always pulsed, but if pulsed at certain frequencies the plasma would flicker dramatically, confine to the center, or extinguish completely. A photo of the apparent acoustic confinement is shown in Figure 5.3.

The largest resonance was observed at a frequency around 30 kHz. A bulb with a radius of 16 mm according to the resonance condition calculated in equation 2.42, for the lowest spherically symmetric mode with $\xi_{02} \approx 4.49$, has a wave number of 280 rad m^{-1}. With this

frequency and wave number the speed of sound in the gas is calculated to be

$$c_s = \frac{2\pi f R}{\xi'_{0,2}} = \frac{2\pi \, (30\,\text{kHz}) \, (0.016\,\text{m})}{4.49} \approx 700\,\text{m s}^{-1}. \tag{5.1}$$

If the sulfur in the bulb is almost all diatomic sulfur, which has molecular weight, $1.1 \times 10^{-25}\,\text{kg}$, the average temperature can be estimated using equation 2.20 to be 2800 K, which is consistent with that suggested by [46]. This estimate is based on a single resonance and assumes the temperature throughout the bulb is uniform - a measurement which will be improved upon in a later section.

The initial probes used to monitor the acoustic field in the sulfur plasma were a microwave diode positioned at the directional coupler monitoring the incident microwave power and a photodiode monitoring the light. Example measurements are shown in Figure 5.3. The microwave trace indicates the power use to heat the plasma. The photodiode trace serves as a probe of the size of the plasma, its average temperature, and the acoustic amplitude. These properties can be discerned by assuming that the light output again depends on temperature based on equation 3.20.

When the acoustic amplitude is small and the microwave pulse is on, the light output increases in a sawtooth pattern as shown in the lower right trace of Figure 5.3. This is due to the plasma absorbing the approximately 20 mJ of energy in each pulse. Based on the thermal mass of sulfur in the bulb such as calculated from Table 10.2, the temperature will increase by approximately 1 K. When the pulse turns off, the light decays linearly, but at a different rate resulting in the sawtooth waveform. When the acoustic amplitude is large as in the lower left trace, however, the diode signal is sinusoidal because the change in temperature due to the sound wave's pressure fluctuation is larger than the temperature oscillation due to the microwave power from a single pulse. Using that premise and equation 2.21, we estimate the Mach number must be greater than

$$\frac{p_1}{p_0} = \frac{\gamma}{\gamma - 1}\frac{T_1}{T_0} > \frac{1.4}{.4}\frac{1}{2800} = .001 \tag{5.2}$$

for the light emission to be dominated by acoustic oscillation in the plasma.
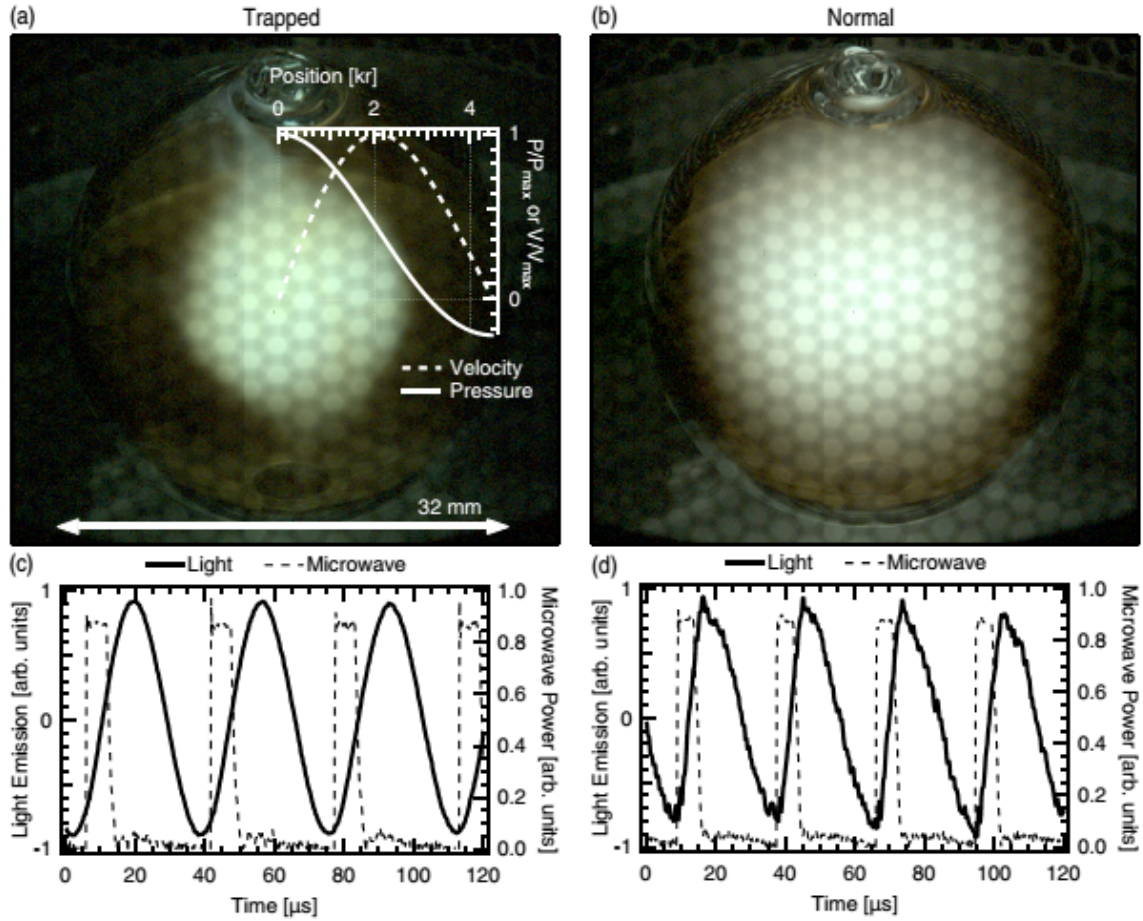
Figure 5.3: A) The pycnoclinic acoustic force due to the lowest spherically symmetric Bessel function confines the sulfur plasma to a spherical region at the center of the quartz cavity. The luminuous edge of the plasma is located near the velocity antinode of the resonant standing wave, which is graphed in the overlay. B) The plasma in the absence of a high amplitude acoustic field apparently fills the bulb. C) The microwave pulse as measured by a microwave diode and a high-passed trace of the visible light photodiode are compared. In the presence of a high amplitude acoustic field the photodiode trace appears sinusoidal because the variation in the light output is dominated by the oscillating pressure of the acoustic field. D) In the absence of the acoustic field, the light output increases linearly while the microwave is on and then cools linearly when the microwave turns off within modulation period. The oscillation amplitude of the photodiode in the confined case is between 20-60 times larger than in the unconfined case. Figure taken from [58].

5.3 Light Based Measurements of Acoustic Effects

The photodiode measurement shown in Figure 5.3 is high pass filtered and scaled on the time axis in order to highlight the effect due to the acoustic oscillations. The high amplitude acoustic field, however, also coincides with slower dynamics that occur over hundreds of acoustic oscillations. For example, the plasma being smaller while trapped as in Figure 5.3 indicates that the total light output is reduced when the plasma is acoustically confined. The change in light output between these two states is shown in Figure 5.4.

Figure 5.4 demonstrates a few aspects of not only the longer timescale effects the high amplitude acoustic field has on the plasma's light output, but also the acoustic trapping process. In that photodiode trace, the plasma sits in its quiescent, bulb filling state for the first $500\,\mathrm{ms}$. During this time, the photodiode signal is a stable value at approximately $2.8\,\mathrm{V}$, the high-passed component of the photodiode is relatively small amplitude and if examined closely is like that of the sawtooth wave shown in Figure 5.3. In the spectrogram, the forcing function is apparent as a dark line at around $33\,\mathrm{kHz}$, which as mentioned before is always pulsed in this device, but in the early times of Figure 5.4 is far from the resonance frequency and so has a low amplitude.

It has been observed that in order to generate sufficient amplitude in the spherically symmetric breathing mode to trap the plasma to the center of the cavity, it is necessary to sweep the driving function's frequency. Such a sweep is shown in Figure 5.4. Just before $500\,\mathrm{ms}$, the forcing function's frequency was swept downward at a rate of around $3.3\,\mathrm{kHz\,s^{-1}}$. As the forcing function's frequency approached the resonance frequency of the cavity, the acoustic amplitude increased as observed by the increasing amplitude in the photodiode. At around 550 ms, the high-passed photodiode amplitude begins to grow larger and more quickly and with intermittent spikes upward approximately every $30\,\mathrm{ms}$. The fluctuations in light output due to the sound field grew so large to be nearly 3% of the total light output when the plasma was quiescent. The largest spikes on the acoustic trace coincide with large drops in the total light output of the plasma as seen in the top trace and a drop in the frequency measured in the spectrogram. These two behaviors suggest that a high amplitude

57
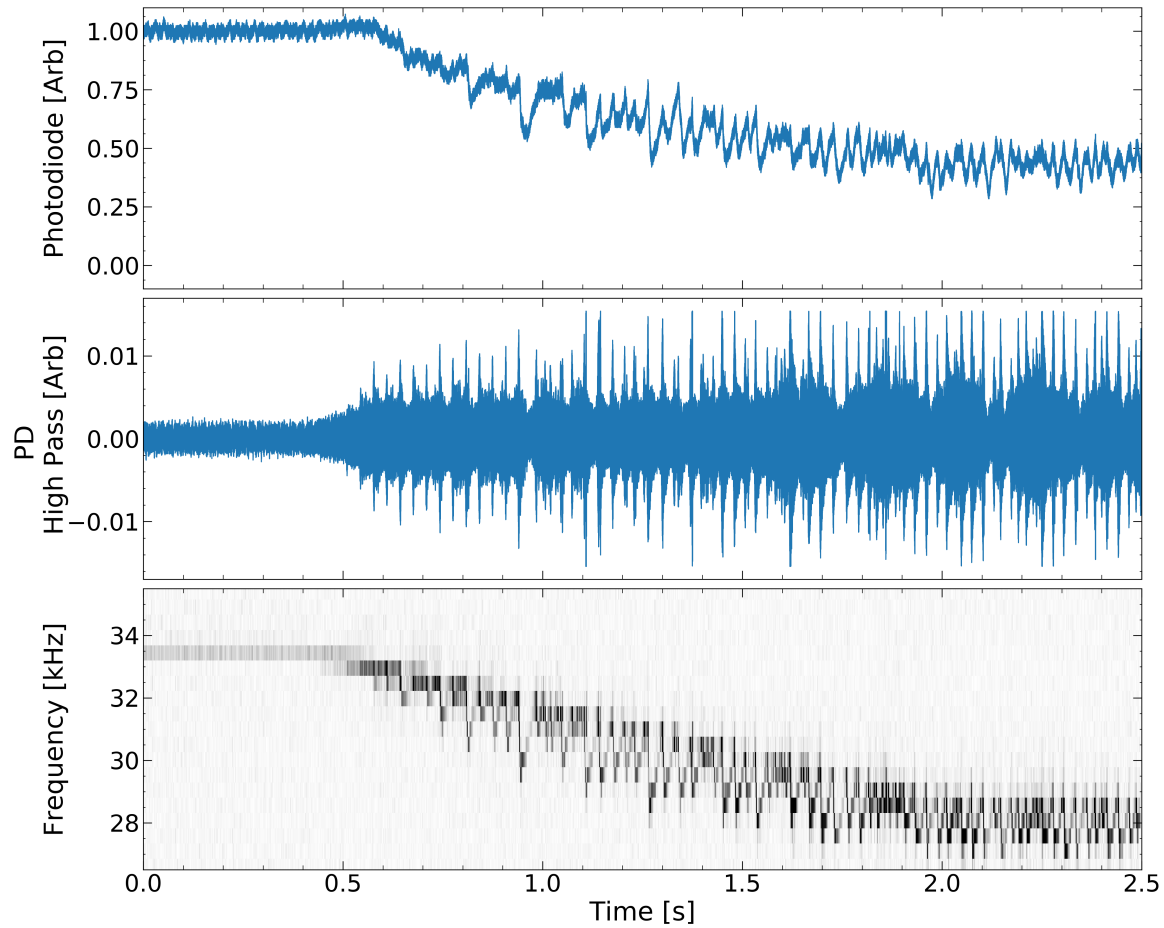
Figure 5.4: These traces demonstrate how the light output of the plasma changes as the driving frequency is swept until it matches the acoustic resonance. The drive frequency starts at around 33 kHz and the sweep begins at around 0.5 s. A) shows the total light output of the plasma as measured by a photodiode. The emission from the confined state is around 1/2 that of the quiescent state. B) is a high-passed version of A which shows the portion of the emission which oscillates due to the acoustic field. The highest amplitudes achieved are not stable because they cause convection within the bulb. Consequences of this convection can be seen both in the total light output and by examining the spectrogram in frame C) which shows the resonance frequency of the cavity varying over 10's of ms. A similar figure was presented in [82].

acoustic field causes the gas in the bulb to cool which simultaneously causes a large drop in the total light output and resonance frequency of the cavity.

When the frequency sweep stopped at around 2 s in Figure 5.4, the total light output was between 1/3 and 1/2 of what it was during the quiescent state indicating how much the luminous portion of the plasma had shrunk. Though the acoustic driving frequency was held fixed around 28 kHz, the acoustic amplitude and resonance frequency continued to oscillate with a frequency around 30 Hz. This oscillation, which occurred over the course of approximately 500 acoustic oscillations was a type of relaxation oscillation. The decreasing acoustic frequency was caused by a cooling event due to a high amplitude acoustic field, and the increase was due to the microwave source heating the plasma until the resonance frequency coincides again with the drive. This recurring process is shown more closely in Figure 5.5. When the high pass filtered photodiode reaches a high amplitude, the DC component drops by as much as 30% over the course of around 5 ms.

5.4 Relaxation Oscillator Model of Pycnoclinic Convection

The change in both the total emission and the acoustic resonance frequency of the cavity indicates that the high amplitude acoustic field drives convection in the gas within the bulb via the pycnoclinic acoustic force (PAF). The changing resonance frequency shown in Figure 5.5 suggests an amplitude dependence of the resonance frequency which is a property of nonlinear oscillators. The delay in the return to the resonance frequency after the amplitude has decayed preclude using a typical nonlinear oscillator model. In the sulfur lamp, the PAF acts on density gradients in the gas in order to hold the central hot region in place, but it also accelerates hot gas in the outer region of the bulb into thermal contact with the bulb. This increase in thermal contact causes the gas temperature to rapidly drop. We will model this convection process first as a global property of the gas in the bulb and so consider how the average temperature within the bulb changes as a function of time due to the amplitude of the acoustic field.
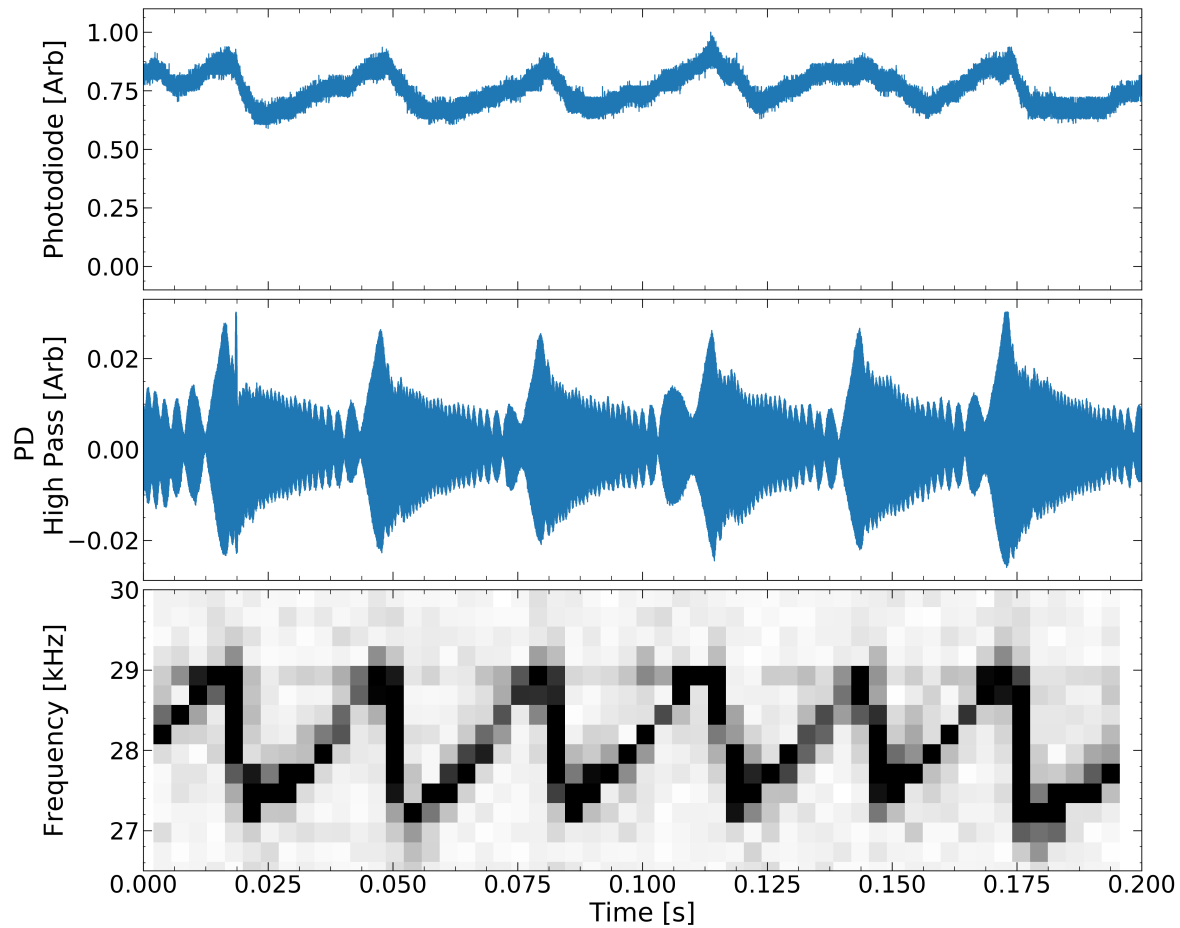
Figure 5.5: When the plasma is in the confined state, its total light output oscillates over the course of around 30 ms. This is shown in the top frame which has been normalized to itself. The second frame which uses the same normalization shows the portion of the light output which oscillates at the acoustic resonance frequency. The amplitude grows and then rapidly decays with an envelope which shows beating at a variable frequency. The beating has a variable frequency due to a change in the acoustic resonance frequency of the cavity shown by the spectrogram in the third frame. The change in the resonance frequency is due to a time varying balance between the microwave absorption which heats and acoustically driven convection which cools the gas. This process causes a relaxation oscillation in the gas which triggers when the resonance matches a fixed drive, in this case around 29 kHz. The frequency resolution in the spectrogram is 244 Hz. A similar figure was presented in [82].

If we consider the acoustic wave equation for the case of a spherically symmetric heating profile as is described in equation 2.48, and keep in mind that the speed of sound and therefore resonance frequency depend on the temperature of the gas within the bulb we can write a coupled set of equations which determine both the fast acoustic and the slow convection dynamics. The first equation, which governs the system on the fast time scales, is the acoustic wave equation for the spherically symmetric mode

$$\frac{\partial^2 \overline{p_1}}{\partial t^2} + 2\alpha \frac{\partial \overline{p_1}}{\partial t} + c(T_{avg})^2 k^2 \overline{p_1} = f \sin(\omega_d t), \tag{5.3}$$

where k is the geometrically determined wave number, and $c(T_{avg})$ is the temperature dependent speed of sound, which evolves according to a time-averaged heating equation of the form

$$D \frac{\partial T_{avg}}{\partial t} = \mu - A T_{avg} - B \left(\frac{\overline{p_1}}{p_0}\right)^2, \tag{5.4}$$

with D as the thermal mass of the gas, μ is the time averaged absorbed microwave power, A is an energy loss which limits the temperature everywhere in the bulb in the absence of acoustics. These losses include the radiation of light, conduction of heat to the container walls, and any other loss that occurs when the bulb is in its quiescent state. The value of D is estimated such that the known power input and the unknown losses balance to a known average temperature - which is again estimated from the resonance frequency of the quiescent plasma. The last term is due to the pycnoclinic acoustic force which induces an acoustically driven convection that causes the gas temperature to change when the sound field grows large in amplitude. The power in the convective term was chosen to be 2, so that it was the smallest power which did not average to zero and it was also based on the pycnoclinic acoustic force depending on the Mach number squared. B is an unknown quantity which determines how strongly an acoustic field might drive convection in a cavity.

Example results of this relaxation model are shown in Figure 5.6. Some aspects of the effects shown in the data, such as variation in resonance frequency have been recreated, but a firmer mechanistic picture of convection is necessary to go further.
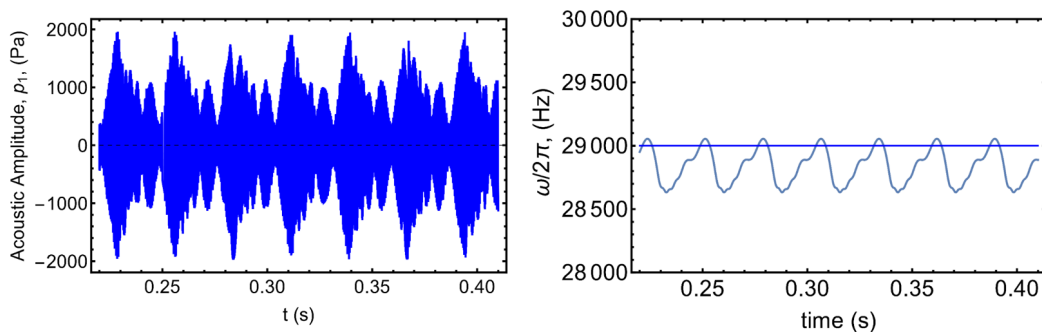
Figure 5.6: Results of a calculation made using equations 5.3 and 5.4. At high amplitude, the acoustic field causes enhanced convection and therefore changes the cavity's resonance frequency. The figure was adapted from [82].

5.5 High Speed Videography for Plasma Acoustics Measurements

High speed videography was used to diagnose many of the observations made with the photodiode, offered a means of measuring the acoustic amplitude, and also revealed acoustically driven convection which became a subject of a sustained research effort. The camera used to make these measurements was a Vision Research Phantom v2512. Using this device at frame rates as high as 1 million frames per second, we were able to make measurements of the total light output of the plasma as a function of the time in addition to a measurement of the plasma's size and shape.

A quantitative measurement of the size of the plasma was made by considering a lineout of the light emission of the plasma - as indicated by the horizontal, dashed redlines across the plasma in Figure 5.7. The result of the lineout is shown as an orange trace in the plots below. The ripple in the lineout is due to the hexagonal pattern in the mesh of the microwave cavity - the wide region of interest was chosen in order to minimize the impact of the ripple. The size of the plasma while in the acoustically confined state is a few millimeter smaller than in the quiescent state. In order to find the size of the plasma as it changes rapidly in time it was necessary to find a function to fit to the lineouts of the light emission which has the radius as a fitting parameter. In order to do this, an initial measurement of the plasma size assumed

the luminous portion of the plasma to be a volume emitter with a nearly constant emission per unit volume. With this assumption, the measured brightness of the plasma as viewed in the photo would be proportional to the depth of the chord into the plasma at that point as indicated in the inset of Figure 5.7. From the perspective of the spherical plasma shown the photo, the chord starts to have a nonzero length at the edges of the plasma and increases to be the diameter at the center of the plasma. Using these assumptions, we estimated that the brightness of the plasma as indicated in a simple 2 dimensional image should follow the relationship

$$I = I_0\sqrt{R(t)^2 - x^2}. \tag{5.5}$$

Where I is the the total light output measured by the camera, I_0 is the brightness per unit length of the chord, R is a fitting parameter which approximates the radius of the plasma, and x is the horizontal position across the width of the plasma. Results of a least squares fit across a lineout is indicated by the blue lines in the plots of Figure 5.7.

When the plasma was in its confined state the luminous boundary was located at a velocity antinode, so the acoustic displacement was maximized. Because the sulfur itself fluoresces, monitoring the motion of that luminous edge enables a direct measurement of the acoustic velocity field without the need for any tracer particle. By using the fitting method described above and equation 5.5, it was possible to make a quantitative measurement of the acoustic amplitude by tracking the radius of the plasma as a function of time for a video taken with a frame rate more than twice the acoustic frame rate. In this case, the framerate was 170,000 fps, so was high enough to resolve the acoustic field. An example trace of the radius as a function of time is shown in figure 5.8.

Based on the oscillation of the plasma's radius, the acoustic displacement exceeds 0.1 mm. At the acoustic frequency of this resonance, which is around 30 kHz, this displacement leads to a velocity amplitude, $v_1 = 2\pi \times 0.1\,\mathrm{mm} \times 30\,\mathrm{kHz} = 20\,\mathrm{m\,s^{-1}}$. This velocity amplitude corresponds to a Mach number of .03 and a sound level of 180 dB re 20 µPa. This Mach number used in equation 2.21 with the approximate guess for the temperature indicates that the temperature during a compression could be as much as much as 50 K hotter than
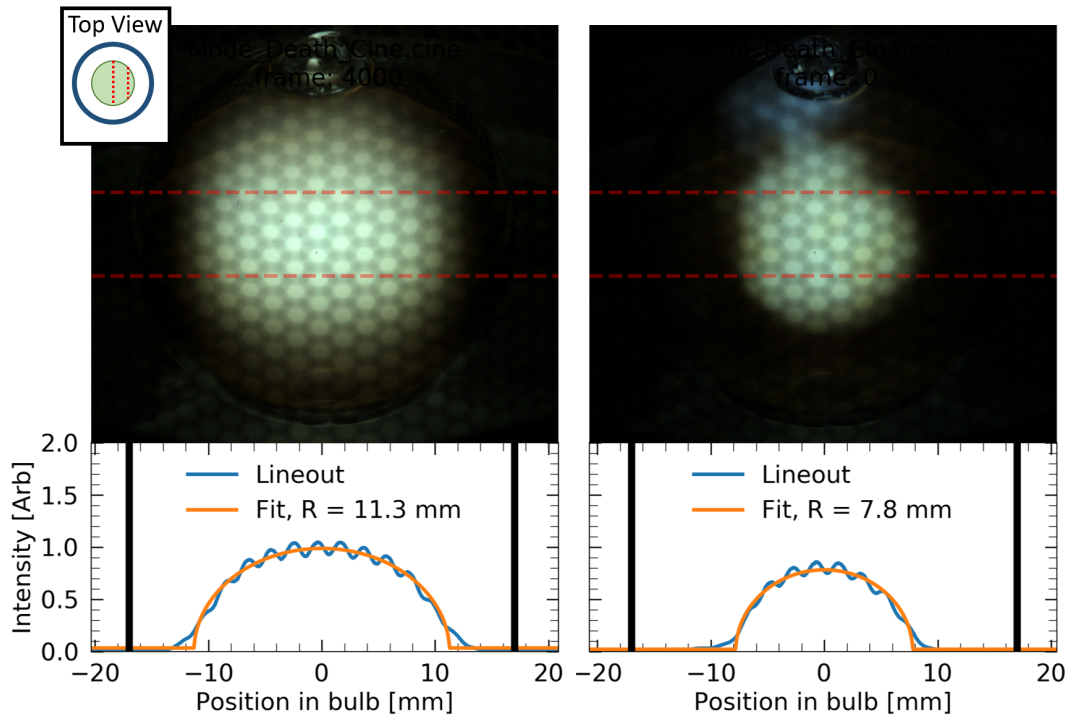
Figure 5.7: By assuming the plasma is a uniform volume emitter it is possible to measure its size by assuming the intensity of a square region in the 2D image is due to contributions of a chord of plasma as shown in the inset. The radius is then measured by using a fit of the form shown in equation 5.5. The measured radius is shown for the plasma while in the quiescent state and also while in the acoustically confined state. The vertical black bars indicate the location of the edges of the quartz sphere.
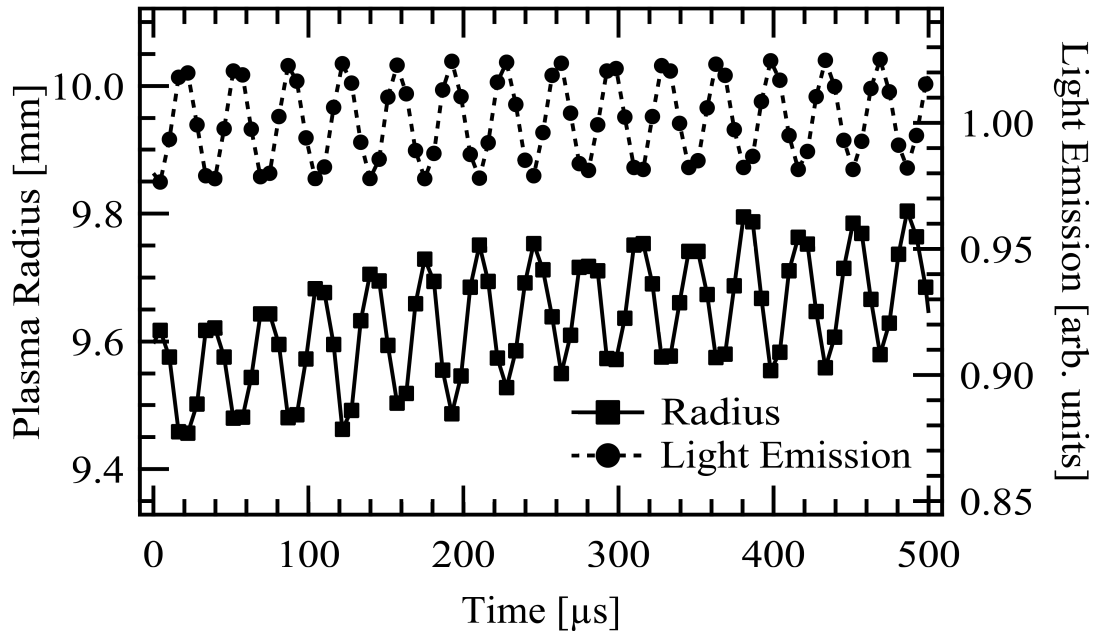
Figure 5.8: By measuring the plasma with a 170 kfps camera it is possible to resolve the acoustic motion and by using the best fit of equation 5.5, we plot the radius, which was a fitting parameter, as a function of time. Tracking the luminous edge of the plasma in this way is a direct measurement of the acoustic displacement, which leads to a measurement of a Mach number around .03. Image from [58].

the rarefaction. This temperature swing across the phase of the acoustic cycle agrees well with the observation in Figure 5.8 that the light emission is greatest when the plasma is the smallest.

With this calibrated measurement of the acoustic amplitude, we can also compare the amplitude of the pycnoclinic acoustic force to that of the competing forces in this system, namely the rotation and gravity. For the plasma to be held in the center and not float upward due to buoyancy, or be deformed due to the rotation, the following series of inequalities must hold

$$\zeta = \frac{\langle v_1^2 \rangle_t \nabla \overline{\rho}}{\overline{\rho} g} \gg \frac{\Omega^2 R}{g} > 1. \tag{5.6}$$

To estimate these values, $\Omega/2\pi = 50\,\text{Hz}$, leading to $\Omega^2 R/g \approx 150$, and with the velocity calculated above, and a variation in density, $\frac{\nabla \overline{\rho}}{\overline{\rho}} \approx 1$, the ratio, ζ exceeds 1000 [58]. These considerations lead us to believe that the pycnoclinic force derived above is likely playing a significant role in the plasma confinement, which causes the luminous region's radius to decrease by around $3\,\text{mm}$ as observed in Figure 5.7.

5.6 Inception of Pycnoclinic Acoustic Convection

The rapid change in the acoustic resonance frequency shown in Figure 5.4 and in Figure 5.5 indicates a change in the temperature of the gas as high as a few hundred Kelvin occurring over a few thousandths of a second. This temperature change occurs when the pycnoclinic acoustic force accelerates hot plumes of gas toward the quartz wall as shown schematically in 5.9. The velocity antinode, which is shown as a white dotted line, according to equation 2.90 is a boundary of convective stability. While it is in effect, the pycnoclinic acoustic force will tend to overturn a temperature profile which decreases from the velocity antinode toward the wall, causing convection. This convection causes a significant increase in the heat transport between the plasma and its container. The temperature of the quartz container, as measured by a FLIR-T400/HT ThermaCam, increases by as much as $100\,\text{K}$ as shown in Figure 5.10.
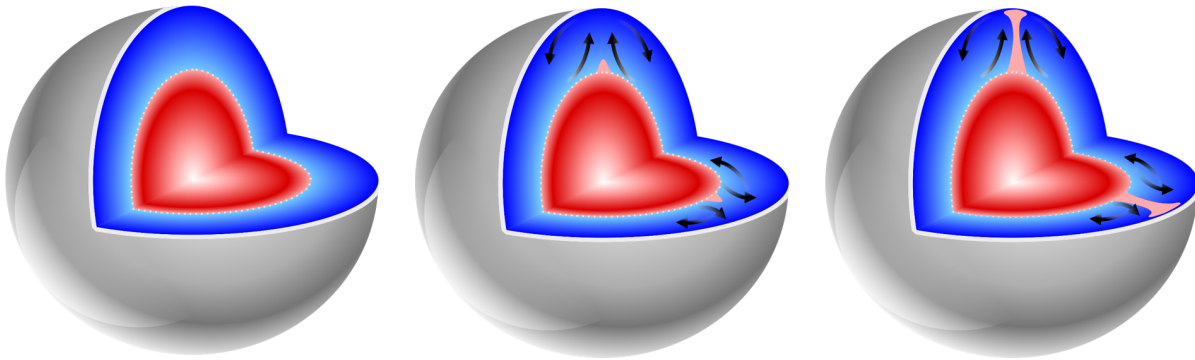
Figure 5.9: Small hot plumes which breach the acoustic velocity antinode surface of the spherically symmetric resonant mode (shown as a dashed line) are accelerated by the pycnoclinic acoustic force until they collide with the quartz bulb. Still images taken from a high speed video show this process in Figure 5.12.
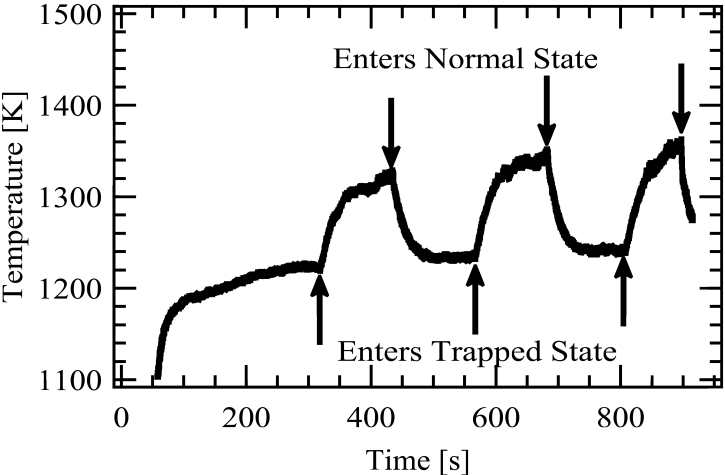
Figure 5.10: When the acoustic amplitude is sufficient to trap the plasma, there is an increase in acoustic convection which causes the quartz sphere to increase in temperature. Figure taken from [58].
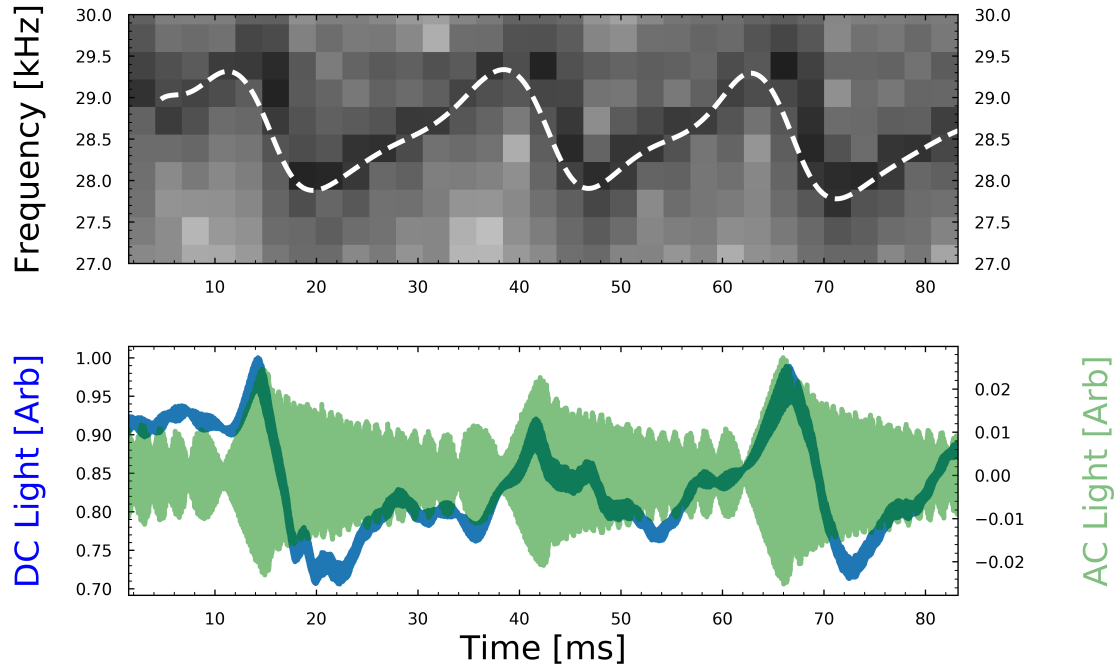
Figure 5.11: The images in Figure 5.12 correspond to the time between 10 ms and 18 ms in this trace. The drop in acoustic resonance frequency of around 1.5 kHz corresponds to a temperature drop in the gas of approximately 300 K and a change in the thermal energy of the gas of around 5 J. The temporal resolution of the spectrogram is 2.6 ms and the frequency resolution of the spectrogram is 330 Hz.

The total light output as measured by the high speed camera as shown in Figure 5.11 reproduces the relaxation oscillation observed with a single photodiode. When the frames of the high speed video corresponding to the high amplitude oscillations are considered individually, plumes can be observed such as are seen in Figure 5.12. Note that the time stamps corresponding to each image correspond to the time in the trace. This plume travels between the velocity antinode and the wall in around 5 ms indicating a characteristic velocity of around $2 \, \mathrm{m \, s^{-1}}$. The plume's role in convection is apparent by noting that the moment the plume begins to touch the quartz wall at around 15 ms, the total light output and the acoustic amplitude drop because the deposition of the thermal energy in the plume is removed from the gas and deposited in the quartz. This change in temperature causes both a drop in light output and detunes the resonance frequency of the cavity from the fixed drive.

68
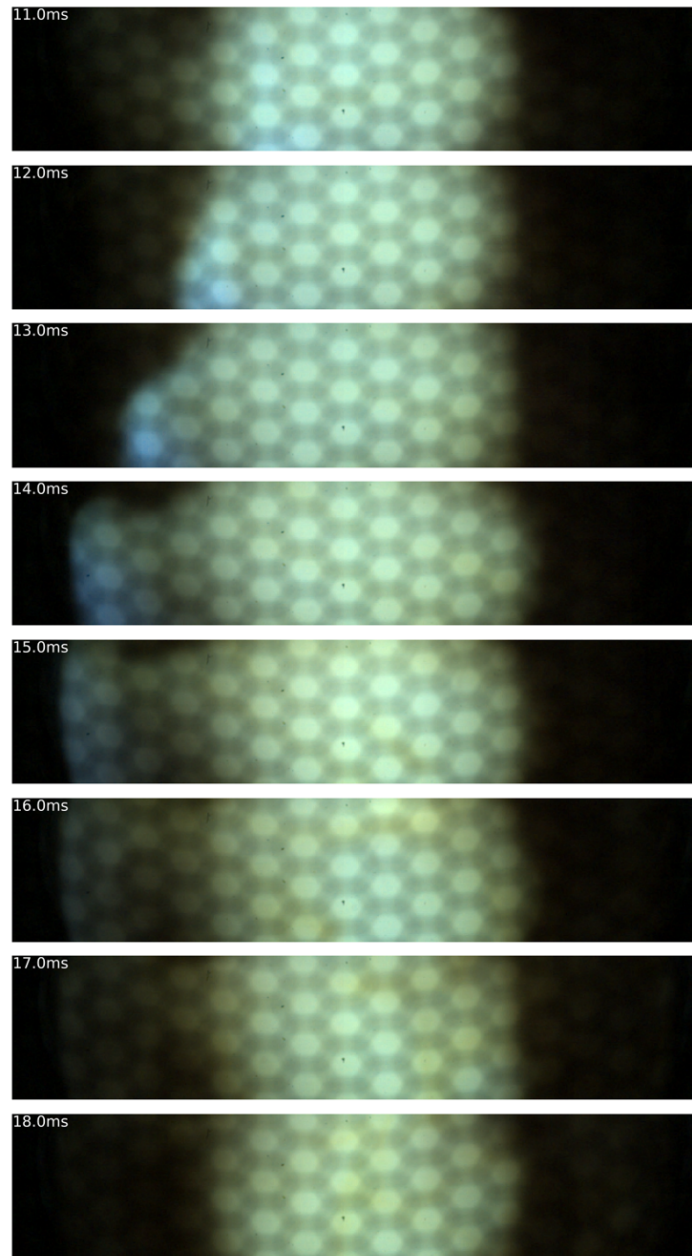
Figure 5.12: A plasma plume breaches the acoustic velocity antinode surface and accelerates toward the quartz wall over the course of 7 ms. The diameter of the luminous plasma is around 20 mm. When the plume reaches the wall it causes the acoustic resonance frequency to drop by 1.5 kHz indicating a drop in temperature of 300 K or the removal of around 4 J of thermal energy from the gas. The time stamps correspond to Figure 5.11.

These plumes are the onset of pycnoclinic acoustic convection. When a hot, less dense pocket of gas breaches the acoustic velocity antinode surface, the pycnoclinic force acts to accelerate it toward the wall where it dumps its energy into the quartz.

In order to consider how the pycnoclinic force drives convection we make an analogy to the Rayleigh number in the simplest convection geometry within a gravitational field, where the gas between two parallel plates separated a distance L undergoes convection. In order for the system to be unstable, the hot plate at temperature T_b must be beneath the cold plate at temperature T_u. The unstable arrangement begins to accelerate when its Rayleigh number exceeds some critical value. In this geometry, the Rayleigh number is

$$Ra = \frac{g\beta}{\nu D_t}(T_b - T_u)L^3, \tag{5.7}$$

where D_t, β, and ν are the thermal diffusivity, expansion coefficient, and kinematic viscosity respectively [63]. In the parallel plate geometry, a Rayleigh number of 2000 indicates the onset of convection. Below that value, a fluid can be held in mechanical equilibrium without being in thermal equilibrium. Above that value are a few regimes. For example, in a Rayleigh-Benard cell in helium gas, the regimes are as follows. When the Rayleigh number increases through about $\sim 2 \times 10^5$ the motion will be chaotic, from $\sim 2 \times 10^5 - 4 \times 10^7$ is a regime labeled soft turbulence, and above that is labeled hard turbulence [38].

In the acoustic case, we follow the example of the the thermal vibrational convection community (e.g. [30]) and pose a modified Rayleigh number based on the experiment at hand. As such we replace the standard force due to gravity, ρg with an acoustic acceleration based on the pycnoclinic force

$$\rho g \to \langle v_1^2 \rangle_t \nabla \rho, \tag{5.8}$$

to estimate a pynoclinic acoustic Rayleigh number due to the temperature difference ΔT across the radius of a bulb,

$$Ra_{paf} = \frac{\langle v_1^2 \rangle_t R^2 \beta}{\nu D_t}\Delta T = \frac{\langle v_1^2 \rangle_t R^2}{\nu D_t}\frac{\Delta T}{T}, \tag{5.9}$$

which can be used to anticipate when the onset of pycnoclinic acoustic convection should begin, and also when it becomes turbulent. If we use the acoustic velocity calculated above,

$v_1 \sim 20\,\mathrm{m\,s^{-1}}$, use a $\Delta T/T \sim 1$, and approximate both ν and D_t as $c_s \lambda_{mfp}$, $Ra_{paf} > 10^6$. This value would correspond to a region of soft turbulence, but such a high value is short lived due to the rapid detuning of the cavity's resonance from the drive and subsequent reduction of the acoustic field mentioned above.

A theory of when such convection becomes significant (i.e. what is the critical acoustic Rayleigh number) is not yet developed, but we will experimentally search for such values by looking for the acoustic amplitude at which a plume causes noticeable change in the acoustic response in section 6.4.

CHAPTER 6

Solid State Plasma Acoustic Drive

The circuit designed by Courret et al limited the microwave modulation schemes to pulse trains. Thus if the pulses were too short or far apart the plasma would extinguish. Another drawback of the magnetron based power supply is that as the magnetron ran its temperature would change and its center frequency could fluctuate by as much as 10 MHz which due to the high quality factor of the cavity could occasionally cause the amount of power delivered to the plasma to change dramatically [59].

In terms of studying the acoustics of the plasma bulb, because the modulation was always 100% on or off, any time the cavity was driven near an acoustic resonance a high acoustic amplitude would be achieved, the pycnoclinic acoustic force would move or deform the plasma, and acoustically driven convection would rapidly change the temperature in the cavity. As such it was difficult to reliably measure the acoustic properties because they were constantly changing.

In order to increase the flexibility with which the microwave power could be modulated, to increase the stability of the experiment, and to allow phase-sensitive detection, the magnetron and pulsed high power source were replaced with a newly available high-power linear solid state amplifier an Empower 2180. This new design enabled nearly arbitrary modulation of the microwave heating with an average power of just over 2 kW. An example modulation of the total power out of the amplifier $P_{\mu W}(t)$ with modulation ratio A_{mod} which can range from 0 to 1 is,

$$H = \frac{P_{\mu W}(t)}{V} = \frac{\overline{P_{\mu W}}}{V} \left(1 + A_{mod} \cos\left(\omega t\right)\right) \tag{6.1}$$

This is the form the driving function in equation 2.36 might take if the power from the
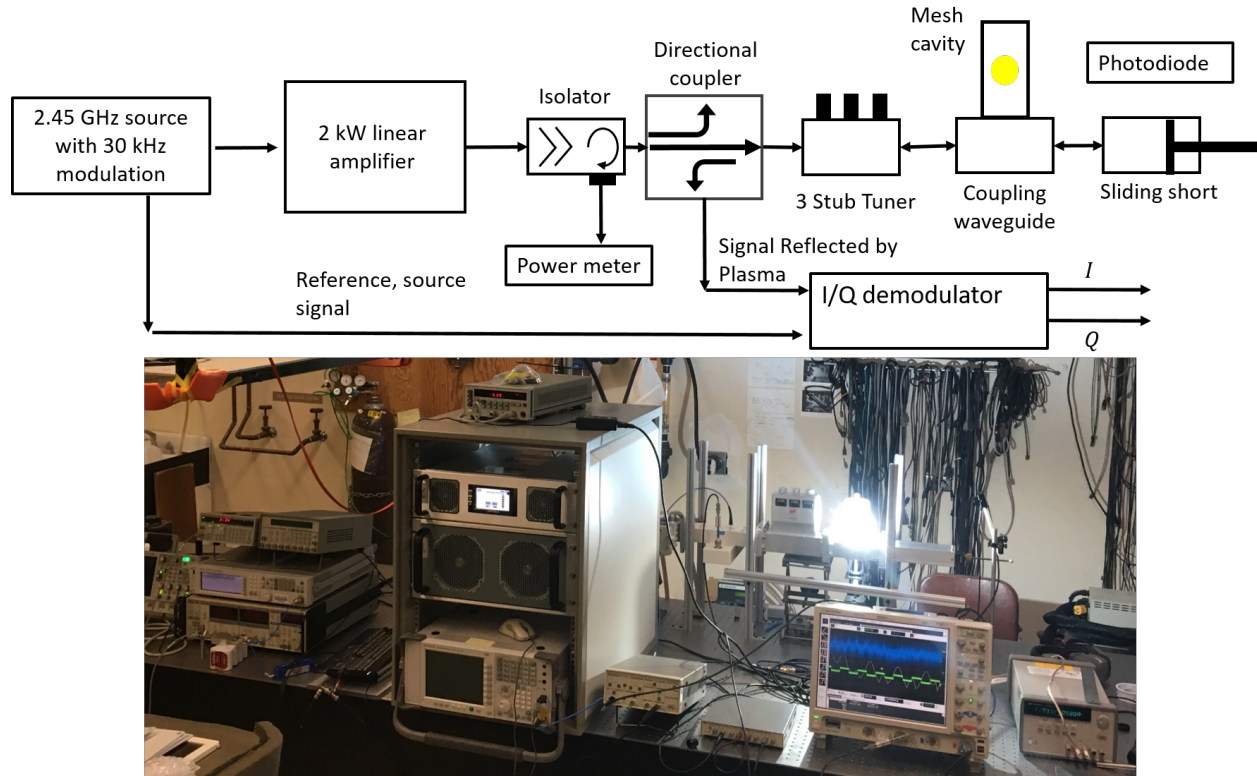
Figure 6.1: A schematic of the plasma acoustic drive at UCLA based on a 2 kW solid state amplifier.

amplifier is distributed evenly over the volume of the bulb V.

One limitation of this device is that the peak power is limited to $2.3\,\text{kW}$ as compared to the magnetron based circuit which could produce a peak power which exceeded the average power as shown in Figure 5.2.

A schematic and a photograph of the apparatus is shown in Figure 6.1.

6.1 Acoustic Spectrum of a Sulfur Plasma

In order to measure the acoustic spectrum of the plasma bulb, we used a frequency sweep on the microwave's modulation frequency to vary the acoustic drive frequency from $5\,\text{kHz}$ to around $100\,\text{kHz}$. By using a shallow modulation depth of 5% and sweep frequency of $5\,\text{Hz}$ or a sweep rate of $475\,\text{kHz}\,\text{s}^{-1}$ it was possible to ensure that the radiation pressure effects
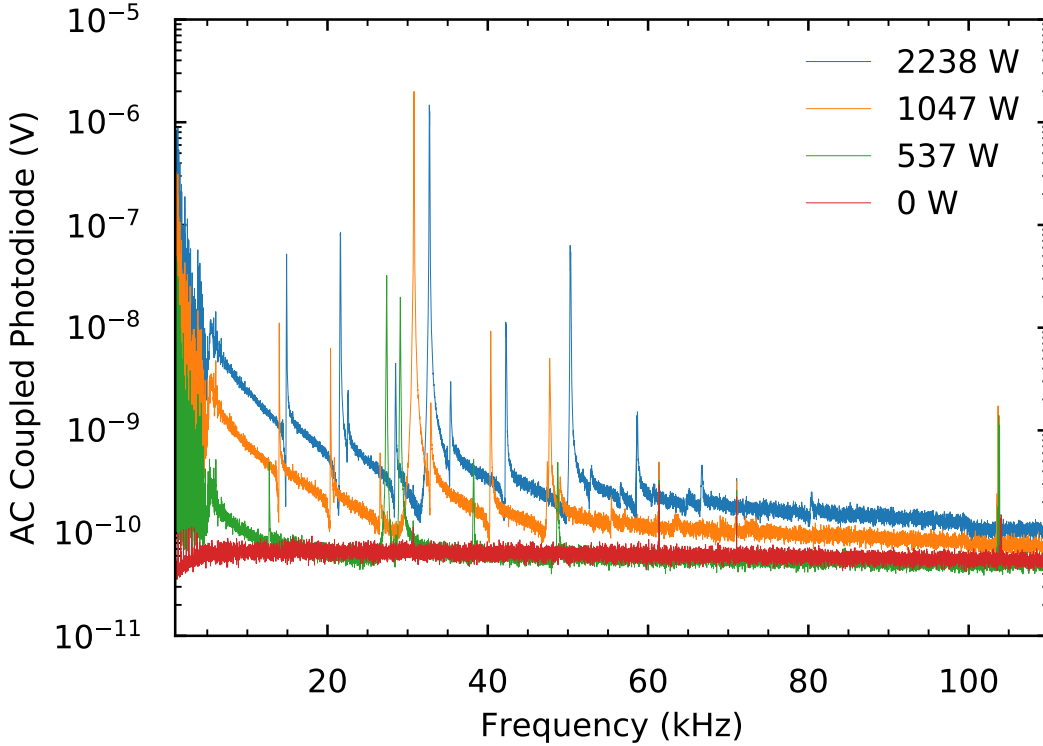
Figure 6.2: The acoustic spectrum of a plasma filled sphere at a few different powers. The spectrum was generated by a constant phase sweep of the microwave power's modulation frequency from 5 kHz to 100 kHz, and measured by monitoring high frequency oscillations in the light output measured with a photodiode. In order to minimize any nonlinear effects, the modulation of the microwave power was 5%.

observed at high acoustic amplitudes would not appreciably change the properties of the resonance cavity over the course of the sweep. A few spectra of plasmas maintained with increasing time-averaged powers are shown in Figure 6.2. The 5% modulation depth was a fixed fraction of incident power, so these sweeps had a proportionally larger drive.

In these spectra, the noise of the measurement is indicated in the 0 W case. In the 500 W case the swept drive is apparent only from 5 kHz to 10 kHz, but 5 acoustic resonances are apparent. The spike around 105 kHz is not of acoustic origin because it does not change with the incident power or the temperature of the gas. For the two higher power sweeps more modes became apparent.

In order to trace the change of modes with acoustic power, these data along with several other traces are plotted in Figure 6.1. In that visualization, the variation of all of the acoustic frequencies with increasing power is apparent.

The resonance frequencies are also highlighted in Table 6.1. If we consider the lowest resonance frequency mode measured here, and compare its value to the analysis in section 2.2.2, and use the speed of sound for diatomic sulfur, we measure an average temperature over the bulb of 2100 K when the plasma is sustained by 300 W which increases to 3200 K when sustained by 2.2 kW.

Comparing the first four measured frequencies to those predicted for a cavity filled with a uniform gas as described in sections 2.2.2 indicates a discrepancy as shown in table 6.2. This discrepancy is most easily observed by noting that in the homogeneous case, there are only two spherical acoustic modes with smaller wave numbers than the lowest spherically symmetric mode, the (1,1) and (2,1) with the (3,1) having a wave number slightly larger than the breather mode. In the data, however, there are three distinct modes with resonances lower than the breather which is that with the largest amplitude. This discrepancy, is due to the variation in temperature throughout the volume of the sphere.

6.2 Acoustic Resonances in a Sphere with a Parabolic Temperature Profile

The resonances predicted by the acoustic wave equation in a sphere discussed in section 2.2.2 were predicted for a fluid was uniform throughout the cavity. The sulfur plasma which is around 4000 K at the center and drops to below 2000 K at the wall less than 2 cm away is not uniform. In order to address this nonuniformity, it is necessary to use the inhomogeneous wave equation derived in equation 2.14 in order to resolve the discrepancy in the resonances shown in Table 6.2. Using the inhomogeneous wave equation as a starting point, a more careful analysis of the expected resonance frequencies of a gas filled sphere with a large temperature gradient was led by my colleague in [56]. In that work the acoustic resonances
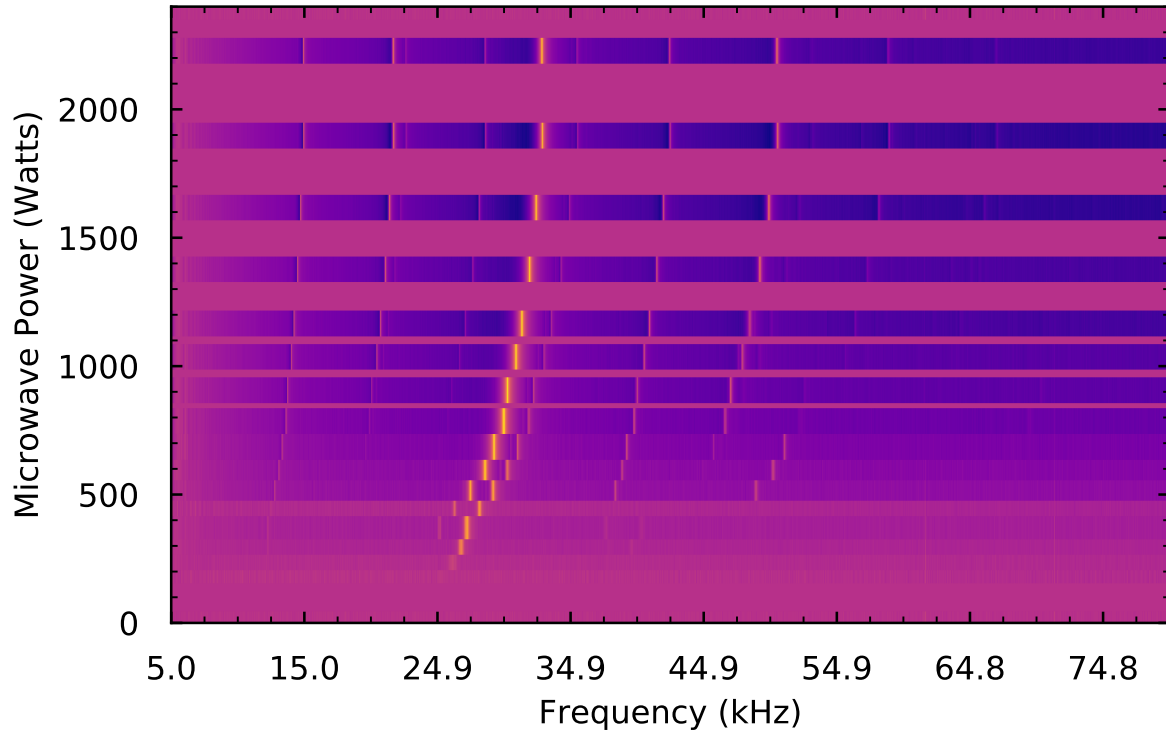
Figure 6.3: The acoustic spectrum of a plasma filled sphere, as measured with a photodiode as a function of average incident power. The spectrum was generated by a constant phase sweep from 5 kHz to 100 kHz In order to minimize any nonlinear effects, the modulation of the microwave power was 5%. Each row was normalized to its highest peak, and the color variation represents a logarithmic scale. For a sense of the relative size of each mode, compare to Figure 6.2, and the find the values corresponding to each mode in table 6.1. The location of the resonances are shown to shift as a function of total incident power and enable a measurement of the plasma's temperature.

Table 6.1:

Here are the first several resonances shown in Figure 6.3, values given are in kHz. The indices given in the column heads are best estimates for which acoustic mode (l,n) is observed in the spectrum.

Power (kW)	(1,1)	(2,1)	(3,1)	(0,2)	(4,1)	(1,2)
0.0						
0.2						
0.3				26.07		
0.3	12.23			26.71		
0.4	12.25			27.16	25.07	37.55
0.5	12.46			28.03	26.20	
0.5	12.74			27.39	29.09	38.23
0.6	13.05			28.47	30.14	38.73
0.7	13.28	19.52		29.15	30.90	39.08
0.8	13.60	19.84	25.68	29.84	31.77	39.59
0.9	13.70	19.99	25.96	30.15	32.09	39.85
1.0	13.98	20.38	26.57	30.80	32.90	40.37
1.2	14.18	20.65	26.99	31.23	33.42	40.76
1.4	14.45	21.01	27.56	31.81	34.15	41.32
1.6	14.68	21.33	28.05	32.29	34.80	41.81
1.9	14.91	21.64	28.52	32.77	35.39	42.32
2.2	14.90	21.63	28.50	32.71	35.38	42.25
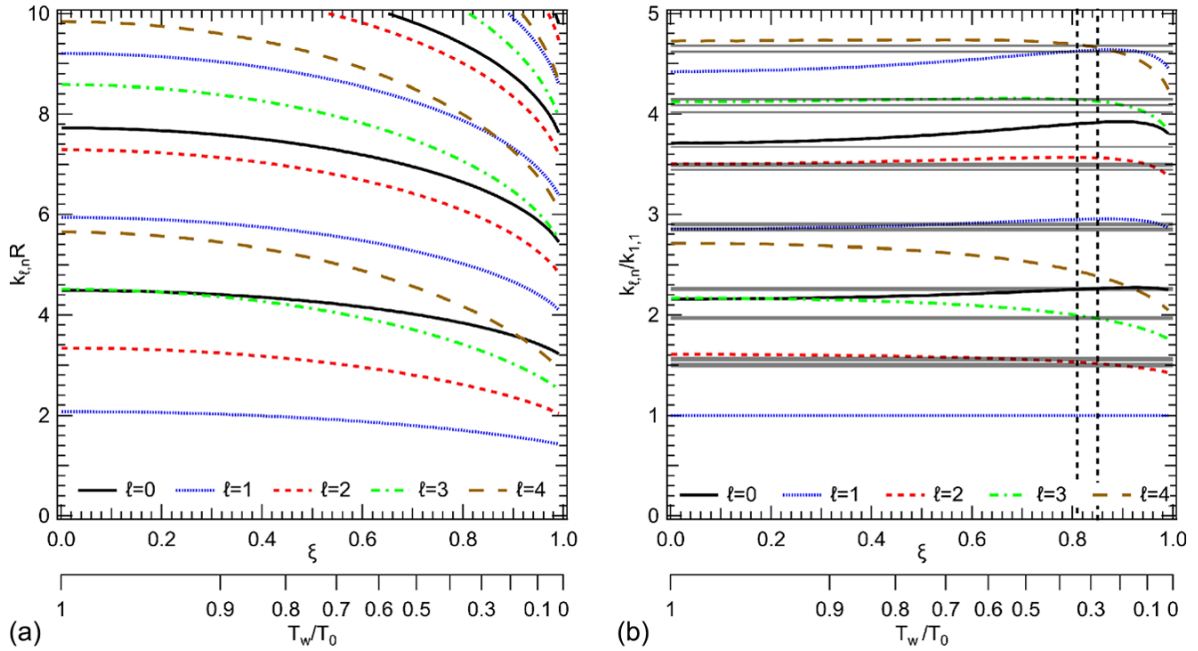
Figure 6.4: A) depicts the change in wavenumber $k_{l,n}$ for the eigenmodes in a gas-filled spherical bulb with a parabolic temperature profile of the form in equation 6.2. B) shows how the modes normalized to the lowest resonance frequency. The gray band indicates the measured shape of the temperature profile determined in the data based on the data in table 6.2. Figure adapted from [56].

of a gas filled sphere with a parabolic temperature profile of the form

$$T(r) = T_0 \left(1 - \xi^2 \frac{r^2}{R^2} \right) \tag{6.2}$$

were calculated. A parabolic temperature profile is interesting to consider because it is both the temperature profile predicted by the steady-state heat equation in a system heated uniformly throughout its volume, and it is also the first useful term in a pertubative expansion of an arbitrary temperature distribution. The eigenmodes for this temperature profile can also be solved analytically to be hypergeometric functions. The variation in the relative wavenumbers and eigenfrequencies as calculated by using the hypergeometric functions is presented in Figure 6.4.

Table 6.2: The ratio of the resonance frequencies to the lowest frequency are compared for the experiment, a homogeneous spherical cavity, and a sphere with a parabolic temperature profile of the form of equation 6.2 as described in [56].

	(1,1)	(2,1)	(0,2)	(3,1)	(4,1)
Measured	1.00	1.45	2.20	1.91	2.37
Homogeneous	1.00	1.61	2.16	2.17	2.72
$\xi = .83$	1	1.55	2.25	1.99	2.4

6.3 Effect of Rotation Rate on Acoustic Spectrum in a Sphere

In these experiments, the sulfur bulb was always rotating in order to stabilize the plasma, but the study of acoustics in a rotating body with large temperature gradients may be of interest to the helioseismology research community. As the techniques to study acoustic resonances of this spherical plasma are developed, one application may be to contribute to the study of study convection in rotating bodies. One particular avenue of research that these experiments could inform or validate are so-called modal acoustic velocimetry experiments. Modal acoustic velocimetry is a technique by which large scale convection or flow in a spherical body is deduced from the acoustic resonant modes in that body. Some recent experiments and accompanying theory have been designed to test shifts in the acoustic modes of a rapidly rotating ellipsoid filled with gas [99, 107]. The sulfur plasma lamp experiment adds the additional feature of a large thermal and density gradient.

We present in Figure 6.5 data of how the (2,n) mode shifts according to the rate of rotation of a plasma bulb. Although the precise reason for the shift is not yet known, I suspect it is basically due to the deformation of hottest regions of the gas into an ellipsoid, which lifts the degeneracy between the quadrupole modes.
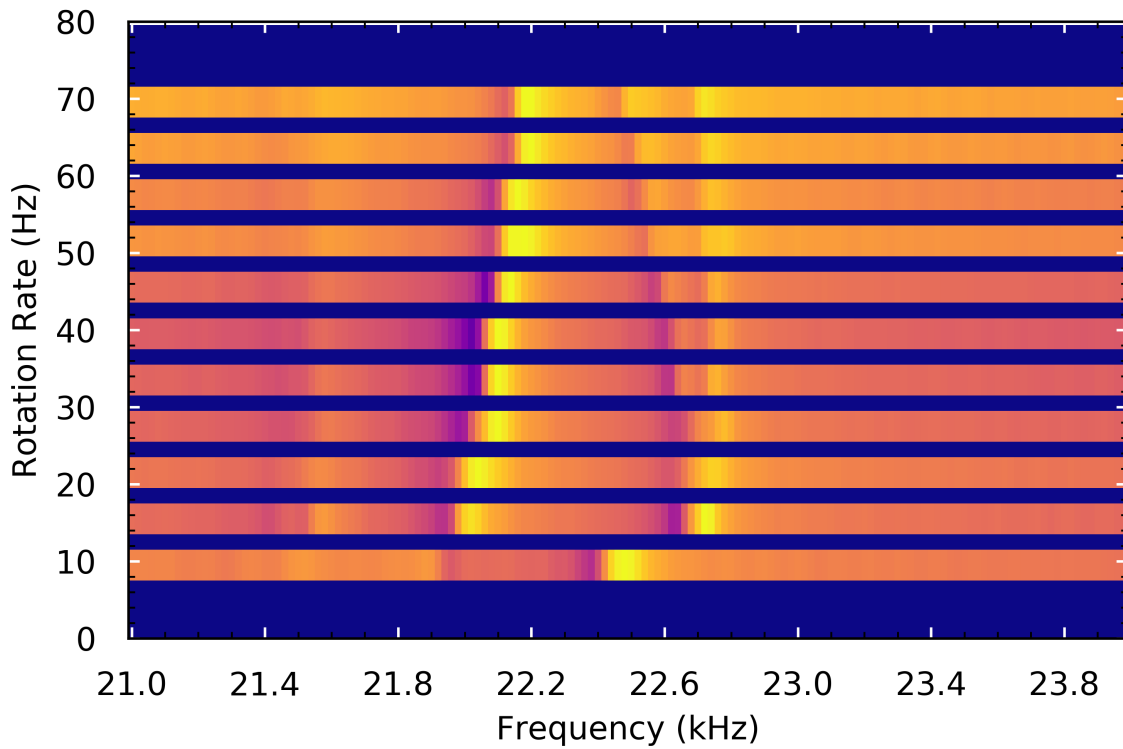
Figure 6.5: As the rotation rate is increased from 10 Hz to over 70 Hz the (2,1) mode shows some variation in its splitting. With a rotation rate below 10 Hz, the plasma floated to the top of the cavity, flickered, or extinguished. The resonance frequencies across the acoustic spectrum were also significantly different at 10 Hz than the higher rotation rates. And we note that some splitting exists at all rotation rates, which may indicate that the plasma has some ellipsoidal shape.

6.4 Resonant Tone Burst to Study Acoustic Amplitude Growth

As mentioned in the previous chapters, whenever the acoustic amplitude is large, the pycnoclinic acoustic force acts on density gradients in the plasma. If the amplitude is high this causes convection which rapidly changes the distribution of the gas and therefore the acoustic properties of the cavity. In order to use acoustics to study the plasma in the absence or at the onset of pycnoclinic convection, we ping the bulb containing a quiescent plasma with a tone burst at a resonant frequency of the cavity. Because the plasma starts in a known state before each ping, it is possible to use these measurements to characterize the distribution of the gas, the temperature, and the acoustic properties of the plasma loaded cavity.

The acoustic response to such a tone burst can again be measured with a photodiode. An example measurement generated by pinging the plasma with a 10% modulation depth 8000 tone burst with a frequency near the acoustic resonance of the lowest spherically symmetric mode is shown in Figure 6.6. The graph is shown at four different time scales. At such a low modulation amplitude, the acoustic response reproduces the familiar damped, driven harmonic oscillator such as is described at length in [81].

We assume that the photodiode response, η_{PD} is linearly proportional to the acoustic pressure in the center of the sphere, and so can be written as

$$\eta_{PD} = \zeta p_1. \tag{6.3}$$

In order to approximately calibrate the photodiode's signal in terms of acoustic pressure we interpret the photodiode's response as a damped, driven harmonic oscillation similar to equation 2.48

$$\ddot{\eta}_{PD} + 2\alpha\dot{\eta}_{PD} + \omega_0^2\eta_{PD} = \zeta f_0 e^{-i\omega t}, \tag{6.4}$$

where 2α is related to the acoustic quality factor, ω_0 is the acoustic resonance frequency, and f_0 is the driving function. Because the cavity is driven at resonance the response initially increases linearly, and so the initial growth of the photodiode's signal depends on the strength

of the driving function and the modulation frequency as

$$\eta_{PD}(t) = \frac{\zeta}{2}\frac{f_0}{\omega_0}t. \tag{6.5}$$

We attempt to calibrate the signal by comparing f_0 to the expected acoustic forcing function based on the incident power and modulation depth according to equation 2.48,

$$f_0 = (\gamma - 1)H_0 * h_{002} * \omega * A_{mod}. \tag{6.6}$$

The Bessel-Fourier weight, h_{002} can be calculated based on the temperature profile predicted in the previous section, an approximate electrical conductivity based on that from Figure 3.5, and the power and modulation depth described above, the predicted h_{002} would be around .5 and f_0 is approximately $4 \times 10^8 \omega A_{mod}(\gamma - 1)$ $\mathrm{Pa\,s^{-2}}$.

We can calibrate η_{PD} by examining the slope in the first two frames of Figure 6.6, where the photodiode's response increases linearly for several milliseconds because the cavity is driven at resonance. The slope in that example is approximately $16\,\mathrm{V\,s^{-1}}$, and so we estimate ζ based on the data in Figure 6.6 to be

$$\zeta \approx 2 \times 10^{-6}\,\mathrm{V\,Pa^{-1}}. \tag{6.7}$$

This value is probably too low, because it indicates a sound field with a Mach number exceeding .02 for the trace in Figure 6.6, and for the data shown in Figure 6.7 would estimate a Mach number ten times larger. I suspect that power does not couple to this acoustic mode as effectively as expected or the linearity of the light emission in terms of the pressure fluctuation is in question.

From these tone burst data it is possible to measure the acoustic quality factor such as by measuring the decay of the signal when the tone burst has ended. The decay of the photodiode signal after the tone burst has stopped at time t_0 is fit to an envelope of the form

$$\eta = \eta(t_0)\exp\left(-\frac{\omega_0}{2Q}(t - t_0)\right). \tag{6.8}$$

The quality factor for this mode is calculated to be approximately 1300, and the fit can be seen the last frame of Figure 6.6.
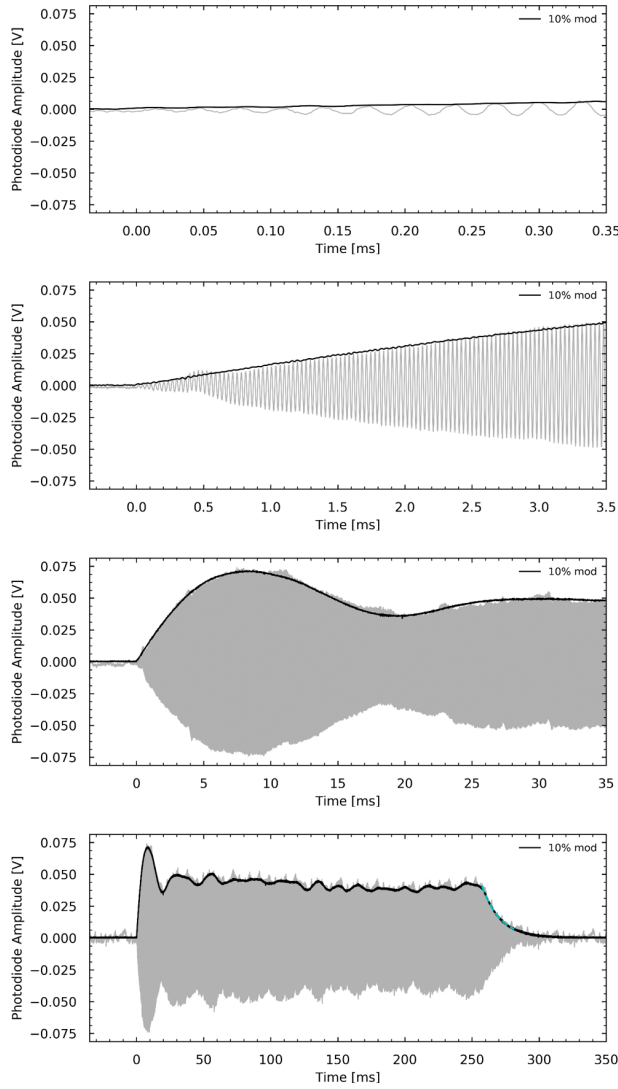
Figure 6.6: A resonant tone burst is used to ping a quiescent plasma sustained by an average incident power of 1.1 kW. The resulting oscillations in the light output are measured with a photodiode. The tone burst was tuned to the resonance frequency of 31 080 Hz, turned on at $t = 0$, and turned off 8000 cycles later at $t = 250$ ms. The modulation depth was 10%. In this case, the drive amplitude was low enough that the acoustic response was that of a linear, damped driven oscillator. The initial linear growth in the first two frames suggests a means of relating the drive strength and the light's response. When the tone burst is turned off at 250 ms, the acoustic field decays. The envelope of the decay was fit with equation 6.8, and shown with a dashed cyan curve, to determine the quality factor which is 1300.

6.5 Effect of Acoustic Drive Strength on Pycnoclinic Acoustic Convection

In order to determine when the transition from linear acoustics to acoustics dominated by nonlinear effects occurs, we varied the microwave modulation depths in order to vary the strength of the acoustic drive while holding other properties of the plasma constant.

The impact of modulation depth is made apparent by probing the microwave plasma's acoustic properties with a series of tone bursts which are tuned to the resonance frequency of the cavity as is shown in Figure 6.7. Note that the black trace from Figure 6.6, is the 10% modulation trace in Figure 6.7. The response to each tone burst again begins with a linear increase due to resonant driving as mentioned. In the modulation depths greater than 10%, the ultimate amplitude by linear theory is never achieved, because the pycnoclinic acoustic convection changes the resonance frequency within a few ms. This process can be seen by observing the beating in the response. This change in resonance frequency can be observed also in an FFT of each trace.

The spectra shown in the lower frame of Figure 6.7 show how the different modulation depths and therefore acoustic amplitudes cause a varying temperature swings in the gas as shown by the change in the resonance frequency. Such data suggests a route to calculating the dependence of pycnoclinic acoustic convection on the acoustic Rayleigh number. The two lowest modulation cases, where no deviation in the resonance frequency is observed can be considered to be subcritical in terms of that acoustic Rayleigh number in equation 5.9, because they never achieve sufficient amplitude to eject a plume. In this system, based on the analysis in previous sections, I estimate the Mach number which causes PAF convection is somewhere between .001 and .01. The Mach number reported in [58] of .03, and the temperature difference measured using the method from [56] would correspond to an acoustic Rayleigh number of 1×10^6 as mentioned above, but a Mach number of .001 corresponds to Ra_{paf} of a factor nearly 1000 times smaller. The change in resonance frequency for the 80% modulation depth of $\sim 2000\,\mathrm{Hz}$ indicates an average temperature drop of around $400\,\mathrm{K}$.

The two lowest amplitude drives reach a stable, steady state amplitude after around 50 ms. Above 15% modulation, however there is significant beating in each trace. Also of interest is that the 40% and 80% traces never achieve the amplitude they do during the first sweep. This is because the PAF driven convection prevents the bulb from returning to its quiescent state and therefore the resonance frequency the tone burst was tuned to. This failure of the amplitude in these two traces to return to the initial high peak is another demonstration of how much the PAF driven convection changes the properties of the acoustic cavity. The comparison between the low and high amplitude cases indicates that the convection causes a chaotic if not necessarily turbulent response in the gas. We believe the opportunity to study convective turbulence due to a 3D central force in the lab is an exciting one.
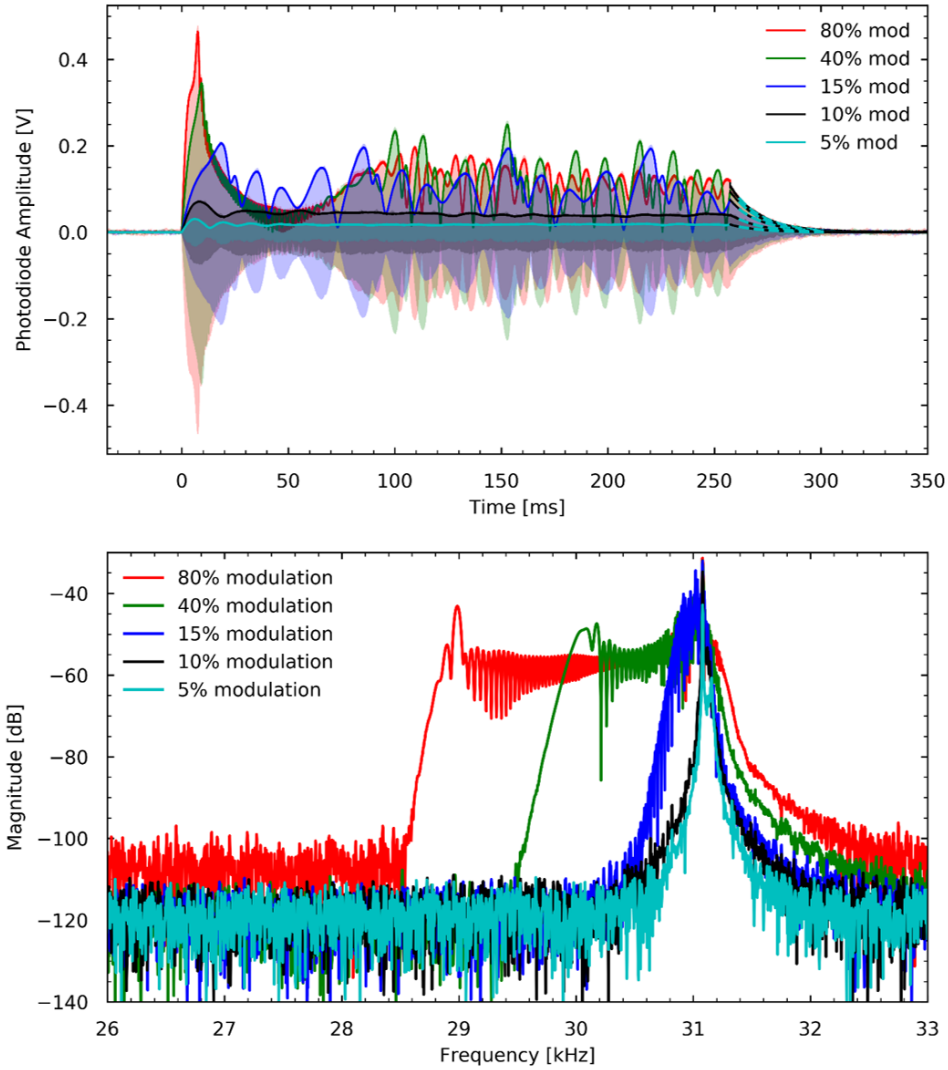
Figure 6.7: When the initially quiescent plasma is driven with tone bursts which are tuned to the resonance of the cavity the acoustic amplitude initially grows as a forced oscillator. If the amplitude is sufficiently high, however, the acoustic response to the drive grows rapidly and nonlinear effects become prominent. Several examples of this process are shown in the top trace. For example, in the previous low amplitude case, the amplitude is apparently limited by damping as is the case in a standard damped oscillator. In the high amplitude case, however, the resonance frequency from the cavity rapidly changes as is evident from the modulated envelope. In order to quantify the tone burst's effect on the gas, the spectrum of each burst has also been included. Note that the resonance frequency for the 80% modulation case drops around 2 kHz, which corresponds to a temperature drop of 400 K.

CHAPTER 7

Microwave Scattering Measurement of Pycnoclinic Acoustic Convection in Plasma

When the acoustic field has sufficient amplitude to cause pycnoclinic acoustic convection the dramatic changes in temperature and shape of the luminous region must also be accompanied by changes in the plasma properties of the gas - after all the free electron density depends strongly on temperature according to Saha's equation (eq. 3.1). As shown above, it is possible to change the strength of convection by changing the strength of the acoustic field driving it. How strongly can pycnoclinic acoustic convection affect the plasma properties? An extraordinary outcome would be the realization of steady-state acoustically driven convective turbulence in a weakly ionized plasma.

Many efforts have been made to study turbulence in plasma induced by flow in the neutral component of weakly ionized plasmas [29, 33, 62]. Alternative efforts have included studying the plasma properties of flames with turbulent plumes [35].

Many of these studies were undertaken in order to study the re-entry communications blackout which occurs when vehicles entering planetary atmospheres accelerate to sufficient velocities that viscous heating of the gas surrounding them causes ionization and disruption of RF communications [34, 74].

Attempts have been made to use plasma acoustics in combination with RF measurements have been used to measure the plasma frequency and collision frequency [91].

This chapter is based on a paper with a preliminary title of "Generation and characterization of chaotic convection in collisional plasma" authored by John P. Koulakis, Seth Pree, and Seth Putterman which has been submitted.

7.1 Microwave Reflection off of Acoustically Convecting Plasma

As discussed above, a microwave cavity coupled to a waveguide is used to start and maintain the plasma. While the plasma is stable (i.e. without any pycnoclinic convection), the cavity can be tuned by configuring the three stub tuner and sliding short so as to reduce the reflected power as much as possible. This occurs when the carrier frequency which is very close to 2.45 GHz matches the resonance frequency of plasma loaded waveguide circuit. When properly tuned, the plasma sits in a region of a resonant electric and magnetic standing wave, and the reflected power is stably less than .1% of the incident power.

When the microwave modulation excites an acoustic resonance, the reflected microwave signal begins to fluctuate because the temperature, electron density, and electron collision time will change. A comparison of the power spectrum of the two cases can be seen in Figure 7.1. We use phase sensitive microwave detection techniques and microwave perturbation theory to understand the fluctuations in the plasma properties responsible for the difference between the two spectra.

7.2 Phase Sensitive Detection

When an RF wave passes through a plasma, it may be both attenuated and undergo variation in its phase relative to a reference signal. By tracking these two variations separately, it is possible via equation 3.9 to determine properties of the plasma. Phase sensitive detection has also been used as a means to measure the time varying properties of an ionized gas such as the afterglow of a high current spark discharge and also to measure the passing of sound waves through that disrupted gas [9].

Although the most conceptually straightforward means of measuring attenuation and phase variation of a signal going through a plasma might be a transmission measurement, our apparatus does not yet have a channel through which such a measurement may be made. Instead, we measure the variation in the reflection of the incident wave off of the plasma loaded cavity.
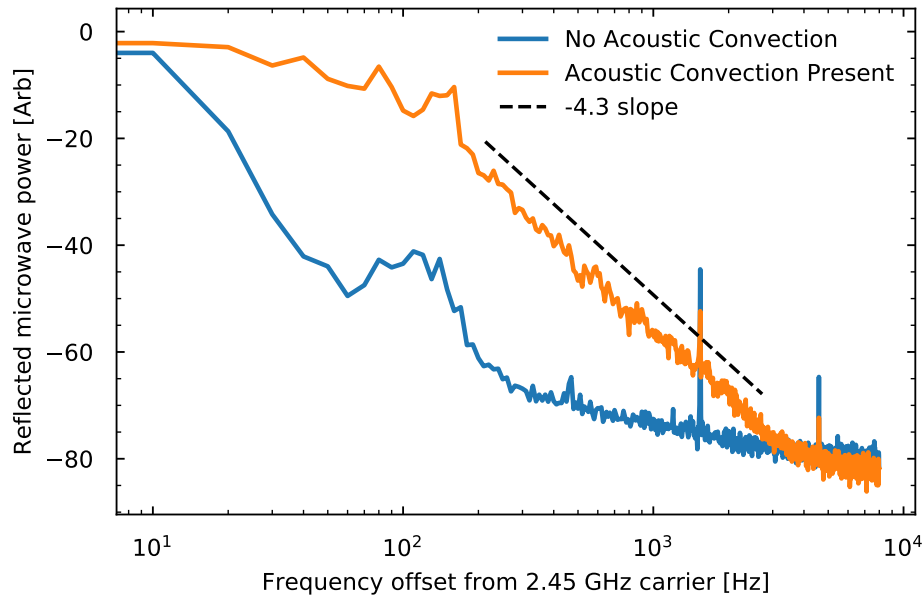
Figure 7.1: The positive side of the power spectrum offset from the carrier as measured by a spectrum analyzer. When the pycnoclinic acoustic convection discussed above is occurring, noise with a bandwidth of around $3\,\mathrm{kHz}$ is observed on the signal.

The complex reflection coefficient, Γ, of the drive field, E_{inc} off of the plasma loaded cavity can be described in terms of the in phase, I, and quadrature Q component of the reflected field, E_{ref} as

$$\Gamma = E_{ref}/E_{inc} \propto I + iQ \tag{7.1}$$

Measurements of each component are made using the directional coupler and a microwave demodulator as shown in Figure 6.1. The reflected signal is compared to a reference from the $2.45\,\mathrm{GHz}$ input.

If the cavity is resonant with the microwave source and the convecting plasma fluctuations only slightly perturb it, the in phase and quadrature signals will vary due to changes in resonance frequency and damping of the cavity [60]. These changes in the complex resonance frequency of the cavity are related to changes in the complex reflection coefficient as

$$\Delta\Gamma \propto \mathrm{Im}[\Delta\omega_{\mu w}] + i\,\mathrm{Re}[\Delta\omega_{\mu w}]. \tag{7.2}$$

The reflection signal can be experimentally calibrated to determine the change in the cavity's

resonance frequency by slightly varying the carrier frequency about the resonance while the plasma is quiescent and measuring the change in the response. If the drive frequency is offset from the resonance frequency, by a small amount (e.g. a few hundred kHz), the imaginary part of the reflection coefficient should shift in the same way as if the real part of the resonance frequency had changed by the same amount. We use this relation to find the absolute phase of the reflection coefficient and rotate the incoming signal such that a frequency modulated carrier signal only impacts the imaginary part of Γ. The size of the deviation also determines the scaling of the deviation of the resonance frequency - the calibration signal plotted in Figure 7.2 was used to scale the axes.

This calibration enables measurement of the change in the cavity's resonance frequency, $\Delta\omega_{\mu W}$, as the plasma it contains changes from quiescent to perturbed by pycnoclinic acoustic convection. Examples of calibrated measurement are shown in Figure 7.2.

As shown in Figure 7.2, the size of deviations in the microwave cavity's resonance frequency from the quiescent state are impacted by the strength of the pycnoclinic acoustic convection which depends on the acoustic amplitude. The variation in the cavity's resonance frequency enables measurement of how the pycnoclinic acoustic force changes the plasma parameters of the gas.

7.3 Microwave Perturbation Theory

If the contents of a microwave cavity are modified either by the addition of or change in a dielectric material within, both the resonance frequency and quality factor of the cavity will change. If the change in the resonance frequency is less than a few percent, properties of the dielectric or changes therein can be discerned using microwave perturbation theory [109]. As shown in Figure 7.2, the pycnoclinic acoustic convection causes deviations in the resonance frequency of a few MHz, and so we can use microwave perturbation theory to study variations in the plasma due to pycnoclinic acoustic convection. In the following analysis, we consider the plasma loaded cavity in the absence of acoustic convection, with a microwave resonance
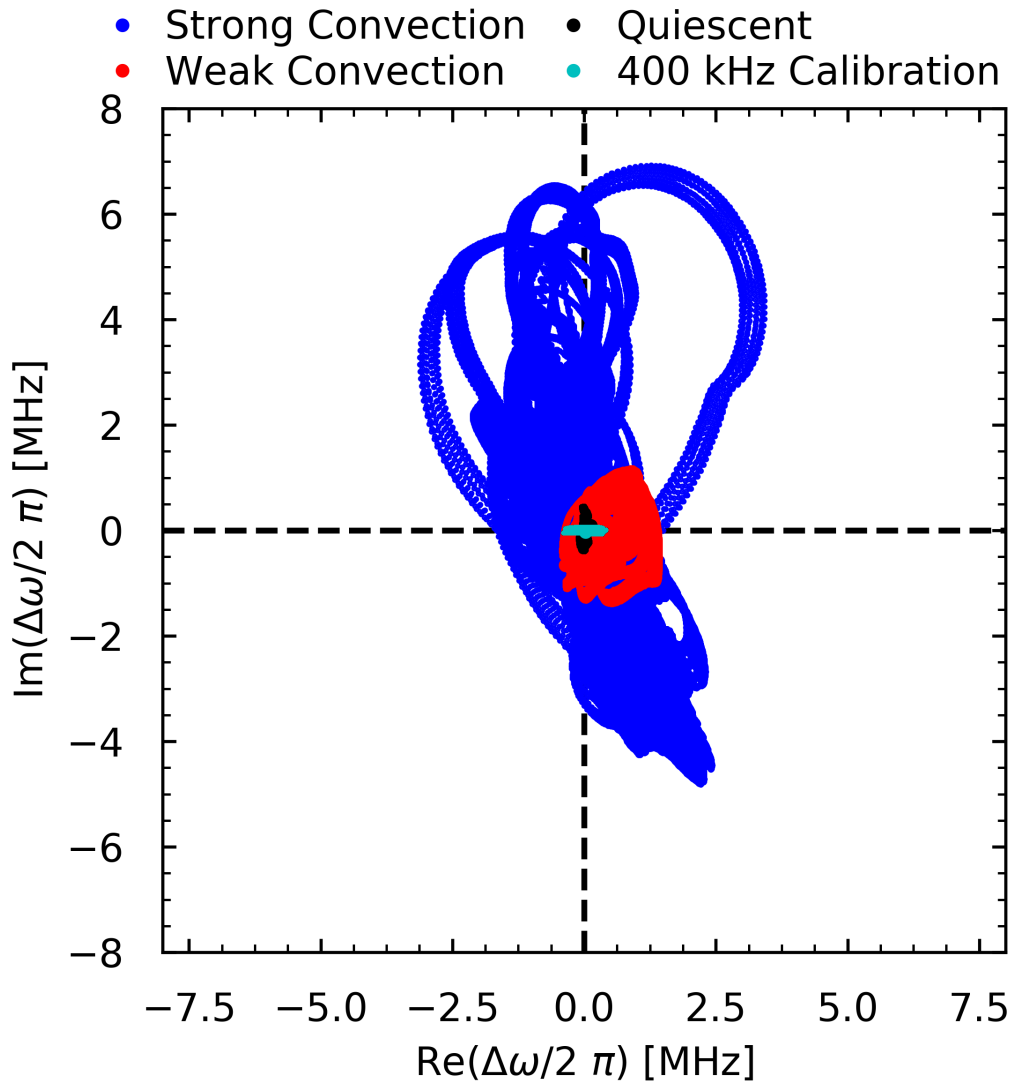
Figure 7.2: The resonance frequency and damping of the plasma loaded microwave cavity is impacted by pycnoclinic acoustic convection. The quiescent, weak convection, and strong convection cases are shown here. The axes are scaled by varying the carrier signal incident on the quiescent plasma by $400\,\mathrm{kHz}$, rotating the resulting signal to be along the $\mathrm{RE}(\delta\omega)$ axis, and scaling the axes to match the width of the frequency modulation.

frequency, $\omega_{\mu w}$ to be the ambient case we perturb around.

In general, the precise modal shape in the compound microwave cavity is difficult to know, but we assume it takes a standing wave form with functional forms

$$E = E_0 e^{i\omega_{\mu w} t}, \tag{7.3}$$

and

$$H = H_0 e^{i\omega_{\mu w} t}. \tag{7.4}$$

where both E_0 and H_0 vary in space.

When the plasma's temperature, density, collision time, or electron density change as may occur due to acoustic oscillations and pycnoclinic acoustic convection, its dielectric properties change according to equation 3.9. A changing dielectric constant subsequently causes the resonance frequency of the microwave circuit to change to $\omega + \Delta\omega$. And the fields will change slightly to

$$E = (E_0 + E_1) \, e^{i(\omega_{\mu w} + \Delta\omega_{\mu w})t}, \tag{7.5}$$

and

$$H = (H_0 + H_1) \, e^{i(\omega_{\mu w} + \Delta\omega_{\mu w})t} \tag{7.6}$$

Inside of the quiescent plasma filled bulb, we consider the complex permittivity to be ϵ_Q, with a corresponding displacement field of $D_0 = \epsilon_Q E_0$ and inside of the convecting plasma filled bulb the permittivity is ϵ_C, which is a function of time and the displacement field is $D_1 = \epsilon_C E_1$. Everywhere else in the cavity, the permittivity is taken to be ϵ_0. This plasma is effectively nonmagnetic, so the relative permeability is considered to be one, and the change in energy due to the magnetic field is negligible. Furthermore, the plasma is placed at a maximum of the electric field. Lastly, the energy in the electric and magnetic field's within the cavity are basically equal. Under these conditions, microwave perturbation theory predicts the change in complex resonance of the plasma-loaded cavity is

$$\frac{\Delta\omega_{\mu w}}{\omega_{\mu w}} = \frac{\int\int\int_{V_p} (E_1 \cdot D_0 - E_0 \cdot D_1) \, dV}{2 \int\int\int_V (E_0 \cdot D_0) \, dV} \; [11, \; 109]. \tag{7.7}$$

The denominator is dominated by the energy stored in the field outside of the plasma. If the permittivities are taken to be constant in space over the volume of plasma, V_P, they can be removed from the integral. These assumptions simplify the perturbation formula to

$$\frac{\Delta\omega_{\mu w}}{\omega_{\mu w}} = \frac{(\epsilon_Q - \epsilon_C)}{2\epsilon_0} \frac{\int\int\int_{V_p} (E_1 \cdot E_0)\, dV}{\int\int\int_{V_0} (E_0 \cdot E_0)\, dV} = \eta_V \frac{(\epsilon_Q - \epsilon_C)}{\epsilon_0}. \tag{7.8}$$

The ratio of integrals on the right hand side, relabeled η_V, is the ratio of the EM energy in the plasma to the total energy in the cavity.

If as a first approximation we assume the energy density of the field within the slightly conducting plasma is not too different from the average throughout the rest of the cavity, this fraction is the ratio of the volume of the plasma-filled bulb to the rest of the cavity which is around .01. This assumed ratio was made more precise and robust by using an Ansys HFSS simulation which included the dimensions of the cavity including the position of the sliding short and tuning stubs determined the weighted volume fraction is around .009 if the resonance frequency is the expected $2.45\,\mathrm{GHz}$.

Using this effective volume fraction, we relate the change in the microwave's complex resonance frequency as measured from the reflection shown in Figure 7.2 to the changes in the dielectric properties of the gas. By comparing the real and imaginary components of the perturbation relation between the permittivity and the cavity's resonance frequency in equation 7.8 to the permittivity of a weakly ionized, collisional gas in equation 3.9, we determine a relation between the variation in each. Using also the approximation that $\omega\tau \ll 1$, the difference in the imaginary component of the permittivity in the convecting and quiescent states relates to the change in resonance frequency as

$$\mathrm{Im}\left(\frac{\Delta\omega_{\mu w}}{\omega_{\mu w}}\right) = -\eta_V \frac{(\omega_p^2\tau)_C - (\omega_p^2\tau)_Q}{\omega_{\mu w}} = \eta_V \frac{\Delta\sigma}{\epsilon_0\omega_{\mu w}} \tag{7.9}$$

where we have also used the drude conductivity (eq. 3.11), $\sigma = \epsilon_0\tau\omega_p^2$. The variation of the average conductivity of the plasma is then shown plotted alongside the change in the imaginary part of the microwave cavity's resonance frequency as is shown in the bottom frame of Figure 7.3.

The real part of the permittivity is plotted in the middle frame of Figure 7.3 in order to suggest how one might expect the phase of an RF wave passing through such a plasma might be distorted.

The data in the lower two frames of Figure 7.3 are taken from a segment of the data shown in Figure 7.2. The top frame is the photodiode signal similar to those in previous sections. Large spikes in the acoustic trace correlate with changes in the reflection and to variation in the plasma's conductivity.

These analyses demonstrate how using pycnoclinic acoustic convection in a conducting gas is a method by which convective turbulence might be generated in a weakly ionized plasma. As mentioned above, an improved experiment may use an RF channel that is separate from the one generating the plasma in the first place. A second such channel should enable not only the observation of the effects of convection, but a more precise measurement of the acoustic oscillations themselves.
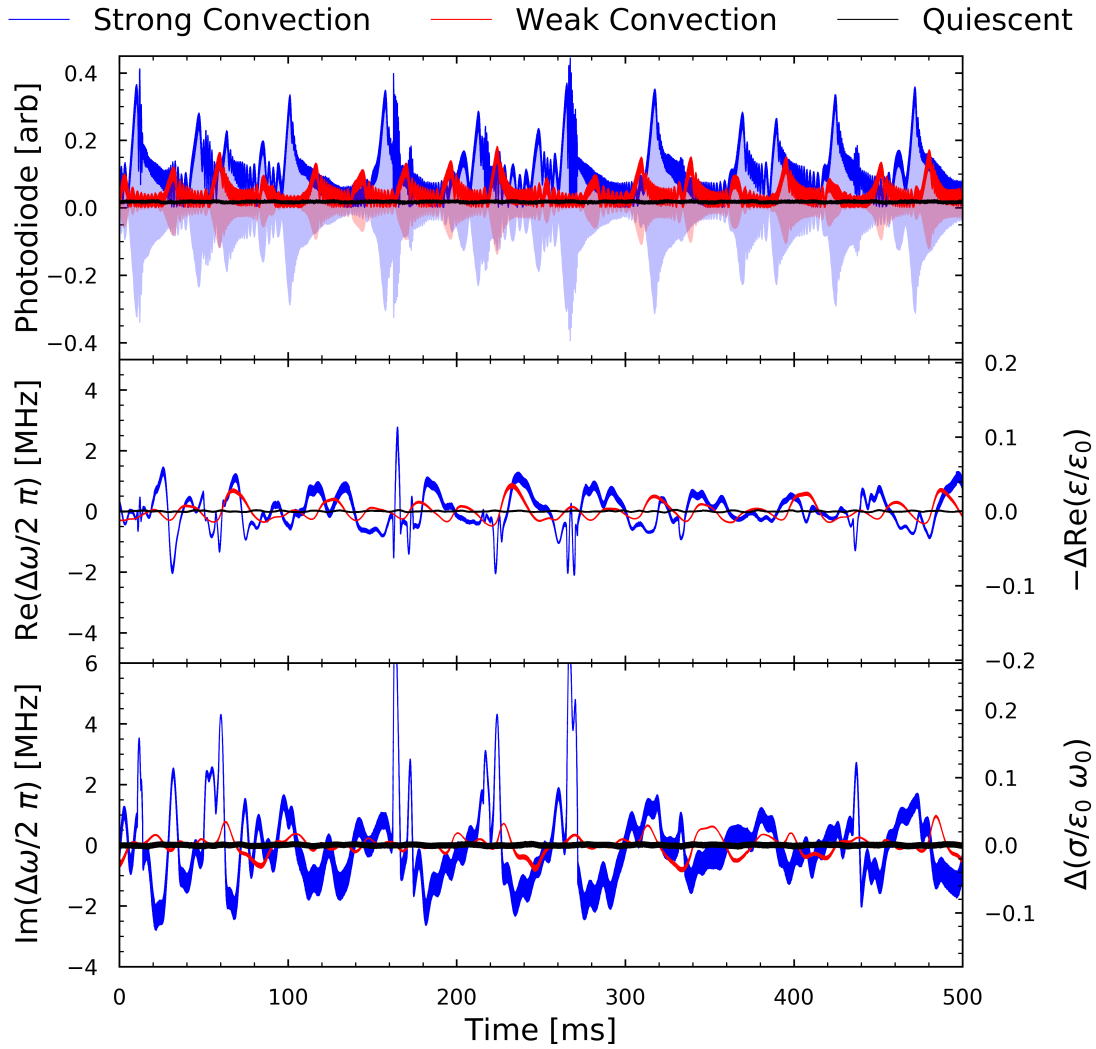
Figure 7.3: Time traces of the pycnoclinic acoustic convection's effect on the plasma-loaded microwave cavity's resonance properties. Microwave perturbation theory and comparison of the changes in the microwave cavity's complex resonance frequency enable measurements of the variation in the plasma properties of the sulfur plasma during acoustically driven convection. The largest spikes in the curves such as can be seen at around 175 ms in the microwave signals are likely due to the constricted arc channels as seen in the title Figure 0.1.

CHAPTER 8

Acoustic Self Oscillation in a Microwave Plasma

In this Chapter, I describe a method of sound amplification in a high pressure partially ionized gas. Piqued by the observation that the total light output increase during the acoustic compression shown in Figure 5.8 and the estimate that the acoustic compression may cause a temperature increase as high as $50\,\mathrm{K}$ we wondered whether the increased temperature during the compression phase may cause a sufficient increase in the electrical conductivity that more microwave power was absorbed during that time. If that were the case, it may be possible to generate acoustic gain in a microwave plasma, and therefore generate sound with a continuous wave microwave source. This chapter is based on [83].

8.1   Thermoacoustics

In section 2.2.1, the ability to generate sound by time-varying an energy or heat source was discussed. In that case the sound is produced by driven or forced oscillations, which are commonly taught in undergraduate differential equations courses. In this section, I will introduce how a constant (i.e. not varying in time) source of energy can generate an oscillating sound field in an acoustic cavity may through a process of positive feedback. Generally, such systems are called self-oscillators or maintained oscillators [81, 43]. Rayleigh's summary of the criteria for such amplification to occur has become a guiding principle of thermoacoustics, "If heat be given to the air at the moment of greatest condensation, or be taken from it at the moment of greatest rarefaction, the vibration is encouraged" [87].

To acousticians and glass-blowers alike it has been well known for hundreds of years that heating the closed end of glass tube can generate a loud sound. This effect is known as the

Sondhauss effect [96, 22]. Other examples include the Rijke tube [89, 21], Knipps tube[55], Hofler tube [112], and also the Taconis oscillations familiar to the cryogenic community [102]. In each of these devices the irreversible process which causes acoustic gain is the interaction of a sound wave with a thermal gradient on some surface against which the oscillating air moves. If the acoustic wave compresses as it moves toward the hotter end of the gradient, the Rayleigh criterion is satisfied.

A similar effect has been shown to cause catastrophe by extinguishing or destroying rockets and jet engines. In those cases the acoustic gain mechanism may either be a surface effect due to the temperature gradient along the tube of the jet as in the Rijke oscillation or the growing sound field causing a time-varying heat release in the flame by choking and throttling the fuel supply [84].

Another system which satisfies the Rayleigh criterion are the Cepheid variables, which are a type of star which oscillates due to what is effectively a spherically symmetric resonant mode. The motion is amplified by a variable absorption of the energy produce via fusion in the star's center, which is due to a variation in the opacity of certain layers in the star [16]. The amplitude of the oscillatory motion is so high that the energy of the oscillatory motion grows to be one-one billionth of the total thermal energy of the star [111]. The gain mechanism in these stars is based on a time-varying opacity. We propose that a microwave plasma may possibly demonstrate a similar volumetric gain mechanism in section 8.3.

An important characteristic of self oscillators is that once the source of gain exceeds the linear means of dissipation the amplitude of the oscillation will grow exponentially until limited by a nonlinear process. This tendency means that studying systems exhibiting spontaneous oscillation often lead to emergent nonlinear processes.

8.2 Ingard's Condition for Plasma Acoustic Amplification

That a sound passing through an ionized gas in the presence of an electric field may cause acoustic amplification was recognized and studied by Ingard in [40]. As shown above, time

varying heating of a gas may act as a forcing function for the acoustic wave equation as in equation 2.36. Although an oscillating electric field was used to generate sound in all of the plasma acoustic examples above, Ingard demonstrated that in the presence of a constant electric field, oscillations in the electrical conductivity or the rate of transfer of heat from hot electrons to the surrounding gas may cause the spontaneous generation of sound.

That research considered two particular classes of experiments - glow discharges and plasma afterglows. The glow discharges were, as mentioned above at a typical pressure of around 1 Torr. In these systems, the collision time is long enough that a significant temperature difference between the electrons and the neutrals was maintained. For example, for a glow discharge in helium a characteristic ratio, $T_e/T_n \approx 40$. Under these conditions, Ingard assumed that the ionization fraction in a given volume of gas was constant, and that a sound wave's primary impact on the plasma's conductivity would be due to an increase in the local density. This approximation is sometimes referred to as a "frozen composition" [94].

As such, the means by which the acoustic field would be driven by a continuous electric field was that the electrons maintained a high enough temperature so as to effectively serve as a high temperature energy source which contributed energy to the rest of the gas via a collision process.

8.3   Acoustic Self Oscillation in a Dense Microwave Plasma

If the density of the neutral gas in which a plasma is generated is sufficiently high that the collisions between electrons and neutrals cause the electron and neutral temperature to come to equilibrium very quickly compared to an acoustic cycle the Ingard mechanism for acoustic amplification may no longer be the dominant one. In particular, if the ionization and recombination rates are faster than an acoustic cycle, the change in temperature due to adiabatic compression of a sound wave may cause variation in the ionization fraction throughout the acoustic oscillation. This opportunity was the subject of [83], the results of

which are summarized here.

If the electron-neutral collision time is shorter than the RF oscillation period, the heat source driving the acoustic wave equation is well described by Joule heating and the Drude model of conductivity (eq. 3.11). In order to highlight the impact the changing ionization fraction has on the absorption of heat, we rewrite the collisional plasma's conductivity, σ_p, as a function of the ionization fraction, the gas temperature, the collision cross section, and fundamental constants,

$$\sigma_p = \frac{N_e}{N_0} \frac{e^2}{m_e a} \sqrt{\frac{\pi m_e}{8 k_B T}} \tag{8.1}$$

We consider a gas with a fairly low ionization fraction, $x = N_E/N_0 \ll 1$, and so the ionization fraction predicted by the Saha equation (eq. 3.1) can be written as an exponential function which depends on the de Broglie wavelength, λ, the ionization energy, χ,

$$x = \sqrt{\frac{2}{N_0 \lambda^3}} \exp -\frac{\chi}{2 k_B T}. \tag{8.2}$$

The Saha equation's prediction of the ionization fraction enables the conductivity of the gas to be determined in terms of the temperature, neutral density, and collision cross section of a gas. Writing the variation of the temperature and neutral density of a partially ionized gas in terms of the oscillating pressure of a sound field,

$$T = T_0 \left(1 + \frac{\gamma - 1}{\gamma} \frac{p_1}{p_0} \right) \tag{8.3}$$

and

$$N_0 = N_{00} \left(1 + \frac{1}{\gamma} \frac{p_1}{p_0} \right) \tag{8.4}$$

Where p_0, T_0, and N_{00} are the pressure, temperature and neutral number density without a sound field. Substituting these linearizations into the Joule heating equation produces a heating function that depends on the acoustic pressure fluctuation

$$H = H_0 \left[1 + \left(\frac{1}{4} \frac{\gamma - 1}{\gamma} - \frac{1}{2} \frac{1}{\gamma} + \frac{\gamma - 1}{\gamma} \frac{\chi}{2 k_B T_0} \right) \frac{p_1}{p_2} \right], \tag{8.5}$$

where H_0 is

$$H_0 = \frac{e^2}{a} \sqrt{\frac{2}{N_{00} \lambda^3}} \sqrt{\frac{1}{2 k_B T m_e}} \exp \left(\frac{-\chi}{2 k_B T} \right) \mathrm{E}_p^2. \tag{8.6}$$

This form of the heating function which is explicitly dependent on the acoustic pressure substituted into the acoustic wave equation with a heating term (eq. 2.36),

$$\frac{\partial^2}{\partial t^2}p_1 - c^2 \nabla^2 p_1 = \frac{(\gamma-1)^2}{c^2 \rho_0}H_0 \frac{\chi}{2k_B T_0}\frac{\partial}{\partial t}p_1, \tag{8.7}$$

shows the opportunity for acoustic amplification to be achieved. The term on the right hand side is opposite that of a typical damping and so is a negative damping or gain term.

Self-oscillation will take place if the acoustic amplification exceeds the acoustic losses in the cavity. To determine the conditions for where the amplification is sufficient to exceed the acoustic damping, we will consider a single mode and compare the gain and damping for that particular mode. Following the method described in [75], we compare the growth time due to the amplification to the decay time due to acoustic damping. As long as the amplitude remains small, which will be the case at the onset of amplification, these quantities can be calculated independently and then compared.

To determine the rate of amplification due to time-varying ionization in a constant electric field, we will consider the spherically symmetric breather mode,

$$p_1(t, r) = P_1 j_0\left(\frac{\xi'_{02}r}{R}\right)\exp i\omega_1 t, \tag{8.8}$$

and substitute it into equation 8.7. This results in a characteristic equation

$$\omega_1^2 + i\frac{(\gamma-1)^2}{c^2\rho_0}H_0\frac{\chi}{2k_B T_0}\omega_1 - \frac{c^2 \xi'^2_{02}}{R^2} = 0. \tag{8.9}$$

By solving this characteristic equation, the resulting real component of ω_1 determines the resonance frequency and is still dominated by the geometry of the cavity. The imaginary term, which is the negative damping, is the amplification's time constant,

$$\tau_{amp} = \frac{2\rho_0 c^2 k_B T_0}{(\gamma-1)^2 H_0 \chi} \tag{8.10}$$

For amplification to occur, the amplification growth time, τ_{amp} must be shorter than the damping time scale. As described in section 2.2.4, the acoustic damping of the spherically symmetric breather mode is due to the isothermal boundary condition at the wall, and so

the damping time scale is

$$\tau_\kappa = \sqrt{\frac{2R^2}{(\gamma-1)^2 \omega_1 D_T}} \tag{8.11}$$

By comparing these two time scales, we can determine whether amplification is possible. When $\tau_{amp} < \tau_\kappa$, the apparent acoustic quality factor will diverge, and self-oscillation will occur. Now we will address which configuration of experimental parameters including gas temperature, incident power, and number density are most likely to cause self oscillation.

The two time constants are plotted in Figure 8.1 for an argon plasma with neutral density of $2.5 \times 10^{19}\,\mathrm{cm^{-3}}$ in a bulb with a $2\,\mathrm{cm}$ radius, and subjected to $2.45\,\mathrm{GHz}$ microwaves with incident power ranging from $500\,\mathrm{W}$ to $2000\,\mathrm{W}$. In this plot, the electron-neutral cross section, a, was taken to be $0.2\,\mathrm{\mathring{A}}^2$, and the thermal diffusivity, extended from [13], was $1 \times 10^{-4}\,\mathrm{W\,m^{-1}\,K^{-1}}$.

Although the amplification time scale written in equation 8.10 suggests that amplification becomes easier at lower temperatures this only holds true while the plasma is sufficiently conducting. For the microwave heating to couple to the sound field, it must first be absorbed by the plasma. When the conductivity of the gas drops too low the energy will dissipate elsewhere such as in the cavity's walls as described in section 3.4, which resulted in a heating per unit volume of

$$H_0 = \frac{P_{in}}{V_p} \left[1 + A\frac{\epsilon_0 \omega V_c}{\sigma Q_c V_p} \right]^{-1}, \tag{8.12}$$

where P_{in} is the total incident power, V_p is the volume of the plasma, and A is a geometric factor which depends on the plasma's effect on the microwave mode. In the limit of low temperature, where $\sigma \to 0$, $H_0 \to 0$, and when the plasma is reasonably conducting, $H_0 \to P_{in}/V_p$.

This form of the power absorption was used to calculate the time scales in Figure 8.1. The increase in the amplification time constant on the low temperature side is due to the diminished power absorption at low temperature. The shaded region of Figure 8.2 shows the region in density and temperature parameter space in which a weakly ionized plasma may spontaneously oscillate via the mechanism described.
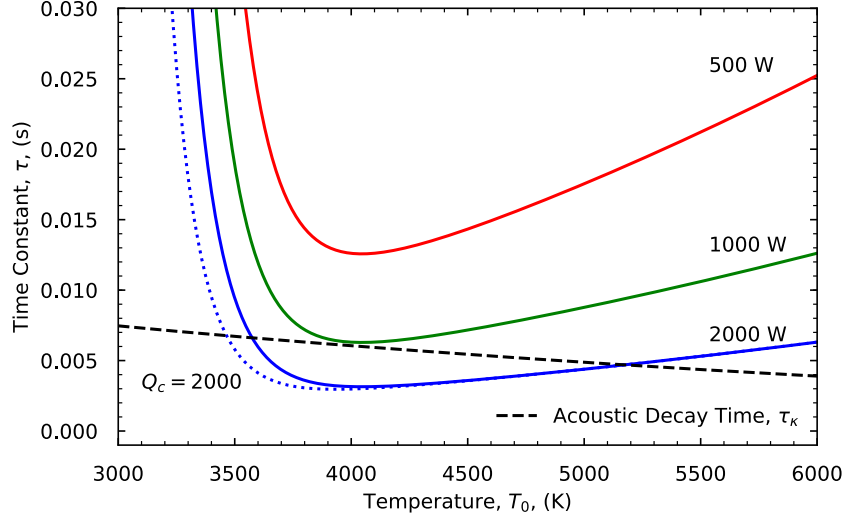
Figure 8.1: A comparison of the acoustic damping time constant, τ_κ, and the acoustic amplification time constant, τ_{amp}, for three incident powers, neutral density $N_0 = 2.5 \times 10^{19}$ /cc, and microwave quality factor $Q_c = 1000$. When $\tau_{amp} < \tau_\kappa$, the energy added to the acoustic field by the absorbed microwave exceeds the acoustic losses. The increase in amplification time at low temperatures is due to the inability of low temperature plasma to absorb microwaves as described in the text. To illustrate how the quality factor impacts the amplification time, the 2 kW case is shown both with $Q_c = 1000$ (solid), and $Q_c = 2000$ (dotted). Figure and caption reproduced from [83]

.

In this chapter we introduced a means by which an ionized gas within a spherical cavity may undergo spontaneous acoustic oscillation. This suggests a feasible path toward generating high amplitude sound in a plasma and a new type of three dimensional gain mechanism in thermoacoustics. Another desirable consequence of such a mechanism is that it no longer requires a drive frequency which is finely tuned to the cavity's instantaneous resonance frequency to generate sound and so may sustain the high acoustic amplitude despite the change in temperature due to pycnoclinic acoustic convection. I think such a capability, if achieved, would be a tool for generating sustained pycnoclinic convective turbulence.
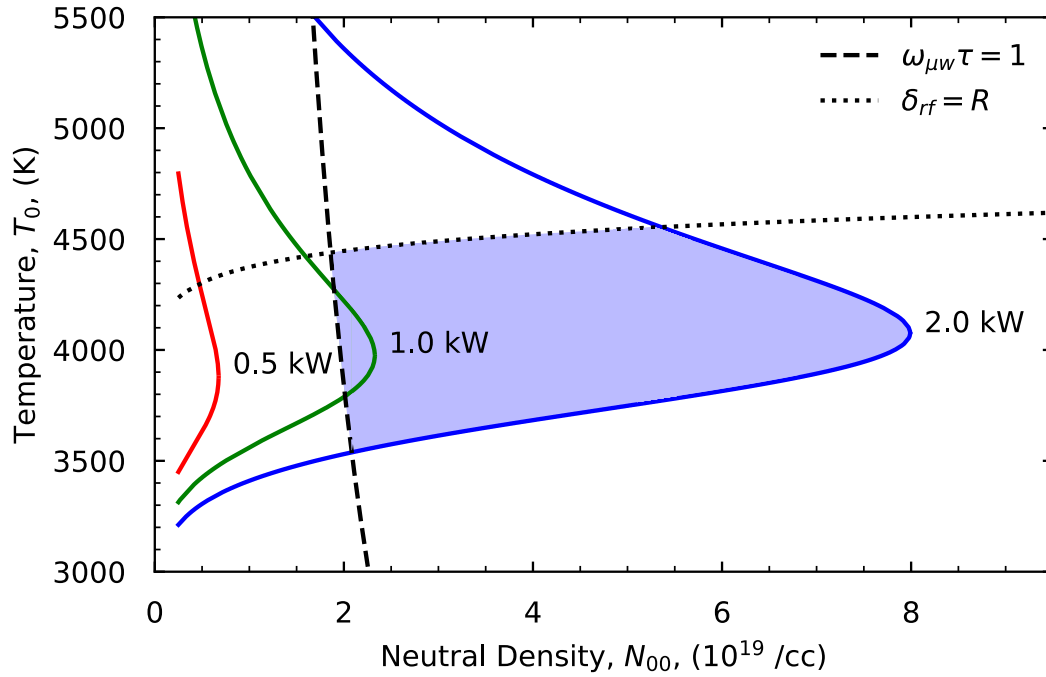
Figure 8.2: For each power, acoustic amplification exceeds thermal acoustic damping, $\tau_{amp} < \tau_\kappa$, to the left of the solid curve. In the region to the right of the dashed line, the electron-neutral collision time is short enough to justify use of the Drude conductivity. Below the dotted line, the microwave penetration depth is larger than the plasma radius, which justifies use of a constant electric field throughout the plasma. The shaded area represents the region in parameter space in which this analysis predicts acoustic self-oscillation for the 2 kW case. Figure and caption reproduced from [83].

CHAPTER 9

Conclusion and Future Work

In this dissertation I have introduced a type of experiment which uses acoustic fields to generate a spherically central confining force to hold a plasma to the center of a bulb. I described the theory, apparatus, and experimental techniques necessary to generate a large acoustic amplitude in a few thousand Kelvin, collisional plasma and described how that acoustic field acts on density gradients in the plasma so as to confine it to some regions and stir it in others.

Modulating the microwave power with a frequency near an acoustic resonance caused an acoustic field with a Mach number of .03. These high acoustic amplitudes acting on the luminous gas revealed a unique consequence of acoustic radiation pressure, which we have called the pycnoclinic acoustic force. The PAF accelerates the gas within the bulb by acting on density gradients within the gas present due to large thermal gradients. The acceleration of the gas in this way both causes the initially observed confinement of the hottest, luminous portions of the gas, but also causes acoustically driven convection in the outer regions of the bulb reminiscent of convection due to gravitational acceleration. The centrally symmetric confining force achieves an amplitude of 1000 times that of gravity and we propose could be an interesting platform to study convective dynamics in a central force. Other experiments designed to simulate a central force have achieved only .1 times the force due to gravity [36].

In order to more carefully study these acoustic effects, I have described an improved experiment which utilized a microwave source capable of arbitrary modulation. The flexibility afforded by the upgraded microwave drive enabled the more careful measurement of the acoustic properties of the plasma filled cavity. For example, measurement of the acoustic

spectrum enabled not only a characterization of the average temperature within the bulb, but also the curvature of the temperature profile within the gas. I then proposed that the ability to measure the acoustic spectrum using the light emanating from the transparent bulb may be a route to studying perturbations to the convection within the gas such as caused by rapidly rotating the bulb. Variation in the amplitude of the modulation depth and therefore the strength of the acoustic drive demonstrated a means to measure the onset of the pycnoclinic acoustic convection which can be classified by a modified acoustic Rayleigh number. At sufficiently high acoustic Rayleigh number, we measure what appears to be the onset of spherically central convective turbulence. Such techniques hopefully may enable new laboratory studies of convection in a central force.

The convection induced by the acoustic field, which causes large temperature fluctuations within the gas also causes variation in the plasma's response to microwave fields. In an attempt to characterize the extent of these fluctuations, I used microwave perturbation theory and the microwave signal reflected off of the acoustically stirred plasma to reveal the time variations in the plasma's conductivity caused by such convection. These time varying fluctuations in the plasma properties may enable a laboratory test-bed for the study of the reentry blackout communications problem.

In the last chapter, I described a potential means of acoustic amplification within a weakly ionized plasma and showed that it may be feasible to achieve. If experimentally realized, such an amplification would be a 3D thermoacoustic oscillator. If an acoustic field can be generated using this amplification mechanism, it may enable a route to scaling up acoustic plasma confinement to much hotter plasmas which are surrounded by a weakly ionized gas such as that studied here.

CHAPTER 10

Appendix

10.1 Extrema of spherical bessel function

Table 10.1: Here are several of the extrema, ξ'_{ln}, of the spherical Bessel functions

l \ n	1	2	3	4	5	6
0	0	4.49	7.73	10.9	14.07	17.22
1	2.08	5.94	9.21	12.4	15.58	18.74
2	3.34	7.29	10.61	13.85	17.04	20.22
3	4.51	8.58	11.97	15.24	18.47	21.67
4	5.65	9.84	13.3	16.61	19.86	23.08
5	6.76	11.07	14.59	17.95	21.23	24.47
6	7.85	12.28	15.86	19.26	22.58	25.85
7	8.93	13.47	17.11	20.56	23.91	27.2
8	10.01	14.65	18.36	21.84	25.22	28.53

10.2 Approximate thermodynamic properties of this experiment

Table 10.2: Several of the thermodynamic properties of the sulfur and argon filled quartz bulb

Quantity	Value	Unit
Quantity of sulfur in bulb	30 (4.7×10^{-4})	mg (moles of S_2)
Sulfur Number Density when vaporized	1.4×10^{19}	cm^{-3}
Specific Heat gaseous Sulfur, S_2 C_p	32	$J\,K^{-1}\,mol^{-1}$
e-S_2 Cross section at 3000 K [76]	22	$\mathring{A}^2$
Argon Number Density	3.2×10^{17}	cm^{-3}
e-Ar Cross section at 3000 K[24]	.2	$\mathring{A}^2$
Radius of Bulb	1.6-1.8	cm
Interior Volume of Bulb	17-24	cm^3
Mass of Quartz	14	g
Specific heat Quartz	700	$J\,K^{-1}\,kg^{-1}$
Melting Point of Quartz	< 2000	K

Bibliography

[1] Eugene Ackerman, Adam Anthony, and Fujio Oda. Corona-type loudspeaker for animal studies. *The Journal of the Acoustical Society of America*, 33(12):1708–1712, 1961.

[2] Farhang Afshar. The theory of acoustic resonance and acoustic instability in HID lamps. *Leukos*, 5(1):27–38, 2008.

[3] John M. Anderson. Irving langmuir and the origins of electronics. *IEEE Power Engineering Review*, 22(3):38–39, 2002.

[4] H. D. Arnold and I. B. Crandall. The thermophone as a precision source of sound. *Phys. Rev.*, 10:22–38, Jul 1917.

[5] W. R. Babcock, K. L. Baker, and A. G. Cattaneo. Musical flames. *Nature*, 216(5116):676–678, Nov 1967.

[6] F. Bastien. Acoustics and gas discharges: applications to loudspeakers. *Journal of Physics D: Applied Physics*, 20(12):1547–1557, Dec 1987.

[7] C. I. M. Beenakker. A cavity for microwave-induced plasmas operated in helium and argon at atmospheric pressure. *Spectrochimica Acta Part B: Atomic Spectroscopy*, 31(8-9):483–486, 1976.

[8] Robert T. Beyer. Radiation pressure—the history of a mislabeled tensor. *The Journal of the Acoustical Society of America*, 63(4):1025–1030, 1978.

[9] Gunthard K. Born and Rudolf G. Buser. Determination of the gas temperature in the afterglow of pulsed discharges by microwave probing of standing acoustic waves. *Journal of Applied Physics*, 37(13):4918–4924, 1966.

[10] John K. Burchard. Preliminary investigation of the electrothermal loudspeaker. *Combustion and Flame*, 13(1):82 – 86, 1969.

[11] Kai Chang and John Wiley. *Encyclopedia of RF and microwave engineering*. Wiley-interscience, 2005.

[12] Francis F. Chen et al. *Introduction to plasma physics and controlled fusion*, volume 1. Springer, 1984.

[13] S. H. P. Chen and S. C. Saxena. Thermal conductivity of argon in the temperature range 350 to 2500 K. *Molecular Physics*, 29(2):455–466, 1975.

[14] P. Collas and M. Barmatz. Acoustic radiation force on a particle in a temperature gradient. *The Journal of the Acoustical Society of America*, 81(5):1327–1330, 1987.

[15] Gilles Courret, Petri Nikkola, Sébastien Wasterlain, Olexandr Gudozhnik, Michel Girardin, Jonathan Braun, Serge Gavin, Mirko Croci, and Peter W. Egolf. On the plasma confinement by acoustic resonance. *The European Physical Journal D*, 71(8):214, 2017.

[16] John P. Cox. *Theory of Stellar Pulsation*. Princeton legacy library. Princeton University Press, 1980.

[17] Lee de Forest. The audion: a new receiver for wireless telegraphy. *Proceedings of the American Institute of Electrical Engineers*, 25(10):719–747, 1906.

[18] Lee de Forest. Audion bulbs as producers of pure musical tones. *The Electrical Experimenter*, 3(8):394–395, Dec 1915.

[19] Thomas D Dreeben and Gregory P Chini. Two-dimensional streaming flows in high-intensity discharge lamps. *Physics of Fluids*, 23(5):056101, 2011.

[20] William Duddell. On rapid variations in the current through the direct-current arc. *Journal of the Institution of Electrical Engineers*, 30(148):232–267, 1901.

[21] K. T. Feldman. Review of the literature on Rijke thermoacoustic phenomena. *Journal of Sound and Vibration*, 7(1):83 – 89, 1968.

[22] K. T. Feldman. Review of the literature on Sondhauss thermoacoustic phenomena. *Journal of Sound and Vibration*, 7(1):71–82, 1968.

[23] Arthur A. Few. Thunder. *Scientific American*, 233(1):80–91, 1975.

[24] L. S. Frost and A. V. Phelps. Momentum-transfer cross sections for slow electrons in He, Ar, Kr, and Xe from transport coefficients. *Physical Review*, 136(6A):A1538, 1964.

[25] Steven L. Garret. *Understanding acoustics*. Springer, 2017.

[26] Serge Gavin, Mauro Carpita, and Gilles Courret. Power electronics for a sulfur plasma lamp working by acoustic resonance: Full scale prototype experimental results. In *2014 16th European Conference on Power Electronics and Applications*, pages 1–7, 2014.

[27] David Gedeon. DC gas flows in Stirling and pulse tube cryocoolers. In *Cryocoolers 9*, pages 385–392. Springer, 1997.

[28] Kenneth W. Gentle and Uno Ingard. Determination of neutral gas temperature in a plasma column from sound velocity measurements. *Applied Physics Letters*, 5(5):105–106, 1964.

[29] Kenneth W. Gentle, Uno Ingard, and George Bekefi. Effect of gas flow on the properties of a plasma column. *Nature*, 203(4952):1369–1370, 1964.

[30] Grigori Zinov'evich Gershuni and Dmitrii Viktorovich Lyubimov. Thermal vibrational convection. *Thermal Vibrational Convection, by GZ Gershuni, DV Lyubimov, pp. 372. ISBN 0-471-97385-8. Wiley-VCH, August 1998.*, page 372, 1998.

[31] Scott R. Goode and Kim W. Baughman. A review of instrumentation used to generate microwave-induced plasmas. *Applied spectroscopy*, 38(6):755–763, 1984.

[32] Lev Petrovich Gor'kov. On the forces acting on a small particle in an acoustical field in an ideal fluid. In *Sov. Phys. Dokl.*, volume 6, pages 773–775, 1962.

[33] V. L. Granatstein. Structure of wind-driven plasma turbulence as resolved by continuum ion probes. *The Physics of Fluids*, 10(6):1236–1244, 1967.

[34] William L. Grantham. Flight results of a 25000-foot-per-second reentry experiment using microwave reflectometers to measure plasma electron density and standoff distance. 1970.

[35] H. Guthart, D.E. Weissman, and T. Morita. Microwave scattering from an underdense turbulent plasma. *Radio Science*, 1(11):1253–1262, 1966.

[36] J. E. Hart, J. Toomre, A. E. Deane, N. E. Hurlburt, G. A. Glatzmaier, G. H. Fichtl, F. Leslie, W. W. Fowlis, and P. A. Gilman. Laboratory experiments on planetary and stellar convection performed on spacelab 3. *Science*, 234(4772):61–64, 1986.

[37] U. Haumman. Used with permission and taken from.

[38] F. Heslot, B. Castaing, and A. Libchaber. Transitions to turbulence in helium gas. *Physical Review A*, 36(12):5870, 1987.

[39] U. Ingard. *Notes on Acoustics*. Physics series. Laxmi Publications Pvt Limited, 2010.

[40] Uno Ingard. Acoustic wave generation and amplification in a plasma. *Phys. Rev.*, 145:41–46, May 1966.

[41] Uno Ingard and Daniel C. Galehouse. Second-order pressure distribution in an acoustic normal mode in a rectangular cavity. *American Journal of Physics*, 39(7):811–813, 1971.

[42] John David Jackson. *Classical Electrodynamics*. Wiley, 1998.

[43] Alejandro Jenkins. Self-oscillation. *Physics Reports*, 525(2):167–222, 2013.

[44] Thomas S. Jerome, Yurii A. Ilinskii, Evgenia A. Zabolotskaya, and Mark F. Hamilton. Born approximation of acoustic radiation force and torque on soft objects of arbitrary shape. *The Journal of the Acoustical Society of America*, 145(1):36–44, 2019.

[45] C. W. Johnston, H. W. P. Van der Heijden, G. M. Janssen, J. Van Dijk, and J. J. A. M. Van der Mullen. A self-consistent lte model of a microwave-driven, high-pressure sulfur lamp. *Journal of Physics D: Applied Physics*, 35(4):342, 2002.

[46] C. W. Johnston and J. J. A. M. Van Der Mullen. Measured and simulated response of a high pressure sulfur spectrum to power interruption. *Journal of Physics D: Applied Physics*, 37(4):573, 2004.

[47] Colin William Johnston. *Transport and equilibrium in molecular plasmas: the sulfur lamp*. Technische Universiteit Eindhoven Eindhoven, 2003.

[48] Finn Jorgensen. The inventor Valdemar Poulsen. *Journal of magnetism and magnetic materials*, 193(1-3):1–7, 1999.

[49] P. L. Kapitza. Free plasma filament in a high frequency field at high pressure. *Sov. Phys. JETP*, 30:973, 1970.

[50] Jonas T. Karlsen, Per Augustsson, and Henrik Bruus. Acoustic force density acting on inhomogeneous fluids in acoustic fields. *Physical review letters*, 117(11):114504, 2016.

[51] Jin Joong Kim, Jung Tae Ko, Dong Ho Won, Jeong Won Kim, SS Kim, and Hong-Young Chang. Rotating plasma discharges of high-pressure molecular vapor using circularly polarized microwaves. *Applied physics letters*, 84(15):2769–2771, 2004.

[52] Louis Vessot King. On the acoustic radiation pressure on spheres. *Proceedings of the Royal Society of London. Series A-Mathematical and Physical Sciences*, 147(861):212–240, 1934.

[53] L. E. Kinsler, L. E. Kinsler, A. R. Frey, A. B. Coppens, and J. V. Sanders. *Fundamentals of Acoustics*. Wiley, 2000.

[54] S. O. Klein. Un nouveau transducteur électroacoustique: l'ionophone. *Acta Acustica united with Acustica*, 4(1):77–79, 1954.

[55] Chas. T. Knipp and Jakob Kunz. A physical explanation of the action of the new singing tube. *Phys. Rev.*, 19:400–401, Apr 1922.

[56] John P. Koulakis, Seth Pree, and Seth Putterman. Acoustic resonances in gas-filled spherical bulb with parabolic temperature profile. *The Journal of the Acoustical Society of America*, 144(5):2847–2851, 2018.

[57] John P. Koulakis, Seth Pree, Alexander L. F. Thornton, Alexander S. Nguyen, and Seth Putterman. Pycnoclinic acoustic force. In *Proceedings of Meetings on Acoustics 21ISNA*, volume 34, page 045005. Acoustical Society of America, 2018.

[58] John P. Koulakis, Seth Pree, Alexander L. F. Thornton, and Seth Putterman. Trapping of plasma enabled by pycnoclinic acoustic force. *Phys. Rev. E*, 98:043103, Oct 2018.

[59] John P. Koulakis, Alexander L. F. Thornton, and Seth Putterman. Magnetron coupling to sulfur plasma bulb. *IEEE Transactions on Plasma Science*, 45(11):2940–2944, 2017.

[60] John Pandelis Koulakis. *Traceable and precise displacement measurements with microwave cavities*. University of California, Los Angeles, 2014.

[61] August Kundt. III. acoustic experiments. *The London, Edinburgh, and Dublin Philosophical Magazine and Journal of Science*, 35(234):41–48, 1868.

[62] Birol Küyel and S. Gruber. Experimental turbulence spectra in neutral and ion components of a weakly ionized gas. *The Physics of Fluids*, 16(11):1842–1847, 1973.

[63] L. D. Landau and E. M. Lifshitz. *Fluid Mechanics*. Number v.6 in Course of Theoretical Physics. Butterworth-Heineman, 1987.

[64] Irving Langmuir. The pure electron discharge. and its applications in radio telegraphy and telephony. *Proceedings of the Institute of Radio Engineers*, 3(3):261–286, 1915.

[65] Irving Langmuir. Oscillations in ionized gases. *Proceedings of the National Academy of Sciences of the United States of America*, 14(8):627, 1928.

[66] C. P. Lee and T. G. Wang. Acoustic radiation pressure. *The Journal of the Acoustical Society of America*, 94(2):1099–1109, 1993.

[67] Ritva Löfstedt and Seth Putterman. Theory of long wavelength acoustic radiation pressure. *The Journal of the Acoustical Society of America*, 90(4):2027–2033, 1991.

[68] Asier Marzo, Adrian Barnes, and Bruce W. Drinkwater. Tinylev: A multi-emitter single-axis acoustic levitator. *Review of Scientific Instruments*, 88(8):085105, 2017.

[69] Kiichiro Matsuzawa. Sound sources with corona discharges. *The Journal of the Acoustical Society of America*, 54(2):494–498, 1973.

[70] Michael S. Mazzola and G. Marshall Molen. Modeling of a DC glow plasma loudspeaker. *The Journal of the Acoustical Society of America*, 81(6):1972–1978, 1987.

[71] Michael R. Moldover, James B. Mehl, and Martin Greenspan. Gas-filled spherical resonators: Theory and experiment. *The Journal of the Acoustical Society of America*, 79(2):253–272, 1986.

[72] Michael R. Moldover, J. P. Martin Trusler, T. J. Edwards, James B. Mehl, and Richard S. Davis. Measurement of the universal gas constant R using a spherical acoustic resonator. *Physical review letters*, 60(4):249, 1988.

[73] Michael R. Moldover, Meyer Waxman, and Martin Greenspan. Spherical acoustic resonators for temperature and thermophysical property measurements. *High Temp. High Pressure*, 11:75–86, 1979.

[74] D. D. Morabito. The spacecraft communications blackout problem encountered during passage or entry of planetary atmospheres. *IPN Progress Report*, pages 42–150, 2002.

[75] P. M. C. Morse and K. U. Ingard. *Theoretical Acoustics*. International series in pure and applied physics. Princeton University Press, 1986.

[76] Rahla Naghma, Minaxi Vinodkumar, and Bobby Antony. Total cross sections for O_2 and S_2 by electron impact. *Radiation Physics and Chemistry*, 97:6–11, 2014.

[77] George W. Nasmyth. The frequency of the singing arc. *Physical Review (Series I)*, 27(2):117, 1908.

[78] Jo Olsen and Thomas D. Dreeben. Experimental and simulated straightening of metal halide arcs using power modulation. *IEEE Transactions on Industry Applications*, 47(1):368–375, 2010.

[79] Jo Olsen and Warren P. Moskowitz. Optical measurement of acoustic resonance frequencies in HID lamps. In *IAS'97. Conference Record of the 1997 IEEE Industry Applications Conference Thirty-Second IAS Annual Meeting*, volume 3, pages 2263–2269. IEEE, 1997.

[80] Ryo Ono, Masaharu Nifuku, Shuzo Fujiwara, Sadashige Horiguchi, and Tetsuji Oda. Gas temperature of capacitance spark discharge in air. *Journal of Applied Physics*, 97(12):123307, 2005.

[81] Alfred Brian Pippard. *The physics of vibration*. Cambridge University Press, 2007.

[82] Seth Pree, John Koulakis, Alexander Thornton, and Seth Putterman. Acousto-convective relaxation oscillation in plasma lamp. In *Proceedings of Meetings on Acoustics 21ISNA*, volume 34, page 045015. Acoustical Society of America, 2018.

[83] Seth Pree, Seth Putterman, and John P. Koulakis. Acoustic self-oscillation in a spherical microwave plasma. *Physical Review E*, 100(3):033204, 2019.

[84] Abbott A. Putnam and William R. Dennis. Survey of organ-pipe oscillations in combustion systems. *The Journal of the Acoustical Society of America*, 28(2):246–259, 1956.

[85] Seth J. Putterman. *Superfluid Hydrodynamics*, volume 3. North-Holland Publishing Co, Jan 1974.

[86] Yuri P. Raizer. *Gas discharge physics*. Springer, 1991.

[87] John William Strutt Baron Rayleigh. *The theory of sound*, volume 2. Macmillan, 1896.

[88] A. S. Richardson. *NRL plasma formulary*. Naval Research Lab., Washington, DC, 1983.

[89] Pieter L. Rijke. Lxxi. notice of a new method of causing a vibration of the air contained in a tube open at both ends. *The London, Edinburgh, and Dublin Philosophical Magazine and Journal of Science*, 17(116):419–422, 1859.

[90] Isadore Rudnick. Measurements of the acoustic radiation pressure on a sphere in a standing wave field. *The Journal of The Acoustical Society of America*, 62(1):20–22, 1977.

[91] William A. Saxton. Excitation of acoustic waves in plasmas. *J. Res. Natl. Bur. Std., Radio Science*, 1965.

[92] Michael Schulz and Uno Ingard. Acoustic kink instability in an argon discharge. *The physics of Fluids*, 10(5):1031–1036, 1967.

[93] John Sheffield, Dustin Froula, Siegfried H. Glenzer, and Neville C. Luhmann Jr. *Plasma scattering of electromagnetic radiation: theory and measurement techniques.* Academic press, 2010.

[94] Mahendra Singh Sodha and Carl James Palumbo. Modulation of electromagnetic waves by acoustic waves in a plasma. *Canadian Journal of Physics*, 42(8):1635–1642, 1964.

[95] Arnold Sommerfeld. *Thermodynamics and statistical mechanics*, volume 5. CUP Archive, 1964.

[96] C. Sondhauss. Ueber die schallschwingungen der luft in erhitzten glasröhren und in gedeckten pfeifen von ungleicher weite. *Annalen der Physik*, 155(1):1–34, 1850.

[97] Klaus Stockwald, Herbert Kaestle, and Herbert Ernst. Highly efficient metal halide HID systems with acoustically stabilized convection. *IEEE Transactions on Industry Applications*, 50(1):94–103, 2013.

[98] Stephen D. Strickler and Albert B. Stewart. Radial and azimuthal standing sound waves in a glow discharge. *Phys. Rev. Lett.*, 11:527–529, Dec 1963.

[99] Sylvie Su, David Cébron, Henri-Claude Nataf, Philippe Cardin, Jérémie Vidal, Max Solazzo, and Yann Do. Acoustic spectra of a gas-filled rotating spheroid. *European Journal of Mechanics-B/Fluids*, 2020.

[100] Yvonne Sutton. *Electro-acoustic coupling in a plasma gas.* PhD thesis, The Open University, 2012.

[101] Gregory W. Swift. Thermoacoustics: A unifying perspective for some engines and refrigerators, 2003.

[102] K. W. Taconis, J. J. M. Beenakker, A. O. C. Nier, and L. T. Aldrich. Measurements concerning the vapour-liquid equilibrum of solutions of He3 in He4 below 2.19 K. *Physica*, 15(8-9):733–739, 1949.

[103] D. M. Tombs. Corona wind loud-speaker. *Nature*, 176(4489):923–923, 1955.

[104] Rudolf Tuckermann, Bernd Neidhart, Ernst G Lierke, and Sigurd Bauerecker. Trapping of heavy gases in stationary ultrasonic fields. *Chemical physics letters*, 363(3-4):349–354, 2002.

[105] B. P. Turner, Michael G. Ury, Y. Leng, and W. G. Love. Sulfur lamps—progress in their development. *Journal of the Illuminating Engineering Society*, 26(1):10–16, 1997.

[106] Han S. Uhm, Yong C. Hong, and Dong H. Shin. A microwave plasma torch and its applications. *Plasma Sources Science and Technology*, 15(2):S26, 2006.

[107] Jérémie Vidal, Sylvie Su, and David Cébron. Compressible fluid modes in rigid ellipsoids: towards modal acoustic velocimetry. *Journal of Fluid Mechanics*, 885, 2020.

[108] H. Volland. *Handbook of Atmospheric Electrodynamics*. Number v. 2. Taylor & Francis, 1995.

[109] R. A. Waldron. Perturbation theory of resonant cavities. *Proceedings of the IEE-Part C: Monographs*, 107(12):272–274, 1960.

[110] John F. Waymouth. Applications of microwave discharges to high-power light sources. In *Microwave Discharges*, pages 427–443. Springer, 1993.

[111] John Wheatley and Arthur Cox. Natural engines. *Phys. Today;(United States)*, 38(8), 1985.

[112] John C. Wheatley, Gregory W. Swift, and Albert Migliori. The natural heat engine. *Los Alamos Science*, 14(2):2–33, 1986.

[113] Harald L. Witting. Acoustic resonances in cylindrical high-pressure arc discharges. *Journal of Applied Physics*, 49(5):2680–2683, 1978.

[114] W. J. Xie, C. D. Cao, Y. J. Lü, Z. Y. Hong, and B. Wei. Acoustic method for levitation of small living animals. *Applied Physics Letters*, 89(21):214102, 2006.

[115] K. Yosioka and Y. Kawasima. Acoustic radiation pressure on a compressible sphere. *Acta Acustica United with Acustica*, 5(3):167–173, 1955.

[116] Y. B. Zel'dovich and Y. P. Raizer. *Physics of Shock Waves and High-Temperature Hydrodynamic Phenomena*. Dover Books on Physics. Dover Publications, 2012.

[117] Likun Zhang. From acoustic radiation pressure to three-dimensional acoustic radiation forces. *The Journal of the Acoustical Society of America*, 144(1):443–447, 2018.